NONLINEAR EFFECTS WITH A FOCUS ON CROSS PHASE MODULATION AND ITS IMPACT ON WAVELENGTH DIVISION MULTIPLEXING OPTICAL FIBRE NETWORKS

Romeo Reginald Gunther Gamatham

Submitted in fulfilment of the
requirements for the degree of

PHILOSOPHIAE DOCTOR

in the Faculty of Science at the
Nelson Mandela Metropolitan University

December 2012

Promoter: Professor A. W. R. Leitch

Co-promoter: Dr T. B. Gibbon

To my lovely wife Adelina Mbinjama-Gamatham and to my family, thank you for all your love and support.

ACKNOWLEDGEMENTS

My sincere thanks and gratitude is extended to my promoter, Professor Andrew Leitch, and co-promoter, Doctor Timothy Gibbon for their support throughout this study.

In 2009 I had the privilege to visit the Technical University of Denmark (DTU) over a three month period. I worked under Professor Idelfonso T. Monroy from the Metro Access group in the Photonics department. We worked on ultra wideband (UWB) radio over fibre transmission. I extend my gratitude to Prof. Monroy, Prof. Xianbin Yu and the rest of the Metro Access team for sharing their knowledge and research experience with me.

Besides my research on nonlinear effects at NMMU in 2011 I spend five months in Italy at the University of Padova. We worked on counter propagating Raman polarization attraction. A great thank you to Professor Andrea Galtarossa for giving me the opportunity to work in his laboratory. I extend my gratitude to Fabrizio Chiarello, whom I worked with personally; I also thank Luca Schenato, Luca Palmieri, Sourab Roy and Leonora Ursini for all their help.

My thanks are extended to staff and students both in the fibre optics laboratory and within the Physics department for their wisdom, experience and general support.

I thank the Nelson Mandela Metropolitan University research partners and the Fibre Optics research group project funders:
African Laser Centre (ALC)
South African National Research Foundation (NRF)
Technology and Human Resources for Industrial Programme (THRIP)
Telkom South Africa
INGOMA Communication Services
Dartcom
National Laser Centre (NLC)

Special thanks go out to Telkom South Africa based in Port Elizabeth for allowing us to carry out measurements on their deployed optical fibre cables.

I thank the African Laser Centre (ALC) for their generous financial support as well as Nelson Mandela Metropolitan University for funding my doctoral studies.

Finally I thank all my colleagues and my family for their continuous support and encouragement during this study.

TABLE OF CONTENTS

ABSTRACT

The demand for faster data transmission is ever increasing. Wavelength division multiplexing (WDM) presents as a viable solution to increase the data transmission rate significantly. WDM systems are based on the ability to transmit multiple wavelengths simultaneously down the fibre. Unlike time division multiplexing (TDM) systems, WDM systems do not increase the data transfer by increasing the transmission rate of a single channel. In WDM systems the data rate per channel remains the same, only multiple channels carry data across the link.

Dense wavelength division multiplexing (DWDM) promises even more wavelengths packed together in the same fibre. This multiplication of channels increases the bandwidth capacity rapidly. Networks are looking into making use of technology that will ensure no electronic signal regeneration at any point within the DWDM network. Examples are; reconfigurable optical add/drop multiplexers (ROADM) and optical cross connect (OXC) units. These components essentially enable network operators to split, combine and multiplex optical signals carried by optical fibre.

WDM allows network operators to increase the capacity of existing networks without expensive re-cabling. This provides networks with the flexibility to be upgraded to larger bandwidths and for reconfiguration of network services. Further, WDM technology opens up an opportunity of marketing flexibility to network operators, where operators not only have the option to rent out cables and fibres but wavelengths as well.

Cross phase modulation (XPM) poses a problem to WDM networks. The refractive index experienced by a neighbouring optical signal, not only depends on the signal's intensity but on the intensity of the co-propagating signal as well. This effect leads to a phase change and is known as XPM. This work investigates the characteristics of XPM. It is shown that, in a two channel WDM network, a probe signal's SOP can be steered by controlling a high intensity pump signal's SOP. This effect could be applied to make a wavelength converter. Experimental results show that the degree of polarization (DOP) of a probe signal degrades according to a mathematical model found in literature. The pump and probe signals are

shown to experience maximum interaction, for orthogonal probe-pump SOP vector orientations. This may be problematic to polarization mode dispersion compensators. Additionally, experimental results point out that the SOP of a probe signal is much more active in the presence of a high intensity pump, as compared to the single signal transmission scenario.

Keywords: wavelength division multiplexing (WDM), time division multiplexing (TDM), dense wavelength division multiplexing (DWDM), reconfigurable optical add/drop multiplexers (ROADM), optical cross connect (OXC), polarization mode dispersion compensator (PMDC).

ABBREVIATION LIST

CD chromatic dispersion
DCF dispersion compensating fibre
DFB distributed feedback laser
DGD differential group delay
DOP degree of polarization
DSF dispersion shifted fibre
DWDM dense wavelength division multiplexing
EDFA erbium doped fibre amplifier
FPC fibre polarization controller
FWM four-wave mixing
GVD group velocity dispersion
IDF inverse dispersion shifted fibre
MZM Mach-Zehnder modulator
OXC optical cross connect
PC polarization controller
PDF probability distribution function
PDL polarization dependent loss
PMD polarization mode dispersion
PMF polarization maintaining fibre
PSP principal state of polarization
PSPs principal states of polarization
RMS root mean square
ROADM reconfigurable optical add/drop multiplexer
SBS stimulated Brillouin scattering
RI refractive index
SMF single mode fibre
SPM self phase modulation
SOP state of polarization
SOPs states of polarization
SRS stimulated Raman scattering

XPM cross phase modulation

XPolM cross polarization modulation

WDM wavelength division multiplexing

WSON wavelength switched optical networks

CHAPTER 1

INTRODUCTION

In the eighth century B.C. the Greeks used to relay information by means of a fire signal. The invention of the telegraph by F. B. Morse revolutionised up distance communication, by using an electrical signal for transmitting information over a long distance. Generally, the data was superimposed onto a sinusoidal varying electromagnetic wave. The sinusoidal wave is known as the carrier, and an increase in the frequency of the carrier implied an increase in the transmission bandwidth, and consequently a greater information capacity. This subsequently led to radio, television, radar and microwave transmission. Until the mid 1960's the options were to send information by either electrical wire or by radio.

The invention of the laser in the late 1950's presented a new means of transmitting data. It took several decades to reduce the attenuation in optical fibres down to an acceptable level. In the 1970's the attenuation in optical fibres was approximately 4 dB/km. This made transmission through the fibre practical. Optical fibre amplifiers were invented in the 1980's. This enabled transmission over longer distances. The demand for more bandwidth rapidly increased. The source of this demand came from a rapid proliferation of personal computers and their advances in storage capacity and processing capability. The widespread availability of the internet and all the functionality that comes with it has fuelled this ever growing demand even more.

The basic components of a fibre optic communication system are as follows. The information is presented to the modulator or directly to the laser in electrical form. The data is then encoded in the light signal from the optical source, which is most often a laser diode. The medium of transport is the glass optical fibre or a polymer fibre. The light travels down the fibre and a receiver detects the data at the end. Some passive components such as filters, isolators, couplers, and Bragg gratings may be present in the network. In some instances the light signal is amplified with an optical amplifier. A photodiode detects the light signal at the end of the network and converts it into an electrical signal. Network service providers are known as carriers. Today's carriers not only provide voice traffic services but some are only dedicated to interconnecting internet service providers. The network carriers are divided into several specialisation groups such as the metro carriers and long haul carriers, where the

network architecture and requirements differ for the networks who deliver metro and long haul services. Local area networks span at most over a few kilometres, whereas metropolitan area networks cover a metropolitan area and span over a few hundred kilometres and wide area networks refer to even longer networks in the hundred to thousands of kilometres range.

Optical fibre cables are installed either aerially, in ducts, undersea or buried in the ground. As the signal propagates through the fibre, the signal is affected by various effects. These effects include attenuation, dispersion and nonlinear effects. Silica fibres are highly transparent over certain wavelength windows. The signal attenuation is mainly due to absorption, Rayleigh scattering, Fresnel reflections and bend induced loss. Chromatic dispersion (CD) and polarization mode dispersion (PMD) are the primary dispersive effects that broaden the input signal. Pulse broadening by dispersive effects may lead to inter-symbol interference as well as power fading. Chromatic dispersion is solved by manufacturing fibres with low CD and by using dispersion compensating fibre to negate the CD from the fibre link. Fibre companies such as OFS and Corning have managed to draw fibre with very low PMD coefficients, which serves working at 10 Gbps to 40 Gbps very well.

Two factors that play a major role in optical networks are, the physical cost of a network and the transmission speed. The idea is to lower the cost and to increase the transmission rate. A practical and straightforward way to decrease the network cost is to increase the initial transmission power of the optical signal, this allows for fewer amplifiers in the link or none at all depending on the link length. This approach is unfortunately in conflict with nonlinear effects. Nonlinear effects become significant at high power levels and threaten to degrade the signal quality. In optical fibre these effects include; stimulated Raman scattering (SRS), stimulated Brillouin scattering (SBS), four-wave mixing (FWM), self phase modulation (SPM) and cross phase modulation (XPM). Effects such as FWM, SPM and XPM have deleterious effects on the transmitted signal at high power levels. The transmission rate in optical networks may be increased by multiplexing several wavelengths together and transmitting them over a fibre simultaneously. This method of transmission is known as wavelength division multiplexing (WDM). This increases the overall transmission speeds considerably. FWM and XPM entail cross-talk which refers to the interaction among neighbouring optical signals, hence FWM and XPM may occur in WDM networks.

This thesis concentrates on the effect of XPM. XPM refers to the interaction where an optical signal is influenced by its neighbouring signal. This interaction is such that the phase of the neighbouring signal is changed by either an intensity variation or polarization variation of the co-propagating signal. The degree of polarization (DOP) of a continuous wave signal may be

degraded by modulating the intensity of a neighbouring signal. This effect may present a problem if the network makes use of a polarization sensitive receiver or other polarization sensitive components. It also presents a problem to PMD compensators placed at the end of a fibre link. PMD compensators use the DOP to indirectly monitor the link PMD; the signal as a result of XPM will be misleading to the PMD compensator.

This thesis is organised as follows. Chapter 2 introduces the optical fibre structure. This is followed by a brief historical background that mentions key discoveries pertaining to the nature of light. Topics such as guided modes and polarization concepts of light are introduced. The chapter then mentions different types of optical fibre and their characteristics. The chapter ends with discussions of the effects of attenuation, chromatic dispersion and polarization mode dispersion. Chapter 3 discusses the theory of SBS, SRS, FWM, SPM and XPM in detail. SBS is a back-scattered optical signal; in chapter 3 the origin and principle of operation of SBS is discussed. Further, the fundamental theory of SRS is presented. The different Raman amplification techniques as well as their operating principles are covered. The Raman amplification section ends with a detailed literature review of Raman polarization attraction, which is a newly contested topic in fibre amplification. Two sections cover the topics of FWM and SPM. Chapter 3 concludes with a detailed presentation of XPM. Theory from referenced books as well as journal articles is presented. The theoretical arguments of XPM presented have direct relation to the work on XPM presented further in this thesis.

Chapters 4, 5 and 6 are results chapters, each presenting the experimental work, results and discussions. Chapter 4 shows experimental schemes and results of several experiments. The following topics are investigated in chapter 4: the stability of the probe SOP in the absence and presence of a pump signal, remote control of a probe signal with a co-propagating pump signal and finally, indirect intensity modulation of a probe signal utilising the XPM effect. Chapter 5 looks into the effect of XPM induced DOP degradation. Experimental results are presented outlining this effect. Chapter 6 focuses on SOP drift over a long period of time and probes the role of XPM in the SOP drift. The thesis concludes with an overall summary found in chapter 7, which is followed by an appendix of research outputs and the references used in this thesis.

CHAPTER 2

OPTICAL FIBRE TRANSMISSION BACKGROUND

There has always been a demand for an increase in data transmission capacity. This demand is driven by continual technological advances, coupled with increasing demands from end-users. Currently the structure of optical networks is based on transmitting a modulated light source over a fibre and detecting the signal using a photodiode. Hence the basic network consists of a transmitter, a link and a receiver. The transmitter is usually a laser or a light emitting diode light source. The light from the source is modulated by either modulating the source directly or by externally modulating a specific component, such as the phase, polarization or intensity of the light source. The light is then transmitted over a link of fibre and the data recovered at the end of the link by a receiver.

2.1 Optical fibre structure

Typical optical fibre consists of a dielectric core with a high refractive index surrounded by a cladding which has a lower refractive index.

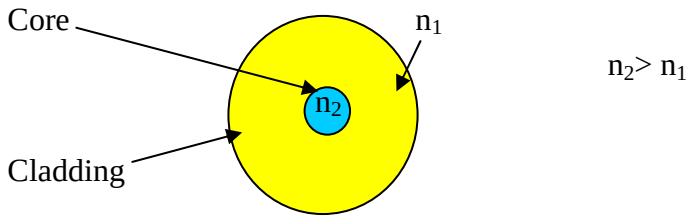

Figure 2.1 Fibre cross-section.

In the case of glass fibres, the core is made up of highly purified silica (SiO_2) which is then doped, normally with Germanium (Ge), to achieve a higher refractive index as compared to the cladding region. Germanium is the preferred doping agent because it absorbs less light energy at 1300 nm and 1550 nm than other dopants [17].

This core cladding configuration allows the optical fibre to act as a light waveguide, through which optical pulses carrying information can be transmitted. Typically the core diameter will range between 5 and 10 μm in single mode fibres, and the cladding will have a diameter of 125 μm. In multimode fibre the core diameter is slightly larger with a size of 50 μm.

2.2 Nature of light

2.2.1 Introductory remarks

The first scientific observation of the polarization effect of light was by a Danish mathematician named Erasmus Bartholinus from the University of Copenhagen in 1669 [8]. He observed that the incident light beam that passed through Iceland spar crystal ($CaCO_3$) was split into two beams [3, 4]. The two beams that exit from the crystal differed as the one beam obeys the law of refraction whereas the other beam does not [3, 4]. Due to the insufficient understanding of the physical nature of light, no accurate explanation was provided. In 1672 Christiaan Huyghens, a Dutch physicist, discovered that the two light beams can be extinguished by placing another Calcite crystal and rotating the crystal about the direction of the beam [32]. In reference [32], which is a translation of the original Traité de la Lumière, Huyghens presented his wave theory of light and explained the phenomena of reflection, refraction and double refraction for the first time.

In 1803 Thomas Young proclaimed that light waves vibrate transverse to the direction of propagation [76]. In 1816 Brewster discovered strain birefringence: he noticed that an isotropic transparent optical medium can be made optically anisotropic by applying some mechanical stress [8].This was followed by Augustine Jean Fresnel's equations of reflection and transmission of a plane wave incident on a static plane interface between two dielectric isotropic media [8].

A major advance regarding the description of the state of polarization of light came in 1852 by George Gabriel Stokes. Stokes introduced four measurable parameters which can be used to describe the polarization properties of light in his paper entitled, "On the composition and resolution of streams of polarized light from different sources" [66]. His description was unique because instead of concentrating on the field vectors, the Stokes description is based on intensities which are measurable quantities of optical frequencies. Later on in 1892 Henri

Poincaré, a French mathematician and mathematical physicist, introduced the Poincaré sphere, a geometric representation of all possible states of polarization of light.

The above facts are a selected list of pioneering contributions to the field of optics. These discoveries all play a major role in our understanding of optics today. Another key milestone which forms the cornerstone in our present view of optics is the electromagnetic theory by James Clerk Maxwell [45]. Maxwell presented his theory in a memoir entitled "A dynamical theory of the electromagnetic field", in 1864 [45]. Maxwell's theory describes the propagation of electromagnetic waves.

2.2.2 Guided modes

Consider Maxwell's equations for a linear, isotropic dielectric material having no currents and free charge:

$$\nabla \times \overline{\mathrm{E}} = -\frac{\partial \overline{\mathrm{B}}}{\partial t} \tag{2.1a}$$

$$\nabla \times \overline{\mathrm{H}} = \frac{\partial \overline{\mathrm{D}}}{\partial t} \tag{2.1b}$$

$$\nabla \cdot \overline{\mathrm{D}} = 0 \tag{2.1c}$$

$$\nabla \cdot \overline{\mathrm{B}} = 0 \tag{2.1d}$$

where $\overline{\mathrm{D}} = \in \overline{\mathrm{E}}$ and $\overline{\mathrm{B}} = \mu \overline{\mathrm{H}}$ [37]. The parameter $\in$ is the permittivity and μ is the permeability of the medium. Decoupling these equations gives the standard wave equation of the electric field

$$\nabla^2 \overline{\mathrm{E}} = \in \mu \frac{\partial^2 \overline{\mathrm{E}}}{\partial t^2}. \tag{2.2}$$

The electric field is taken to be

$$\overline{\mathrm{E}}(\bar{\mathrm{r}}, t) = \overline{\mathrm{E}}(x, y) e^{i(\omega t - \beta z)}. \tag{2.3}$$

Substituting equation 2.3 into 2.2 gives

$$\nabla^2\bar{\mathrm{E}}(\bar{\mathrm{r}}) + k_0^2 n^2(\bar{\mathrm{r}})\bar{\mathrm{E}}(\bar{\mathrm{r}}) = 0 \tag{2.4}$$

where the susceptibility is related to the refractive index as$n^2 = 1 + \chi_e$, the permittivity is given by $\in = \in_0 (1 + \chi_e)$ and $k_0^2 = \omega^2 \mu \in_0$.

Before looking at wave propagation in optical fibres, it is imperative to examine guided modes. Yariv shows a detailed simplified description of the existence of guided modes in [75]. Here follows a summary of this discussion. Substituting the electric field given by equation 2.3 into equation 2.4 gives

$$\left(\frac{\partial^2}{\partial x^2} + \frac{\partial^2}{\partial y^2}\right)\bar{\mathrm{E}}(x,y) + [k_0^2 n^2(\bar{\mathrm{r}}) - \beta^2]\bar{\mathrm{E}}(x,y) = 0. \tag{2.5}$$

For the sake of mathematical simplicity the discussion is limited to a planar waveguide which gives equation 2.5 to have the form

Region I (RI is n_1) $$\frac{\partial^2}{\partial x^2}\mathrm{E}(x,y) + [k_0^2 n_1^2 - \beta^2]\mathrm{E}(x,y) = 0 \tag{2.6a}$$

Region II (RI is n_2) $$\frac{\partial^2}{\partial x^2}\mathrm{E}(x,y) + [k_0^2 n_2^2 - \beta^2]\mathrm{E}(x,y) = 0 \tag{2.6b}$$

Region III (RI is n_3) $$\frac{\partial^2}{\partial x^2}\mathrm{E}(x,y) + [k_0^2 n_3^2 - \beta^2]\mathrm{E}(x,y) = 0. \tag{2.6c}$$

Here it is assumed that the refractive index (RI) $n_2 > n_3 > n_1$, hence there are three layers where layer 2 has the highest refractive index. The partial differential equations from 2.6a to 2.6c have an exponential solution when $k_0^2 n_i^2 - \beta^2$ is negative and a sinusoidal solution when $k_0^2 n_i^2 - \beta^2$ is positive. These different scenarios are illustrated in figure 2.2.

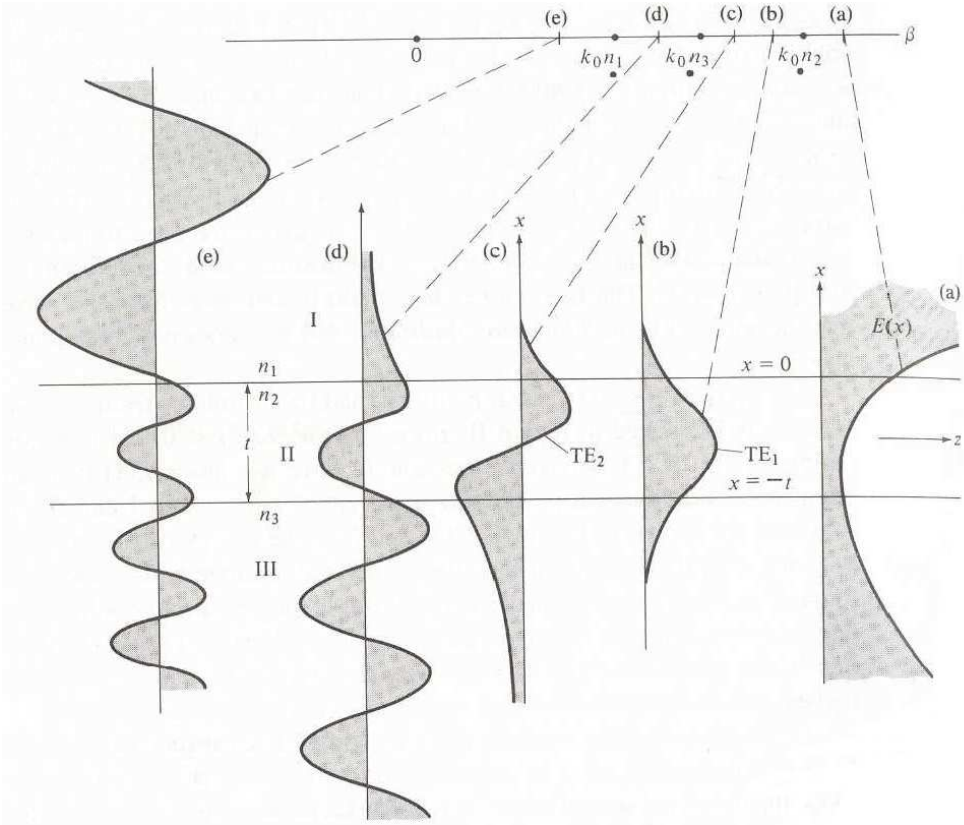

Figure 2.2Electric field distribution across three layers with different refractive index, figure from Yariv [75] pg. 494.

Case (a) shows the electric field solutions when $\beta^2 > k_0^2 n_2^2 > k_0^2 n_3^2 > k_0^2 n_1^2$, hence the solution is exponential for all the layers. The boundary condition states that the electric field must be continuous at the boundary. This yields a situation where the electric field increases away from the waveguide which is physically not possible. Cases (e) and (d) lead to substrate and radiation modes. The only cases that lead to guided modes are cases (b) and (c), where $k_0^2 n_2^2 > \beta^2 > k_0^2 n_3^2 > k_0^2 n_1^2$. Here the electric field is oscillatory within the layer with refractive index $n_2$and decays exponentially in the two other layers. Therefore guided modes in optical fibre are defined as solutions to the wave equation that satisfy the boundary conditions.

The number of confined modes depends on the width of the waveguide, the frequency of the light, and the refractive indices of the layers. Maxwell's equations show that only transverse electric (TE) modes and transverse magnetic (TM) modes are found in metallic waveguides [37]. In optical fibres though, the core-cladding boundary conditions lead to coupling between the electric and magnetic field components. This leads to hybrid modes designated as HE or EH modes, depending on whether the transverse electric or the transverse magnetic field is larger for that particular mode [37]. The lowest order mode in optical fibre is HE_{11}.

2.2.3 Polarization concepts of light

Light is an electromagnetic wave consisting of electric and magnetic fields which are orthogonal with respect to each other. These waves are transverse waves with respect to the direction of propagation. Consider the light wave to propagate along the z-axis. When viewing the electric field as it propagates towards you, the transverse wave will have an appearance of a vector. This electric vector will trace out a path as it propagates; the mapping of this path describes the state of polarization of the light wave. When fully polarized the light wave will either be linearly, elliptically or circularly polarized.

The electric field vector can be broken up into E_x and E_y components respectively; this allows the electric field vector to be written as

$$\overline{\mathrm{E}}(z,t) = \hat{e}_x \mathrm{E}_x(z,t) + \hat{e}_y \mathrm{E}_y(z,t). \tag{2.7}$$

The component waves travelling in the z-direction with phases φ_x and φ_y are written as

$$\mathrm{E}_x = \mathrm{E}_{0x} e^{i(kz-\omega t+\varphi_x)} \tag{2.8}$$

and

$$\mathrm{E}_y = \mathrm{E}_{0y} e^{i(kz-\omega t+\varphi_y)}. \tag{2.9}$$

Substituting the x and y component of the electric field into equation 2.7 allows the electric field to be written as

$$\overline{\mathrm{E}} = \left[\hat{e}_x \mathrm{E}_{0x} e^{i\varphi_x} + \hat{e}_y \mathrm{E}_{0y} e^{i\varphi_y}\right] e^{i(kz-\omega t)} = \widetilde{\mathrm{E}}_0 e^{i(kz-\omega t)} \tag{2.10}$$

The state of polarization of the light is determined by the relative amplitudes and phases of these components, therefore it is only necessary to concentrate on the complex amplitude, [51],

$$\widetilde{\mathrm{E}}_0 = \begin{bmatrix} \mathrm{E}_{0x} e^{i\varphi_x} \\ \mathrm{E}_{0y} e^{i\varphi_y} \end{bmatrix} = \begin{bmatrix} \widetilde{\mathrm{E}}_{0x} \\ \widetilde{\mathrm{E}}_{0y} \end{bmatrix}. \tag{2.11}$$

Equation 2.11 is a representation of the Jones vector described by Jones in 1941[36]. These Jones vectors can be used to describe any state of polarization of light. The state of polarization of the light wave depends on the relative phase between the x and y components of the electric field vector. Figures 2.3 to 2.5 show the relative phase associated with linear, elliptical and circular polarized orientations. The phase difference is denoted by φ.

In addition to the linear polarization states of light shown in figure 2.3 (a) and (b), the light signal can also be vertically and horizontally linearly polarized. This occurs when either the x or y component of the electric field is zero.

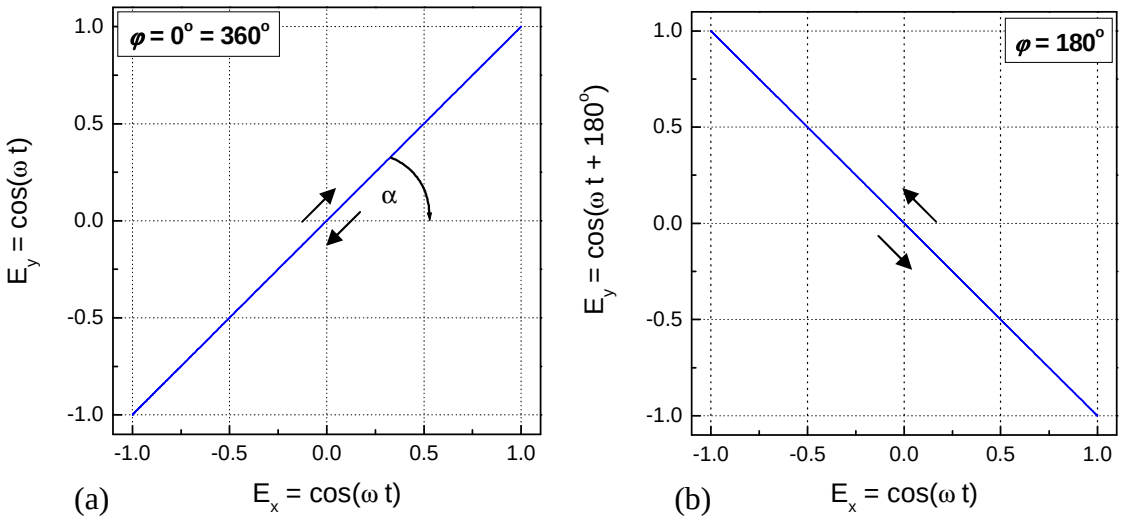

Figure 2.3Representation of linearly polarized light.

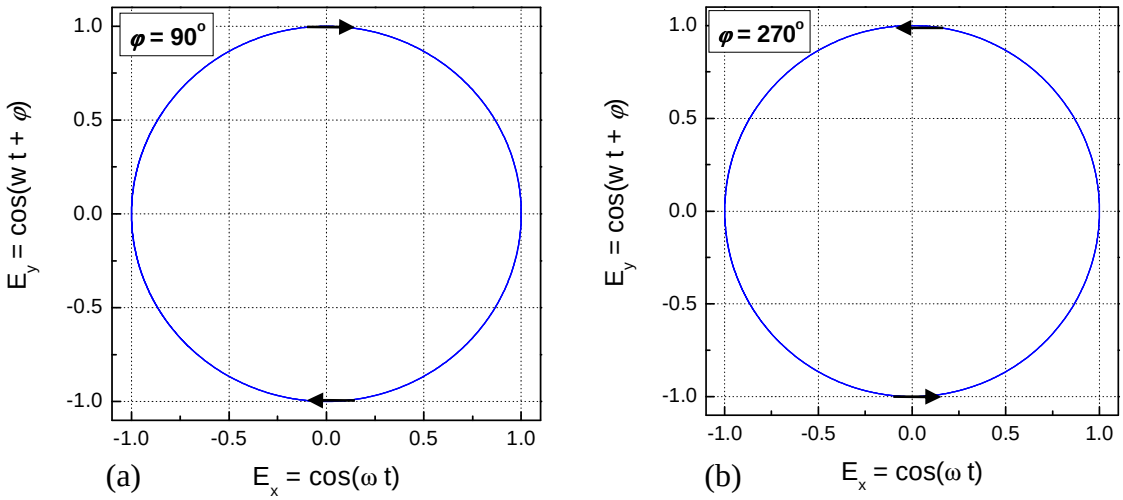

Figure 2.4 Representation of circularly polarized light: (a) Right circular polarized, (b) Left circular polarized.

There exist two possibilities for circular polarized light. The light is circularly polarized when the waves are either 90^o or 270^o out of phase as seen in figure 2.4 (a) and (b). Any other phase differences, other than those shown in figure 2.3 and 2.4 yields, elliptically polarized light. Figure 2.5 shows specific examples for the relative phases required, for the light to be elliptically polarized. As shown in figure 2.5 (a), the difference between the phase differences 45^o and 315^o is the direction of rotation, where the phase difference 45^o has clockwise sense of rotation and 315^o rotates anticlockwise. Similarly, the difference between 135^o and 225^o is that 135^o rotates clockwise while 225^o rotates in an anticlockwise direction.

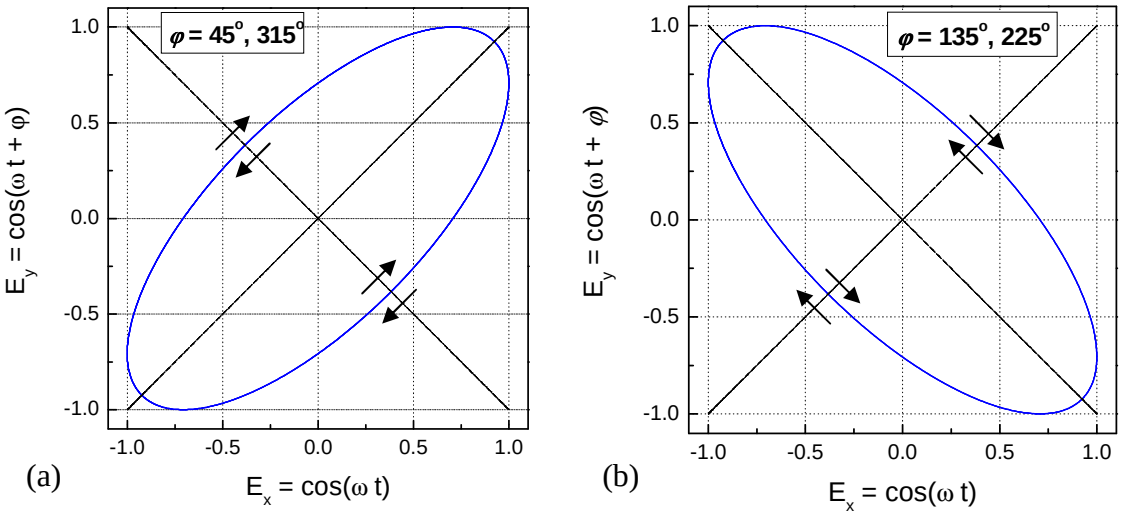

Figure 2.5 Representation of elliptical polarized states: (a) For a phase difference of 45^o the electric field rotates clockwise in the direction of travel and rotates anticlockwise for 315^o, (b) The electric field rotation is clockwise for 135^o and anticlockwise for 225^o.

2.2.4 Stokes formalism

An alternative manner to represent the state of polarization (SOP) of a light signal is to use the Stokes formalism proposed by Stokes in 1852 [66]. The Stokes formalism has the advantage of describing both polarized and unpolarised light. The Stokes vector is an array consisting of optical power values which are in reference to polarization states [17]. Four units make up the Stokes vector; S_0, S_1, S_2, S_3 [17].

The following abbreviations are used to define the Stokes parameters; LV for left vertical, LH for left horizontal, RC for right circular, LC for left circular, L ±θ for linear polarization at an angle.

S_0 = Total power (polarized + unpolarised)

S_1 = Power through LH polarizer – power through LV polarizer

S_2 = Power through L +45 – power through L -45 polarizer

S_3 = Power through RC polarizer – power through LC polarizer

These Stokes parameters are normalized by dividing all by S_0 which yields a range between -1 and 1. The degree of polarization (DOP) is defined as the ratio of polarized to the total light signal. Using the normalized Stokes parameters it is expressed as

$$\text{DOP}=\sqrt{s_1^2 + s_2^2 + s_3^2}. \tag{2.12}$$

All possible states of polarization can be represented by a unit sphere. This sphere is known as a Poincaré sphere and is shown in figure 2.6.

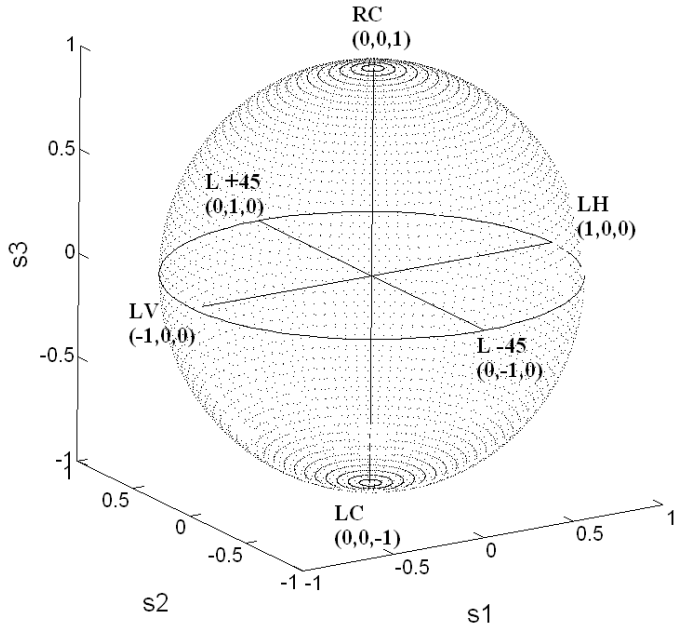

Figure 2.6 Poincaré sphere.

The location of the Stokes parameters for the main poles is indicated in figure 2.6. The circular states of polarization (SOPs) are at the top and bottom poles of the sphere. The linearly polarized SOPs are located along the equator of the sphere, while the elliptical SOPs are located everywhere else on the sphere. Fully polarized light is located on the surface of the Poincaré sphere and partially polarized light somewhere within the sphere.

2.3 Types of optical fibre

Fibre materials need to meet three requirements. It should be possible to draw the material into thin flexible fibres, the material must be transparent, at minimum for a particular wavelength, and it should be possible to alter the refractive index of the fibre in order to obtain a core and cladding. Glass and plastic meet these criteria. The majority of fibre is made of silicon dioxide or silica (SiO_2). There are many variations of this type of fibre.

The refractive index distribution in the core of the fibre can be varied by varying the material composition of the core of the fibre. Generally there exist two of these fibre types, step index fibre and graded index fibre. With step index fibre the refractive index remains the same throughout the full diameter of the fibre core but changes abruptly at the core cladding boundary. In graded index fibre the refractive index varies as a function of the radial distance from the core of the fibre [37]. These fibre types can be found as either single mode or multimode fibres.

In single mode fibres only one mode propagates through the fibre, whereas multimode fibres allow several modes to propagate through the fibre simultaneously. Typically single mode fibre (SMF) has a core diameter between 8 to 12 μm and a cladding diameter of 125 μm. Multimode fibres (MMF) have larger core areas compared to single mode fibre. Typical core sizes of multimode fibre vary from 50 to 200 μm with a cladding size of 125 to 400 μm. Multimode fibres allow the use of light emitting diodes which are much cheaper and have a longer lifetime than laser diodes. Multimode fibres are more expensive than single mode fibres but have a much cheaper system cost than single mode fibres. Current limits for multimode fibre transmission are 100 Gbps over 150 m multimode fibre and 10 Gbps over 550 m. Their overall transmission distance limit is 2 km. Multimode fibres suffer from intermodal dispersion, have a higher attenuation than SMF and generally are not suitable for long distance transmission. Single mode fibres are preferred for long distance transmission as they have a lower loss.

Chromatic dispersion is made up of waveguide and material dispersion. Material dispersion depends on the composition of the material, whereas waveguide dispersion is a function of the core radius, refractive index difference and the shape of the refractive index profile. Conventional single mode fibre has zero dispersion at 1310 nm. The optical signal is attenuated less at 1550 nm. This motivated the design of dispersion shifted fibre (DSF). By keeping the material dispersion fixed and altering the waveguide dispersion of the fibre, the

zero dispersion can be shifted to larger wavelengths [2, 35, 37]. The zero dispersion wavelength for DSF is 1550 nm [2]. The international telecommunications unit (ITU) standard for dispersion shifted fibre is abbreviated ITU-T G.653 [35]. At high power and long distance transmission DSF has a poorer performance as nonlinear effects come into play. This problem is solved by using non-zero dispersion shifted fibre (NZDSF) instead. Here the fibre dispersion is slightly offset from zero, hence a small amount of dispersion reduces the effects of nonlinear effects on the signal. The ITU standard of NZDSF is denoted as ITU-T G.655 [34].

Polarization maintaining fibre (PMF) is a special fibre that maintains the input state of polarization (SOP) as the signal propagates through the fibre. PMF has one slow and one fast axis. The birefringence in PMF is much higher than the birefringence in ordinary SMF. The refractive index between the fast and slow axis differ and the input SOP is maintained only when the electric field of the light signal is aligned with either the fast or the slow axis.

The birefringence is induced by stressing one of the orthogonal axes which results in a refractive index difference. Figure 2.7 shows four basic birefringent stress geometries, these are called panda, bow tie, oval core and elliptical stress member. The principle of operation of the panda, bow tie and elliptical jacket geometries is that the fibre core is flanked by high expansion glass that shrinks more during the manufacturing process [46]. This freezes the fibre in tension which induces tension birefringence [46]. Two axes which differ in refractive index are created, a higher index parallel and a lower index perpendicular to the direction of the applied stress [46].

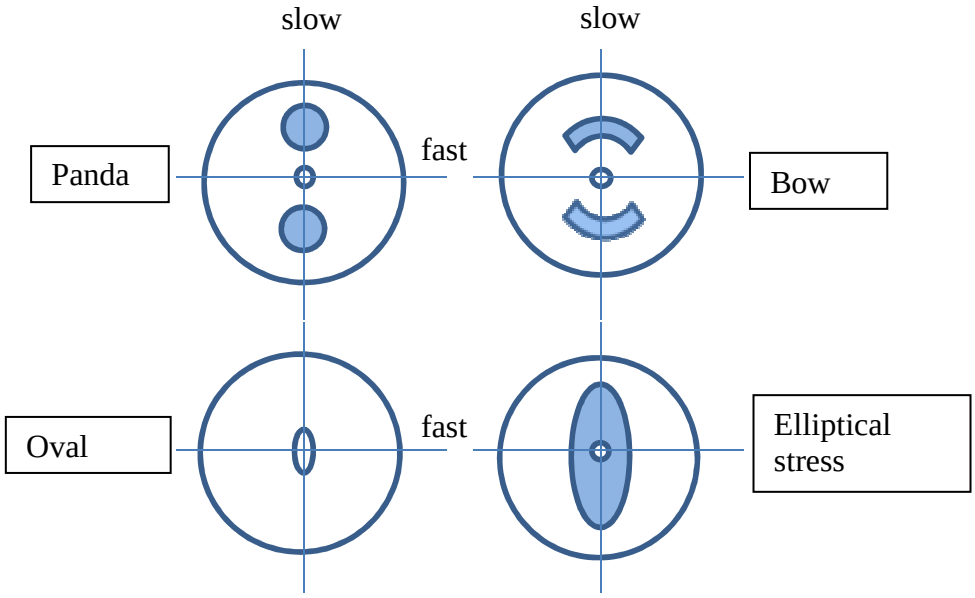

Figure 2.7 Cross section of well known PMF geometries.

2.4 Optical effects

2.4.1 Attenuation

SMF is made of pure silica which is pure silicon diode (SiO_2). Silica has the lowest absorption within the C and L band of any available material. The refractive index of silica can be altered with dopants. The refractive index of the core can be increased by doping the core with germanium dioxide (4% to 10%), or the refractive index of the cladding can be reduced by doping it with boron trioxide (B_2O_3) [19]. The doping process needs to be well controlled as it changes other characteristics of the silica, for example the thermal expansion coefficient [19]. If the core and cladding differ significantly in their thermal expansion coefficients, they may crack apart at some point in time. Other dopants that increase the refractive index are phosphorus pentoxide (P_2O_5), titanium dioxide (TiO_2) and aluminium oxide (Al_2O_3) [19]. The common feature among dopants is that they all increase the attenuation of the silica. MMF has a higher attenuation than SMF because MMF contains more dopants than SMF.

Light is attenuated exponentially with distance as the light signal propagates along the optical fibre by

$$P(z) = P(0)e^{-\alpha_p z} \tag{2.12}$$

where α_p is the attenuation coefficient in units of per km, while $P(0)$ is the initial power and $P(z)$ the power at distance z.

From a broad perspective, attenuation in optical fibres is caused by absorption, scattering, bending loss and core/cladding losses. Absorption is caused by atomic defects in the glass, extrinsic absorption by impurities and absorption by the atoms of the fibre material [37].

In 1970, the attenuation of silicon fibre was 20 dB/km, by 1980 researchers had reduced it to 1 dB/km. Since the 1990's typical SMF had an attenuation of 0.2 dB/km. Figure 2.8 shows the attenuation per kilometre as a function of wavelength for SMF.

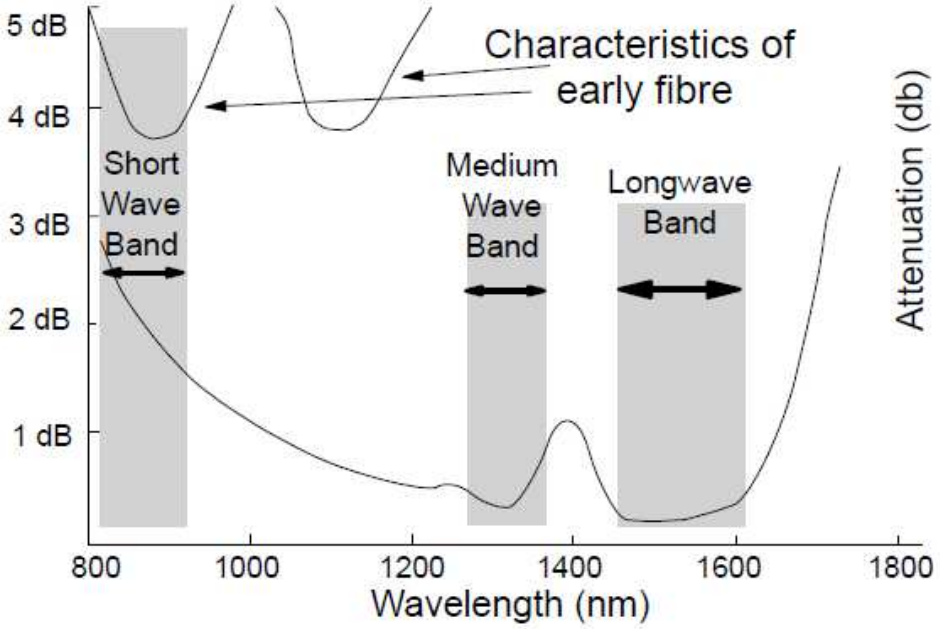

Figure 2.8 Optical fibre attenuation as a function of wavelength. Figure is from Understanding Optical Communications [19] pg. 32.

Three wavelength windows with minimal attenuation are evident in figure 2.8. The short wavelength band, from 800 nm to 900 nm, was made use of in the early days of optical fibre communication, 1970's, because of the cheap optical sources available at that wavelength.

The wavelengths where attenuation is minimum are 1310 nm and 1550 nm. At 1400 nm the attenuation increases sharply as indicated in figure 2.8. This is known as the water peak and is caused by OH ions. The OH ion is resonant at this wavelength hence the increase in absorption. The water peak is no longer a problem though, as researchers found a solution to the problem. The OH ions are removed by exposing porous glass to chlorine gas at high temperatures, for example 1200 ^{o}C [20]. This process allows companies such as Optical Fiber Solutions (OFS), to manufacture SMF such as the AllWave zero water peak SMF, which is a full spectrum fibre design that operates from 1260 nm to 1625 nm.

Another form of scattering is Mie scattering. Mie scattering has to do with scattering caused by imperfections comparable to the wavelength size. Modern day fibres don't experience this problem at all.

Assuming that the optical fibre has no physical defects, the dominant loss mechanism in today's fibres is caused by Rayleigh scattering [19]. This scattering is caused by the minute variations in the density or composition, 1/10th the wavelength, of the glass. Rayleigh scattering is inversely proportional to the wavelength power 4.

2.4.2 Chromatic dispersion

Dispersion in optical fibres occurs whenever some components of the light signal travel faster or slower than other components of the light signal. This leads to broadening of the optical pulse. Chromatic dispersion (CD) is made up of material and waveguide dispersion, where both depend on the spectral width of the source [28]. Typical spectral widths are 40 nm for light emitting diodes (LEDs), 1-2 nm for multimode laser diodes and 0.0001 nm for single mode laser diodes. The effects of material dispersion worsen with increasing spectral width [37].

Material dispersion occurs because the refractive index varies with wavelength; hence different wavelengths propagate with different velocities through the fibre. All optical sources have a particular bandwidth in wavelength. A larger bandwidth implies more wavelengths. Therefore material dispersion will cause the optical pulses to spread out. The expression for the pulse width, σ_{mat}, for a source is given by

$$\sigma_{mat} = \sigma_{\lambda} L |D_{mat}(\lambda)| \tag{2.13}$$

whereσ_{λ} denotes the spectral width, L is the fibre length and $D_{mat}(\lambda)$ the material dispersion [37].

Waveguide dispersion occurs because not all of the light propagating down the fibre travels within the core. About 80 % of the light signal travels within the core region [37]. Both the electric and magnetic fields extend into the cladding region. Generally the light signal travels faster in the cladding than in the core because the cladding has a lower refractive index. Longer wavelengths extend further into the cladding than shorter wavelengths. The light signal experiences an average refractive index. Hence, because a smaller percentage of the shorter wavelengths travel in the cladding the refractive index experienced by the shorter wavelengths is higher than that experienced by the longer wavelengths. Therefore, the shorter wavelengths propagate slower than the longer wavelengths. Since the light signal consists of a band of wavelengths, the optical pulse will spread out.

Material and waveguide dispersion have opposite signs, so they counteract each other. The zero dispersion wavelength for conventional single mode fibre, for example G.652 fibre, is at 1310 nm. Thus at 1310 nm the material and waveguide dispersion cancel each other out. The units for chromatic dispersion are ps/km.nm, it describes the time delay per spectral width

fibre distance. Chromatic dispersion is managed by making use of dispersion compensating fibre (DCF). DCF has a much higher dispersion value than SMF. This allows for short lengths of DCF to compensate for SMF kilometres in length. DCF has a negative dispersion with a high dispersion coefficient. The negative dispersion cancels the positive dispersion of the SMF, thus compensating for the chromatic dispersion in the SMF. Fibre Bragg gratings are also used to compensate for chromatic dispersion. Another dispersion management fibre is inverse dispersion fibre (IDF). IDF has a negative and less steep dispersion slope as compared to DCF. IDF has the advantage over DCF of extending the network reach as it can be used to manage dispersion while extending the network reach.

2.4.3 Polarization mode dispersion

Polarization mode dispersion refers to a dispersion effect that arises because the fibre core is non-symmetric (with respect to geometry or the refractive index distribution) and this causes different polarizations of the signal to travel with different group velocities. A light signal is made up of two orthogonal polarizations. These modes experience birefringence, hence the ray paths of the two orthogonal modes exhibit different refractive indices. Polarization mode dispersion (PMD) is made up of birefringence and mode coupling. PMD can be modelled as a concatenation of birefringent sections where each section has its own fast and slow axis. The phenomenon of PMD has been well researched and documented. There exist several good review papers on PMD in the literature, [29, 31, 57].

Various mechanisms lead to birefringence in the fibre. Normally, the combination of these mechanisms and their extreme sensitivity to the environment causes the instability of the output SOP of the fibre. Enhancement of the birefringence leads to other beneficial properties such as maintaining the input state of polarization, for example PMF maintains the input SOP. In a birefringent fibre section the two orthogonal modes will propagate with different velocities because of the effective refractive indices each polarization component experiences. The birefringence is the difference between the effective refractive indices. Birefringence occurs whenever the circular symmetry of the fibre core is disrupted. This produces an anisotropic refractive index distribution in the fibre. Anisotropic distribution of the refractive index can be caused by either a geometric deformation of the fibre core or by a change in the elasto-optic, magneto-optic or electro-optic index [62]. Birefringence can be

introduced by the following mechanisms: noncircular core, asymmetrical lateral stress, bending, electric field, twist, magnetic field [62]. These mechanisms can be divided into two categories. The first two are internal to the fibre and are introduced during the manufacturing process. The last four occur as a result of some external stress on the fibre. The exception is asymmetrical lateral stress which has both internal and external triggers [62]. External is from any applied external mechanical pressure on the fibre. Internal causes refer to when the cladding is constrained by the fibre jacket. The induced birefringence for all of the above mechanisms is linear except for the last two where the induced birefringence is circular.

The principal states of polarization (PSPs) are defined as the states of polarization that remain invariant with frequency at the output over a small frequency change (to first order) for any input SOP that is aligned with the PSPs [56, 54].The principal state of polarization (PSP) that gives the faster group velocity is the fast PSP and the PSP that gives the slower group delay is the slow PSP. These PSPs are oriented orthogonal with respect to each other in the absence of polarization dependent loss (PDL) or polarization dependent gain (PDG) and nonlinear effects [56, 54]. A consequence of the PSP model suggests that the first-order effects of polarization dispersion arises from a differential time of flight between the two principal states [54].

When considering a long fibre link then mode coupling becomes an apparent phenomenon, hence the PMD in the fibre link is a result of birefringence and mode coupling. When the birefringence is not strong enough to maintain the SOP of the orthogonal polarization components then coupling will occur. Each birefringent section has an orthogonal axis; these axes differ from section to section. A portion of the energy of the fast mode will couple into the slow mode and visa versa.

In practical fibres a combination of birefringence mechanisms, both internal and external, will act on the fibre [62]. Their number, strength, distribution and orientation are all unknown, and they generally vary with time and temperature [62]. This implies that there will be random coupling throughout the fibre. Gisin presents a model that represents a fibre as a combination of birefringent fibre sections, with random mode coupling sections distributed along the fibre where the light may change velocity [25]. This model yields the probability density as

$$\frac{\partial^2 \rho_l(\tau)}{\partial l^2} = B^2 \frac{\partial^2 \rho_l(\tau)}{\partial \tau^2} - \frac{2}{h}\frac{\partial \rho_l(\tau)}{\partial l} \tag{2.14}$$

where ρ denotes the probability density function, τ the time of flight, z the distance and $B = 1/v\,(\Delta v/v)$ where v is the average velocity and Δv is the differential group velocity between fast and slow axes. Equation 2.14 is also known as the telegrapher's equation [25]. After finding the solutions of equation 2.14, the mean square deviation of the probability distribution function $\rho_l(\tau)$ gives the PMD as

$$\text{PMD}=\frac{Bh}{\sqrt{2}}\left(\frac{2L}{h}-1+e^{-2L/h}\right)^{1/2} \tag{2.15}$$

where h is the polarization mode mean coupling length and L the fibre length [25, 22, 26, 27]. Hence the PMD is the root mean square (RMS) width of the polarization mode time of flight distribution. Equation 2.15 has two limiting conditions, (a) L << h and (b) L >> h [25].

(a) Then the probability density function, $\rho_l(\tau)$, is flat and PMD $= BL$.

(b) Then $\rho_l(\tau)$has a Gaussian distribution and PMD $= B\sqrt{hL}$.

In (a) PMD increases linearly with length and in (b) PMD increases with the square root of length. In an independent study Poole found a similar result [55].

In weakly birefringent fibres with random mode coupling, it is found that that both the differential group delay (DGD) and PSPs are statistical variables [9]. When the PMD varies as a function of wavelength then it is known to be stochastic. This occurs because of the random mode coupling between the two PSPs. For a fibre much longer than the mode coupling length the probability density function (PDF) of the differential group delay (DGD) follows a Maxwellian distribution, [9, 16], given by

$$\text{PDF}(\Delta\tau)=\left(\sqrt{\frac{2}{\pi}}\right)\frac{\Delta\tau^2}{\sigma^3}e^{-\Delta\tau^2/2\sigma^2}. \tag{2.16}$$

The form of the probability density function is determined by the form of σ. The two cases are summarised in table 2.1.

Cases	$\boldsymbol{\sigma}$	**PDF**$(\Delta\tau)$	**PMD is equal to**
Quadratic mean value, $\langle\Delta\tau^2\rangle^{1/2}$	$\frac{\langle\Delta\tau^2\rangle^{1/2}}{\sqrt{3}}$	$3\left(\sqrt{\frac{6}{\pi}}\right)\frac{\Delta\tau^2}{\langle\Delta\tau^2\rangle^3}e^{-3\Delta\tau^2/2\langle\Delta\tau^2\rangle}$	RMS DGD,$\langle\Delta\tau^2\rangle^{1/2}$
Mean value, $\langle\Delta\tau\rangle$	$\left(\sqrt{\frac{\pi}{8}}\right)\langle\Delta\tau\rangle$	$\frac{32}{\pi^2}\frac{\Delta\tau^2}{\langle\Delta\tau\rangle^3}e^{-4\Delta\tau^2/\pi\langle\Delta\tau\rangle^2}$	Mean value of DGD,$\langle\Delta\tau\rangle$

Table 2.1 Equations for PMD found in reference [33].

In summary, this chapter discussed the nature of light. Key historical findings regarding optics were pointed out. Maxwell's equations were used to derive the standard wave equation, which was applied to highlight the conditions required to have guided modes in a waveguide. It is found that a number of guided modes may propagate along a waveguide depending on several conditions. The section thereafter, serves as a reminder to the polarization characteristics of light. This is followed by a section which covers different types of optical fibre and a description of their specification as well as their function in fibre optic links. It is pointed out that DSF is prone to nonlinear effects. This explains why DSF was the main fibre used in experiments to investigate cross phase modulation. The coming chapters (4, 5 and 6) present the experimental work where DSF was used. The chapter then goes on to discuss attenuation, chromatic dispersion (CD) and polarization mode dispersion (PMD) in optical fibres. The chapter that follows hereafter reviews nonlinear effects found in optical fibres.

CHAPTER 3

NONLINEAR EFFECTS IN OPTICAL FIBRE

Below a particular optical power threshold within an optical fibre, the loss and refractive index of the fibre are independent of the input signal power. Beyond this low power threshold the impact of nonlinear effects on the fibre network become notable. Nonlinear effects place limitations on high speed networks as well as optical wavelength division multiplexing (WDM) networks. This chapter discusses the theoretical background of various nonlinear effects which occur in optical fibre networks. Nonlinear effects in fibre can be subdivided into two categories. The first entails the interaction of light waves with phonons, this includes stimulated Brillouin and Raman scattering. The second deals with the dependence of the refractive index on the optical power, this includes four-wave mixing, self phase modulation and cross phase modulation.

3.1 Stimulated Brillouin scattering

It can be shown that the product of the launched power and effective length increase with amplifier spacing indicating that nonlinearities can be reduced by decreasing the amplifier spacing [61]. In this scenario each amplifier compensates for the power loss between amplifiers. This however increases the network cost as more amplifiers are required.

The process of stimulated Brillouin scattering (SBS) was first observed in 1964 [10]. SBS deals with acoustical phonons. A pump wave generates an acoustic wave through electrostriction. This acoustic wave in turn modulates the refractive index of the medium. The pump signal is then scattered by the pump induced index grating through Bragg diffraction. The frequency of the scattered light is downshifted because of the Doppler shift associated with the refractive index of the grating moving at the acoustic velocity [1]. SBS only occurs in the backward direction in optical fibres. The Brillouin shift is given by

$$\nu_B = \frac{2n\nu_A}{\lambda_p} \tag{3.1}$$

where a typical value for the refractive index (n) in silica is 1.45 and the acoustic velocity (v_A) in silica fibres is 5.96 km/s, yielding a Brillouin shift of 11.1 GHz for a pump wavelength (λ_p) at 1550 nm [1].

Nonlinear effects are challenging to model because nonlinear effects become more significant with increasing fibre length which is offset by the fact that the optical power is attenuated along the fibre. An effective approximation is to use the effective fibre length which takes into account power absorption along the fibre [37]. The effective length (L_{eff}) is defined as the length such that

$$L_{eff}P_0 = \int_0^L P(z)dz. \tag{3.2}$$

P_0 is the initial power and L the total length of the fibre. It is assumed that the optical power decays exponentially along the fibre length, hence the effective length is given by

$$L_{eff} = \frac{1}{P_0}\int_0^L P(z)dz = \frac{1}{P_0}\int_0^L P_0 e^{-\alpha z}dz = \frac{1-e^{-\alpha L}}{\alpha}, \tag{3.3}$$

where α is the fibre attenuation [37]. The threshold power is defined as the measured power at which the nonlinearity becomes significant. The approximation of the threshold power for Brillouin scattering is given by

$$P_{th} \approx \frac{21bA_e}{g_B L_e}, \tag{3.4}$$

found in [64], where the value of b ranges between 1 and 2 depending on the relative orientation between the pump and Stokes wave, A_e is the effective area, g_B is the Brillouin gain coefficient and L_e is the fibre effective length. Assuming the worst case, b is 1 and using typical values found in fibre the effective area and length take on the values 50 μm^2 and 20 km. The Brillouin gain coefficient is approximately equal to 5 x 10^{-11} m/Watt [1]. Hence according to equation 3.1 the Brillouin threshold for typical fibre parameters is 1 mW. It can be inferred from equation 3.1 that the threshold power for the case of Brillouin scattering increases with the core effective area of the fibre. Equation 3.4 assumes that the pump wave is narrow band and that its spectral width falls within the 20 MHz spectral width of

stimulated Brillouin scattering (SBS). The threshold power for Brillouin scattering is two orders of magnitude lower than the threshold power for stimulated Raman scattering.
An approximate expression of the threshold power which accounts for the spectral width of the source is given by [61]

$$P_{th} \approx \frac{21bA_e}{g_B L_e}\left(1 + \frac{\Delta f_{source}}{\Delta f_B}\right) \tag{3.5}$$

where Δf_{source} is the spectral width of the source. For a source with a spectral width of 200 MHz, equation 3.2 gives the threshold power to be 12 mW. Hence broader spectral sources increase the spectral power considerably. Several means to mitigate the SBS penalty are: to reduce the power per channel, to directly modulate a laser source which will generate chirp causing spectral broadening, to dither the frequency of the laser and to apply phase modulation which will lower the power of the carrier [61].

3.2 Stimulated Raman scattering

Stimulated Raman scattering (SRS) refers to the transfer of power from lower wavelengths to higher wavelengths. The energy of a photon is given by hc/λ where h is Plancks's constant. Photons of lower wavelengths have higher energy than photons of higher wavelengths. Hence SRS may be viewed as photons of higher energy prompting the emission of photons of lower energy. SRS has a broader gain spectrum than SBS and a much lower peak gain coefficient than SBS.
Spontaneous Raman scattering can cause the transfer of a small fraction of optical energy from one optical field to another in a molecular medium. The spontaneous Raman scattering effect was discovered by Raman in 1928 [59, 60]. The frequency of the boosted optical field is determined by the vibrational modes of the medium. Unlike SBS, SRS can occur in both the forward and backward directions; hence forward, backward and bidirectional pumping are all possible with SRS. SRS was first observed in 1972 [67] when fibre losses became low enough to make this effect measurable.
When a pump signal propagates through a medium such as silicon, the pump photon, v_p, excites the molecules of the medium to a higher virtual energy level as shown in figure 3.1.

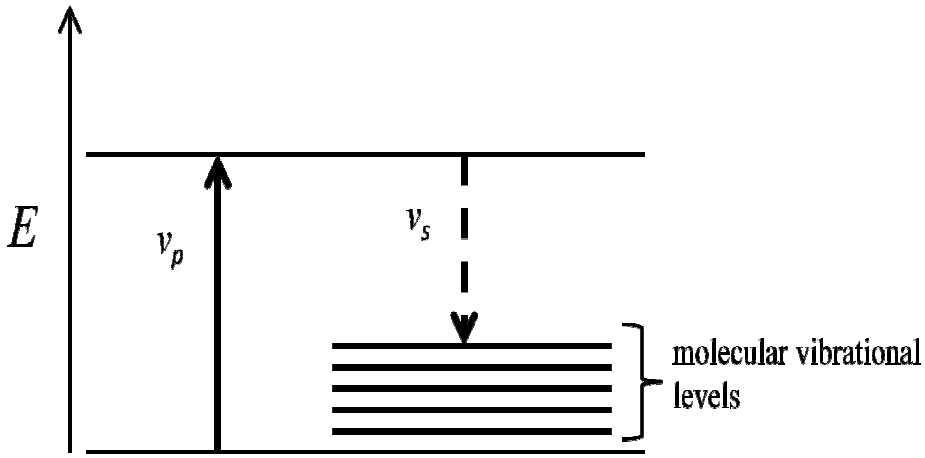

Figure 3.1 Illustration of the stimulated Raman scattering effect.

The molecule then decays to a lower energy level emitting a signal photon, v_s, in the process. The energy difference between the pump and signal photons is dissipated by the vibrational modes of the medium [30]. These vibrational levels determine the frequency shift of the signal as well as the shape of the Raman gain curve. The amorphous nature of silica ensures a broad Raman gain curve. The peak of this Raman gain is 13.2 THz away for a pump wavelength of 1550 nm in silica fibres. This shift is known as the Stokes shift, as the shift is towards higher wavelengths (lower energies) than the pump wavelength.

Different types of optical fibres have different gain curves. For example the Raman gain curve of single mode fibre, dispersion shifted fibre and dispersion compensating fibre have the same width, however dispersion compensating fibre has a much higher peak gain than the other two fibre types. DCF has a much higher Raman gain coefficient. The order for the Raman gain efficient in fibres from highest to lowest is; DCF, DSF and SMF. If another wavelength is placed 13.2 THz, 100 nm in wavelength, away from a pump wavelength at 1550 nm Raman amplification occurs. Raman amplification has several advantages [30]. It can occur over a broad wavelength range just over a 100 nm, hence any wavelength slightly greater than the pump wavelength and falling within this range may be amplified. Raman amplification can occur in any optical silica fibre. SRS has a fast response time in the order of femtoseconds [68].

Figure 3.2 illustrates the general pumping configuration used for Raman amplification.

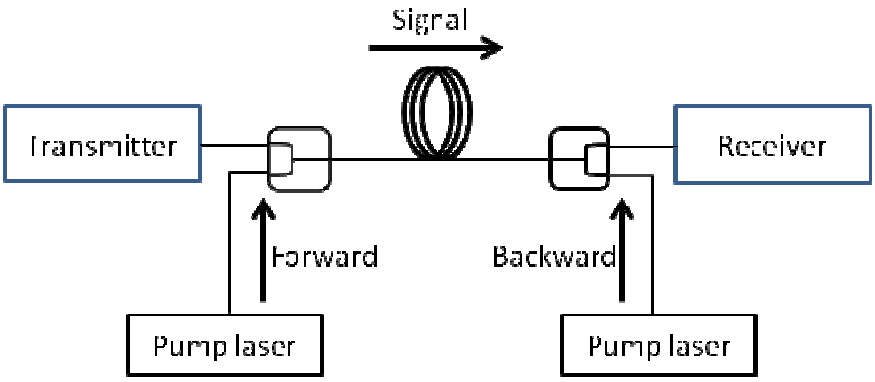

Figure 3.2 Co- and counter-propagating Raman pump scheme.

Forward or co-propagating pumping refers to the scenario when the pump and signal being amplified propagate in the same direction. Backward or counter-propagating pumping refers to when the signal to be amplified and the pump laser are at opposite ends of the fibre link. Raman amplification can either be discreet or distributed. Discreet Raman amplification occurs when the fibre through which amplification takes place is located in a box near the transmitter or receiver. Distributed Raman amplification takes place when the fibre through which amplification occurs also forms part of the network; hence the amplification is distributed over a particular distance.

The interaction of the pump and signal waves along the fibre for the case of continuous waves may be described by the propagation equations as follows [30]:

$$\frac{dP_s}{dz} = g_R P_p P_s - \alpha_s P_s \tag{3.6}$$

and

$$\pm \frac{dP_p}{dz} = -\frac{\omega_p}{\omega_s} g_R P_p P_s - \alpha_p P_p. \tag{3.7}$$

where P_p and P_s refers to the pump and signal waves, g_R ($W^{-1}m^{-1}$) is the Raman gain coefficient, ω_s and ω_p are the signal and pump angular frequencies, and α_s and α_p are the attenuation coefficients of the signal and pump wavelength. The ± in equation 3.7 represents the case for co- and counter-propagating Raman. The threshold or critical power for Raman amplification may be derived by solving equation 3.7 for the case of an un-depleted pump, and substituting the solution into equation 3.6 [1]. The critical threshold power is derived in [1] and takes the form

$$P_{th} = \frac{16A_{eff}}{g_R L_{eff}}. \quad (3.8)$$

Using an effective length of 20 km for standard single mode fibres, an effective area of 50 μm^2 and a pump wavelength of 1550 nm, equation 3.8 gives the Raman threshold power as 600 mW or 27.8 dBm. Beyond this threshold, power is rapidly transferred from the pump wavelength to the signal wavelength.

Additionally, Raman amplification shows an improved noise figure. Generally, when an optical signal is amplified in fibre some noise is added onto the signal. Discrete amplifiers have a worse performance since signals with low power require more gain from the amplifier which in turn leads to more amplified spontaneous emission (ASE) generated in the amplifier as well as amplification of the ASE. Distributed amplifiers are exempted from this problem as the power level delivered to each amplifier remains high hence less gain is required. Therefore, distributed amplifiers show an increased performance to discrete amplifiers in this regard. Raman distributed amplifiers, where the fibre acts as the transmission span that links two points, have the same advantage as the gain is evenly distributed along the fibre length resulting in an improved performance.

In wavelength division multiplexing (WDM) systems, it is important that all the channels have the same optical power after passing through the amplifier. Gain flatness is defined as the difference in signal power after the signals have passed through the amplifier. It is possible to flatten the spectral profile by using multiple pump lasers of different wavelengths. This technique is complicated by interpump Raman amplification, where the power is transferred from the lower pump wavelengths to the longer pump wavelengths resulting in a slanted gain spectrum for the signal wavelengths. Numerical simulations can be used to determine the required wavelength and power of the pump waves.

Several limiting factors arise in Raman amplification such as multipath interference, pump noise transfer and noise figure tilt. For further reading, please see [30].

Recently, polarization attraction has received considerable attention as an alternative means of repolarising the optical signal. Nonlinear polarization pulling refers to using nonlinear effects to control the SOP of a signal. Nonlinear effects such as Brillouin amplification [70, 77], counter-propagating four-wave mixing [52, 53], cross phase modulation and Raman amplification [21, 44, 71] have all been used for the purpose of polarization pulling. Making use of nonlinear effects for polarization pulling has the advantage of not depreciating the input signal as is the case with inline polarizers. For the case of Brillouin scattering,

polarization pulling is made possible because of the strong polarization dependence of SBS [70]. SRS features a strong dependence on polarization as well.

In [77], researchers looked at the polarization evolution of the pump and signal for the case of co-propagating Raman amplification. It is shown that pump depletion plays a key role in the efficiency of Raman polarization pulling [77]. The model used in [77] accounted for pump depletion as well as for nonlinear polarization rotation (NPR) due to self- and cross-phase modulation. Simulation results show that pump depletion degrades the signal DOP only slightly, because pulling effectively takes place before the pump is completely depleted [77]. However at high pump power in the presence of pump depletion, NPR dominates and disrupts the pulling process. The output SOP of the signal after Raman polarization pulling is not predictable for the case of co-propagating Raman amplification [77].

Polarization pulling by Raman amplification is made possible by the great polarization dependence of SRS [44]. Additionally, Raman amplification has a large gain bandwidth, over 5 THz, making it very suitable for optical communications. Raman polarization attraction exploits the fact that for parallel pump and signal SOP orientation the signal has a much higher gain than when the pump and signal SOPs are orthogonal. Polarization pulling by Raman amplification offers the advantage of polarization pulling with amplification. From a vectorial point of view of the pump signal and birefringence, the signal rotates around the birefringence vector. Since birefringence is stochastic along the fibre length, this results in randomization of the signal SOP [44], thus preventing effective pulling when the birefringence is large. Conversely, when the signal and pump vectors are orthogonal, polarization pulling is not effective, hence a certain amount of birefringence is required to break the orthogonality between the pump and signal vectors [44]. From [44], the rate of the local rotation due to birefringence is about 30 times more for counter-propagating Raman than for co-propagating Raman. This implies that a much higher pump power is required for counter- than for co-propagating Raman in order to overcome the effects of fibre birefringence.

Martinelli et al. (2009) has shown an experimental demonstration of co-propagating Raman polarization attraction. In [21], experimental results show the stabilization of any input polarization into a single polarization state. Numerical and experimental results show the interplay between pump power, fibre PMD and fibre length to achieve the best pulling efficiency [21]. Numerical results show in particular that the higher the pump power, the shorter the fibre length should be. At very high pump powers and long fibre lengths the signal is amplified such that the signal starts to altar the pump SOP, hence disturbing the pulling

effect. Simulation results also show that pulling improves with an increase in fibre length, however beyond a critical length pulling worsens with increased fibre length. As mentioned previously for high pump powers, very long fibre lengths lead to high amplification of the signal which in turn modifies the pump SOP. Long fibre lengths also lead to the signal being attenuated to such an extent that the Raman gain is not enough to counteract birefringence SOP randomization. Regarding PMD, low pump power combined with SOP randomization caused by fibre birefringence will prevent Raman pulling from taking place effectively. Hence low PMD fibres improve pulling. Experimental results show that by choosing the optimum fibre length, pump power and low PMD fibres, efficient polarization pulling can be achieved [21].

A realistic model describing backward pump Raman amplification is presented in [23]. The model in [23] makes use of the equations found in [42] describing the evolution of the pump and signal SOPs:

$$\xi \frac{d\bar{P}}{dz} = -\alpha_p \bar{P} - \frac{g\omega_p}{2\omega_s}[(1+3\mu)S_0\bar{P} + (1+\mu)P_0\bar{S} - 2\mu P_0\bar{S_3}] + \left(\omega_p\bar{\beta} + \overline{W_p}\right) \times \bar{P} \qquad 3.9\ (a)$$

and

$$\frac{d\bar{S}}{dz} = -\alpha_s \bar{S} + \frac{g}{2}[(1+3\mu)P_0\bar{S} + (1+\mu)S_0\bar{P} - 2\mu S_0\bar{P_3}] + \left(\omega_s\bar{\beta} + \overline{W_s}\right) \times \bar{S} \qquad 3.9\ (b)$$

where ξ may take on the value of +1 or -1 depending on whether the Raman scheme is forward or backward Raman pumping. The coefficient $\mu = 0.0118$ is the ratio between orthogonal and parallel silica Raman gain coefficients. The vectors $\overline{W_p}$ and $\overline{W_s}$ account for the nonlinear polarization rotation due to self phase modulation and cross phase modulation. The pump and signal angular frequencies are represented by ω_p and ω_s, while g is the Raman gain co-efficient. The fibre linear birefringence vector is represented by $\bar{\beta}$. Using equations 3.9 (a) and 3.9 (b) the model in [23] looks into the effects of linear and nonlinear birefringence on Raman gain.

In [11], researchers show simulation results for counter-propagating Raman polarization pulling. Although co-propagating Raman pulling is very efficient with respect to Raman pulling, counter-propagating Raman has the advantage that the output signal SOP is determined by the pump input SOP [11]. The simulation results show that PMD leads to SOP scattering making polarization attraction less efficient for high PMD, hence there is a

compromise between PMD, fibre length and signal gain. It is found that pump depletion aids polarization pulling in counter-propagating Raman for high PMD values, whereas depletion hampers pulling for co-propagating Raman [11]. The signal output DOP is finally plotted as a function of the mean gain [11], hence providing the expected signal DOP for a given mean gain.

3.3 Four-wave mixing

The Kerr nonlinearity does not only produce phase shifts within a channel but also leads to the generation of new frequencies. This effect is known as four-wave mixing (FWM). FMW is a third-order nonlinearity in silica fibres [37]. FWM is bit rate independent but depends heavily on the channel spacing and fibre chromatic dispersion [61]. Decreasing the channel spacing enhances the FWM effect, so does decreasing the chromatic dispersion.
When three signals v_i, v_j and v_k propagate through a fibre near the zero dispersion point, these signals will mix to produce a fourth product v_{ijk} given by

$$v_{ijk} = v_i + v_j - v_k \text{ with } i, j \neq k. \tag{3.10}$$

This new frequency product may cause crosstalk when its frequency spacing between the original frequencies is small. As an example, two frequencies v_1 and v_2 will mix to generate sidebands at $2v_1 - v_2$ and $2v_2 - v_1$. Three waves propagating may generate nine optical sidebands. In general for N wavelengths propagating through a fibre, the number of optical sidebands M is determined by the expression (found in [37])

$$M = \frac{N^2}{2}(N - 1). \tag{3.11}$$

While propagating alongside the original signal waves, these sidebands will grow in strength at the expense of signal strength depletion.

3.4 Self phase modulation

Self phase modulation (SPM) is a result of the refractive index, known as the nonlinear refractive index, having an intensity dependent component. The Kerr nonlinearity describes the process where the refractive index depends on the intensity of the optical signal within the medium [1]. This gives rise to the expression

$$n = n(\lambda) + \left(\frac{n_2}{A_{eff}}\right) P \tag{3.12}$$

where n_2 is the nonlinear Kerr coefficient, A_{eff} the effective mode area and P the optical power of the signal.

The nonlinear refractive index induces a phase shift which is proportional to the intensity of the pulse. Hence, since a pulse has an intensity profile, different parts of the pulse undergo different phase shifts [61]. This gives rise to pulse chirp which together with chromatic dispersion leads to pulse broadening.

Consider a Gaussian pulse which varies in intensity with time as shown in figure 3.3. The time axis is normalized to t_0.

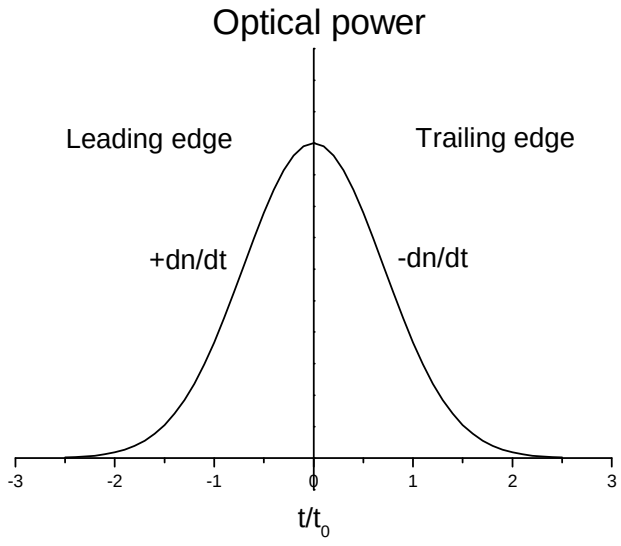

Figure 3.3 Gaussian optical pulse at the input of the fibre.

The front edge of the pulse rises rapidly to a maximum and the trailing edge of the pulse decreases to zero. According to the Kerr nonlinearity the refractive index (n) in silica fibre is

intensity dependent, therefore since the pulse intensity varies with time, the refractive index also varies over time [37]. In figure 3.3 the derivative of n with respect to time, dn/dt, is positive and the trailing edge has a negative dn/dt.

The temporal refractive index change leads to a temporal phase change, dΦ/dt. Therefore, since the phase change is intensity-dependent, different parts of the pulse experience different phase changes. This leads to frequency chirping where the frequencies of the leading edge of the pulse shift to higher frequencies (referred to as red shift), and the frequencies of the trailing edge shift to lower frequencies (referred to as blue shift) as illustrated in figure 3.4 [37].

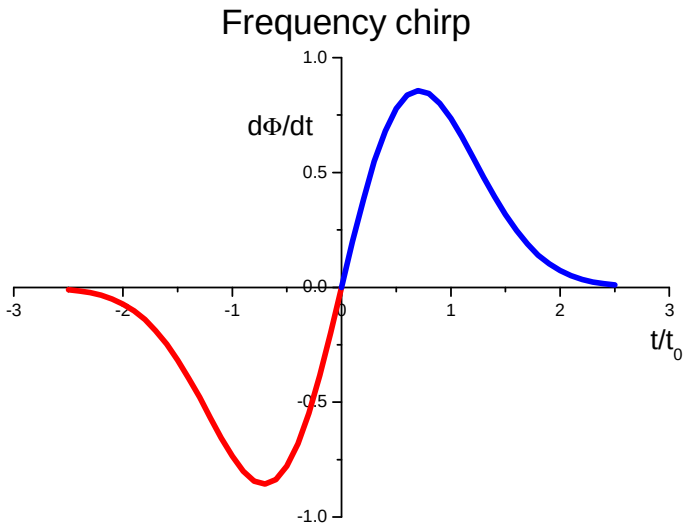

Figure 3.4 Schematic of temporal varying phase change of Gaussian pulse.

Self phase modulation is more prominent for higher intensity pulses as the degree of chirping is proportional to the transmitted power. For the case when chromatic dispersion is negative, SPM causes pulse broadening. This occurs because for negative chromatic dispersion, the red-shifted leading edge travels faster and the blue-shift trailing edge travels slower. Hence the frequency chirping worsens the pulse broadening effects by dispersion. However for positive chromatic dispersion the red shifted leading edge travels slower and the blue shifted trailing edge travels faster, hence in this case SPM compensates for chromatic dispersion.

3.5 Cross phase modulation

Wavelength division multiplexing (WDM) systems are made up of several signals; hence the intensity of the overall signal is much higher than a single signal propagating through the fibre on its own. Therefore, nonlinear effects are enhanced by the higher intensity due to the multiple signals travelling down the fibre. The intensity dependent phase shift and consequent chirping by self phase modulation is thus enhanced. This is referred to as cross-phase modulation. Cross- phase modulation (XPM) worsens the effects of SPM.

The principle behind XPM is that the effective refractive index that an optical beam experiences in an optical fibre does not only depend on the intensity of that beam but also on the intensity of the co-propagating beams. The nonlinear contribution to the refractive index can be seen directly by writing the simplified expression for the nonlinear polarization (P_{NL}) as a function of the carrier frequency, derivation shown in [1],

$$P_{NL}(\omega_j) = \varepsilon_0 \varepsilon_j^{NL} E_j, \tag{3.13}$$

where ω_j is the carrier frequency, E_1,E_2 are the corresponding amplitudes of the electric field of the two pulses and j = 1 or 2. It is assumed that phase matching does not occur. When combining it with the linear part, the total induced polarization is

$$P(\omega_j) = \varepsilon_0 \varepsilon_j E_j, \tag{3.14}$$

where

$$\varepsilon_j = \varepsilon_j^L + \varepsilon_j^{NL} = \left(n_j^L + \Delta n_j\right)^2. \tag{3.15}$$

The linear and nonlinear dielectric constants are represented by $\varepsilon_j^L$and ε_j^{NL}. The linear part of the refractive index is given by n_j^L and the refractive index change due to third order non-linear effects is Δn_j. Making the approximation $\Delta n_j << n_j^L$ allows the refractive index change to be expressed as

$$\Delta n_j \approx {\varepsilon_j^{NL}}\Big/{2n_j} \approx n_2 \left(\left|E_j\right|^2 + 2\left|E_{3-j}\right|^2\right) \tag{3.16}$$

where n_2 is the nonlinear index coefficient. Equation 3.16 shows that the refractive index seen by an optical field does not only depend on the intensity of that signal but also on the intensity of co-propagating fields. As the optical field propagates down the optical fibre, the intensity dependent phase fluctuations can be expressed as

$$\Phi_j^{NL}(z) = (\omega_j/c)\Delta n_j z = n_2(\omega_j/c)\left(\left|E_j\right|^2 + 2\left|E_{3-j}\right|^2\right)z \tag{3.17}$$

where Φ_j^{NL} represents the nonlinear phase and j =(1 , 2). The first term in equation 3.17 represents SPM. By substituting j with the values 1 or 2 it is evident that phase modulation of one optical wave is caused by the co-propagating wave. This phenomenon is known as cross-phase modulation (XPM). Further, the factor 2 on the right hand side of equation 3.17 (in front of the term for XPM) shows that XPM is twice as effective as SPM [1].

In 1984, the first experimental results of XPM in fibre was demonstrated in [14]. Laser light from two injection locked lasers were multiplexed, transmitted over a 15 km single mode fibre link (SMF) and the nonlinear phase effects measured using an interferometer [14]. An optical field can be characterised by its electric field which can be expressed as

$$E(z,t) = Ee^{i(\omega t - \beta z)} \tag{3.18}$$

where ω is the angular optical frequency and β is the propagation constant of the wave. When the two waves propagate together down the fibre each wave will affect the propagation constant of the other because of the nonlinear refractive index. Therefore, the propagation constant of wave 1 will be changed by the intensity of wave 2, hence wave 1 will experience a phase shift $\Delta\Phi_1$, in radians, of

$$\Delta\Phi_1 = \frac{2\times10^5\pi\omega_2 n_2 L_e P_2}{3nc^2 A_e}. \tag{3.19}$$

The parameters in 3.19 are defined as follows: n is the linear refractive index, n_2 is the intensity dependent nonlinear part of the refractive index, c is the speed of light in a vacuum, L_e is the effective length , A_e is the effective core area and P_2 is the power of channel 2 (measured in milliwatts). Expression 3.19 is derived in [14], it shows that the phase change in wave 1 is directly dependent on the power change of wave 2, P_2. In [14], researchers used a

novel interferometric setup to measure the intensity dependent phase change of one channel while the power of the co-propagating channel was changed. It was found that a 1 mW power change in the one channel leads to a 1.4^{o} phase change in the other channel.

Researchers have found that soliton-soliton collisions alter the polarization states of the colliding solitons [47]. In [47], researchers show that the change in polarization of solitons when colliding them in a WDM system is given by the cross product of the Stokes vectors. It was found that nonlinear channel depolarization was induced by XPM in long-haul soliton systems [47]. The optical field in a fibre may be described by the following expression:

$$\bar{E} = \begin{pmatrix} E_x \\ E_y \end{pmatrix}, \qquad \overline{E^{\dagger}} = \left(E_x^*, E_y^*\right). \tag{3.20}$$

Here, the optical field is a two dimensional complex vector, where $\overline{E^{\dagger}}$ is the conjugate transpose of the row vector. The x and y components are normalized so that the optical power in the fibre is given by

$$\left(\overline{E^{\dagger}}\bar{E}\right) = \left(|E_x|^2 + \left|E_y\right|^2\right). \tag{3.21}$$

A simple version of the Manakov equation from [43] is written as

$$-i\frac{\partial \bar{E}}{\partial z} = \frac{1}{2}\frac{\partial^2 \bar{E}}{\partial t^2} + \left(\overline{E^{\dagger}}\bar{E}\right)\bar{E}. \tag{3.22}$$

Here, polarization dispersion of the two pulses is neglected and the nonlinear term is averaged over all polarizations, while z and t denote the distance and time, respectively. If $\bar{E}$ is made up of two fields with distinct frequencies a and b, the terms of each frequency may be isolated, [47], and the equation for $\overline{E_a}$ written as

$$-i\frac{\partial \overline{E_a}}{\partial z} = \frac{1}{2}\frac{\partial^2 \overline{E_a}}{\partial t^2} + \left(\overline{E_a^{\dagger}E_a}\right)\overline{E_a} + \left(\overline{E_b^{\dagger}E_b}\right)\overline{E_a} + \left(\overline{E_b^{\dagger}E_a}\right)\overline{E_b}. \tag{3.23}$$

The equation for $\overline{E_b}$ is obtained by interchanging the indices. When looking at equation 3.23, there are three nonlinear terms on the right-hand side. The first of these three terms relates to self phase modulation and the last two terms describe cross phase modulation [47].Only the

last term related to XPM produce nonlinear polarization state evolution. When the two fields are co-polarized, the second and third terms become the same and when the fields are orthogonally polarized, the third term becomes zero [47]. The Stokes vector of the field with its three real components may be expressed as

$$S_i = \overline{E^{\dagger}}\sigma_i\bar{E}, \qquad \text{(i=1, 2, 3)} \tag{3.24}$$

whereσ_i represents the three Pauli matrices. As explained in [47] by expanding equation 3.23 into its field components it can be shown that as a result of XPM the Stokes vector of field a is modified as follows:

$$\frac{\partial\overline{S_a}}{\partial z} = \overline{S_a} \times \overline{S_b}. \tag{3.25}$$

Equation 3.25 shows that the Stokes vectors of the two fields precess around each other as a result of the nonlinear effect [47].

It is well known that polarization dependent loss (PDL) and polarization mode dispersion (PMD) perturb the polarization states of optical channels. Researchers have shown that nonlinear polarization rotation can also adversely affect the performance of polarization sensitive receivers. In [15], equation 3.23 is rewritten to include the nonlinear co-efficient γ. From the equation in [15] the expression for the nonlinear polarization state evolution is the cross product between the Stokes vectors of the two fields, similar to equation 3.25. Assuming that both fields have the same power, P_0, the vector average of $\overline{S_a}$ and $\overline{S_b}$ becomes $\bar{S_0} = 1/2 * (\overline{S_a} + \overline{S_b})$, hence the evolution is written as

$$\frac{\partial\overline{S_a}}{\partial z} = \gamma P_0(\overline{S_a} \times \overline{S_b}) = 2\gamma P_0(\overline{S_a} \times \bar{S_0}) \tag{3.26 (a)}$$

and

$$\frac{\partial\overline{S_b}}{\partial z} = \gamma P_0(\overline{S_b} \times \overline{S_a}) = 2\gamma P_0(\overline{S_b} \times \bar{S_0}). \tag{3.26 (b)}$$

Equation 3.26 indicates that the Stokes vectors of both fields precess with the same rate about the stationary vector $\bar{S_0}$ [15]. Additionally, equations 3.26 (a) and (b) also indicate that no polarization evolution takes place between co-polarized and orthogonally polarized signals.

The experimental makeup, found in [15], consists of two wavelengths (in the 1550 nm range) multiplexed and transmitted through 22.7 km of SMF. One channel is filtered through a 0.25 nm tuneable filter and monitored with a polarization analyser while changing the launched power. Experimental results of this nonlinear polarization evolution are given in [15] where it is shown that both vectors rotate around a constant pivot as predicted by equation 3.26 (a) and (b).

Collings and Boivin further show that nonlinear polarization evolution caused by XPM produce time dependent polarization state changes on the time scale of the bit rate [15].In this experiment, five 10 Gbps signals with a channel spacing of 50 GHz are transmitted through 360 km of SMF [15]. Dispersion compensating fibre (DCF) was used to eliminate the CD. A tuneable filter, fibre polarization controller (FPC) and a polarizer were placed at the fibre output in front of the receiver. The results show that the intensity per bit varied along the pattern. The magnitude of this variation is dependent on the polarization controller setting, suggesting that the nonlinear evolution as a result of XPM occurs on the scale of the bit period [15]. Further, the magnitude of this effect is power dependent. In summary, these polarization fluctuations are converted into amplitude fluctuations by polarization sensitive receivers; these fluctuations occur at the bit rate and increase in magnitude with an increase in power.

Before discussing the degree of polarization (DOP) degradation in a WDM system, this section briefly looks at the walk-off parameter related to chromatic dispersion (CD). In [1] parameters β_1 and β_2 are defined as follows

$$\beta_1 = \frac{1}{v_g} = \frac{n_g}{c} = \frac{1}{c}\left(n + \omega\frac{dn}{d\omega}\right) \qquad 3.27\ (a)$$

and

$$\beta_2 = \frac{1}{c}\left(2\frac{dn}{d\omega} + \omega\frac{d^2n}{d\omega^2}\right) \qquad 3.27\ (b)$$

where v_g represents the group velocity of an optical pulse and n_g the group refractive index. The derivative of β_1 is β_2 which is the dispersion of the group velocity and is responsible for pulse broadening [1]. From equation 3.27 (a), $\beta_1$is defined as the time the optical pulse takes to cover a unit distance. Chromatic dispersion (CD) causes different wavelengths to propagate with different velocities through the fibre because of the difference in their group

velocities. This leads to a walk-off effect which plays an important role in nonlinear phenomena involving closely spaced optical pulses. The walk-off is expressed as

$$d_{sp} = \beta_1(\lambda_1) - \beta_1(\lambda_2), \tag{3.28}$$

which is the difference between the β_1 parameter of each central wavelength of two optical pulses [1]. The walk-off indicates the rate at which the faster wave will move away from the slower wave.

Cross-phase modulation can lead to degree of polarization (DOP) degradation in a WDM system which multiplexes several channels into one link [72]. In [72] researchers derive and propose a Carousel model for a two channel WDM system where the signals are on-off key (OOK) modulated. The Manakov propagation equation for two polarized OOK-modulated pump and probe signals with wavelengths λ_s (probe wavelength) and λ_p (pump wavelength) in the Jones domain is as follows [72]:

$$\frac{\partial \bar{S}(z,t)}{\partial z} - j\frac{\beta_{2s}}{2}\frac{\partial \overline{S^2}(z,t)}{\partial t^2} + j\frac{8}{9}\gamma e^{-\alpha z}\left[s_0\sigma_0 + \frac{3}{2}p_0\sigma_0 + \frac{1}{2}\bar{p}\cdot\bar{\sigma}\right]\bar{S}(z,t) = 0 \qquad 3.29\ (a)$$

and

$$\frac{\partial \bar{P}(z,t)}{\partial z} + d_{sp}\frac{\partial \bar{P}(z,t)}{\partial t} - j\frac{\beta_{2s}}{2}\frac{\partial \overline{P^2}(z,t)}{\partial t^2} + j\frac{8}{9}\gamma e^{-\alpha z}\left[p_0\sigma_0 + \frac{3}{2}s_0\sigma_0 + \frac{1}{2}\bar{s}\cdot\bar{\sigma}\right]\bar{P}(z,t) = 0. \quad 3.29\ (b)$$

Here, $\bar{P}(z,t)$ and $\bar{S}(z,t)$ are the complex envelopes of the pump and probe, $d_{sp} \approx D_c(\lambda_s - \lambda_p)$ is the walk-off parameter, the tensor $\bar{\sigma} = (\sigma_1, \sigma_2, \sigma_3)$ is the Pauli spin vector, $\bar{p}(z,t) = (p_1, p_2, p_3)$ is the pump stokes vector and p_0 is the pump intensity. The group velocity dispersion (GVD) coefficients of the pump and probe wavelengths is given by β_{2p} and β_{2s} respectively. Assuming that the GVD terms are equal to zero, the equivalent of equations 3.29 (a) and 3.29 (b) in Stokes space is:

$$\frac{\partial \bar{s}(z,t)}{\partial z} = \frac{8}{9}\gamma e^{-\alpha z}\left(\bar{p}\left(z, t - d_{sp}z\right) \times \bar{s}(z,t)\right) \qquad 3.30\ (a)$$

and

$$\frac{\partial \bar{p}(z,t-d_{sp}z)}{\partial z} = \frac{8}{9}\gamma e^{-\alpha z}\left(\bar{s}(z,t) \times \bar{p}\left(z, t - d_{sp}z\right)\right). \qquad 3.30\ (b)$$

When both the probe and pump are continuous waves then the Stokes vectors of the probe and pump rotate around a pivot $\bar{m} = \bar{s}(z) + \bar{p}(z)$, as is known from [15] and [6]. The expression of the rotation angle for this special case is

$$\Psi(z) = \frac{8}{9}\gamma P_m \int_0^z e^{-\alpha z'} dz' = \frac{8}{9}\gamma P_m L_{eff}(z). \tag{3.31}$$

Equation 3.31 shows that the rotation angle is independent of the wavelength spacing between the two channels. Hence, two continuous wave (CW) channels will continue to undergo rotation no matter how far they are apart in wavelength. Further, the CW model suggests that the WDM channels do not depolarize [72]. The CW model does not account for depolarization due to channel modulation and finite walk-off [72].

Bononi *et al.* presents a Carousel model in [72] which takes finite walk-off and an intensity modulated pump signal into account [72]. Assume a pump and probe wave are multiplexed and transmitted over a piece of fibre. The "carousel" of the two Stokes vectors starts rotating around a common pivot $\bar{m} = \bar{s} + \bar{p} = P_m \bar{m}$ when both the pump and probe are switched on. As soon as the pump is switch off, the carousel stops rotating around the pivot. The expression for the rotation angle for this case becomes:

$$\Psi(z,t) = \frac{8}{9}\gamma P_m \int_0^z e^{-\alpha z'} p\left(t - d_{sp} z'\right) dz'. \tag{3.32}$$

In this case, the rotation angle depends on the pump OOK modulated bits that have walked past the probe signal at distance z.

According to the carousel model, the probe depolarization occurs because of the time varying rotation angle around an average angle $\langle \Psi(\mathrm{z,t}) \rangle = (1/2)(8/9)\gamma P_m L_{eff}(z) = (1/2)\Psi(\mathrm{z})$. At the output of the fibre, $z = L$, the probe swings around the pivot with a rotation angle that swings in time around an average value $\langle \Psi(\mathrm{L,t}) \rangle$ by an amount $\Delta\Psi(\mathrm{L,t}) = \Psi(\mathrm{L,t}) - \langle \Psi(\mathrm{L,t}) \rangle$. A general expression for the DOP is derived in [72] and has the form:

$$\mathrm{DOP} = \sqrt{1 - \sin^2 \theta_s (1 - \langle \cos \Delta\Psi(t) \rangle^2 - \langle \sin \Delta\Psi(t) \rangle^2)}, \tag{3.33}$$

where θ_s is the angle between the probe and pivot. For a periodic modulated pump and a random pump bit sequence (RBS) the DOP simplifies to, [72],

$$\text{DOP} = \sqrt{1 - \sin^2 \theta_s \{1 - \langle \cos \Delta\Psi(t) \rangle^2\}}. \quad (3.34)$$

Equations 3.33 and 3.34 show that the larger the swing angle $\Delta\Psi$ the lower the DOP value. Further, when the Stokes vectors of the probe and pump are aligned (θ_s = 0) or are anti-parallel (θ_s = 180^o), then sin(θ_s) = 0 so the DOP equates to 1 [72].

Nonlinear effects have the potential to be detrimental to optical networks. It is important to take into consideration the threshold power of each nonlinear effect. On the other hand the above literature review also points out that nonlinear effects may be useful to optical networks as well. Potential uses include amplification of optical signals, to create wavelength converters and for nonlinear polarization pulling. Hence it becomes imperative to understand the characteristics and nature of nonlinear effects. The theory on XPM has showed the effect that a change in power and a change in the SOP of a co-propagating pump signal has on a neighbouring probe signal. The Carousel model describes the relation between the rotation angle and the degree of polarization. The experimental results to come in chapter 4 show the effect that a change in SOP of a pump signal has on a probe signal. Chapter 5 investigates the DOP degradation predicted by the Carousel model.

CHAPTER 4

CROSS PHASE MODULATION ROTATION

When two optical waves of different wavelength propagate down an optical fibre they may be coupled through cross phase modulation (XPM) by the fibre nonlinearity. In the case of XPM no energy transfer occurs between the two optical fields. This chapter focuses on the remote control characteristic of XPM, showcasing that the effective refractive index seen by an optical beam is not solely dependent on its intensity but also on the intensity of a co-propagating beam. Various experimental procedures were developed to demonstrate the effect of XPM on a neighbouring probe signal in a two channel 50 GHz WDM system.

4.1 SOP drift over a short period of time

When two optical signals are combined within an optical fibre there is an interaction between the two beams. As mentioned previously in chapter 3 and clearly indicated by equation 3.16, the refractive index that an optical field experiences may be altered by the intensity of a neighbouring field. This leads to a phase change which is dependent of the intensity of the neighbouring signal according to equation 3.17.

The following experiment was conducted to investigate the SOP drift over a short period of time. Two optical waves with different wavelengths were multiplexed using a wavelength division multiplexer (WDM) and transmitted over the fibre under test (FUT) as illustrated in figures 4.1 (a) and (b). In both scenarios the pump signal, indicated by λ_1, was amplified using an erbium doped fibre amplifier (EDFA). Post-transmission, the probe (indicated by λ_2) was filtered out using a digital tuneable filter from OZ optics.

A switch directed both the probe and pump signals to a polarimeter from Adaptif photonics as shown in figures 4.1 (a) and (b). Fibre polarization controllers (FPC) placed directly after the pump and probe signals allowed control of the pump and probe signal states of

polarization (SOPs). The state of polarization (SOP) of both pump (λ_1) and probe (λ_2) signals were monitored over a period of 30 minutes. The pump wavelength was 1552.12 nm and the probe wavelength 1551.72 nm, which amounts to a spacing of 50 GHz.

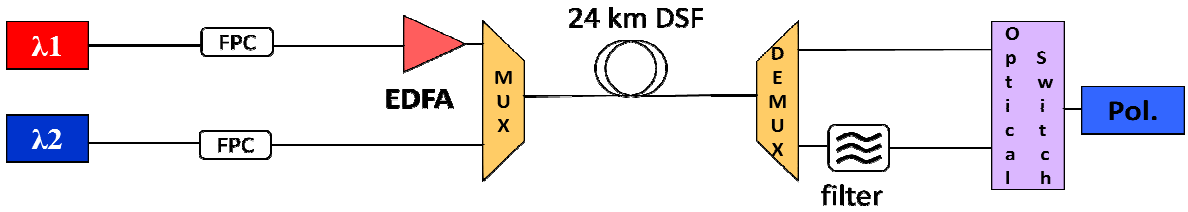

(a)

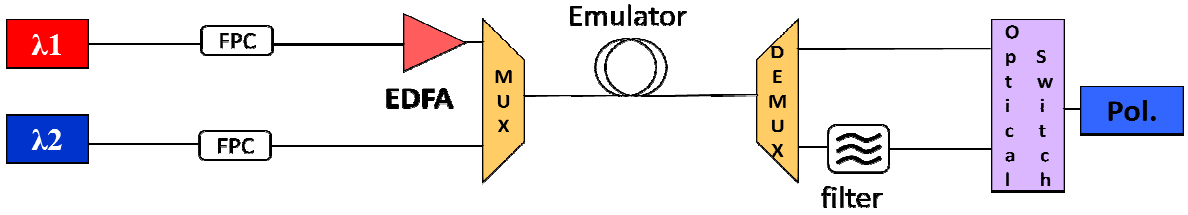

(b)

Figure 4.1 (a) Pump and probe continuous wave transmitted over 24 km DSF, (b) multiplexed pump and probe transmitted over an emulator.

As shown in figure 4.1 (a) the combined signal was transmitted over 24 km of dispersion shifted fibre (DSF) and over an emulator as seen in figure 4.1 (b). The emulator was made up of a concatenation of polarization maintaining fibre (PMF) and single mode fibre (SMF) sections all spliced together.

The probe wavelength power was kept fixed throughout, at a power of 3 dBm. The SOP of the probe signal was logged over a period of 30 minutes. SOPs were recorded at 12 second intervals. The same measurement was repeated for several pump powers ranging from a minimum pump power of 3 dBm and ending with a maximum pump power of 13 dBm. The pump power was increased in increments of 1 dBm. The power ratio (PR) is defined as the ratio between the pump power and the signal power. Hence for example if the signal power is 3 dBm then for a pump power of 13 dBm the corresponding power ratio is 10 dB.

Figure 4.2 is a plot of the cumulative angle against time. As the SOP develops the angle between any two adjacent SOP vectors was calculated. The cumulative angle refers to the summation of the relative angles as the SOP migrates over time. Hence for any particular time over a period of 30 minutes figure 4.2 (a) and (b) shows the additive angle growth up to that particular time.

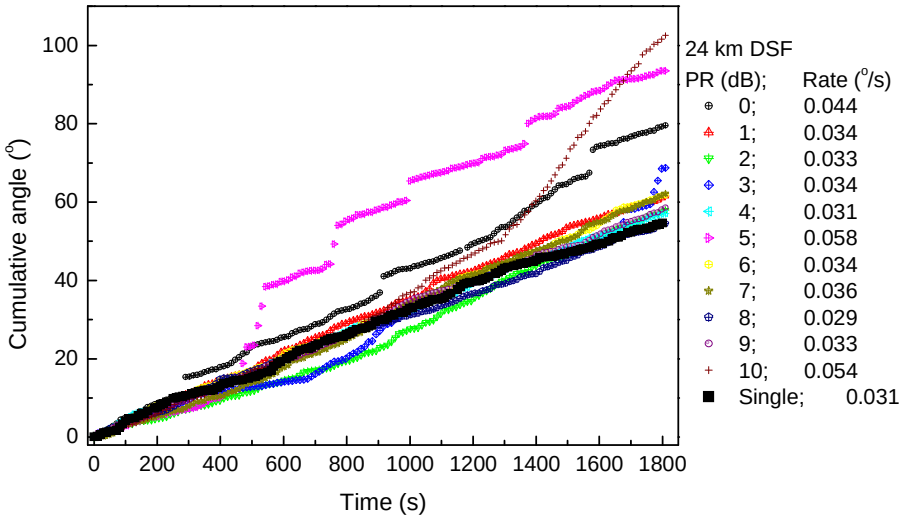

Figure 4.2 (a) Cumulative angle for DSF over 30 minutes.

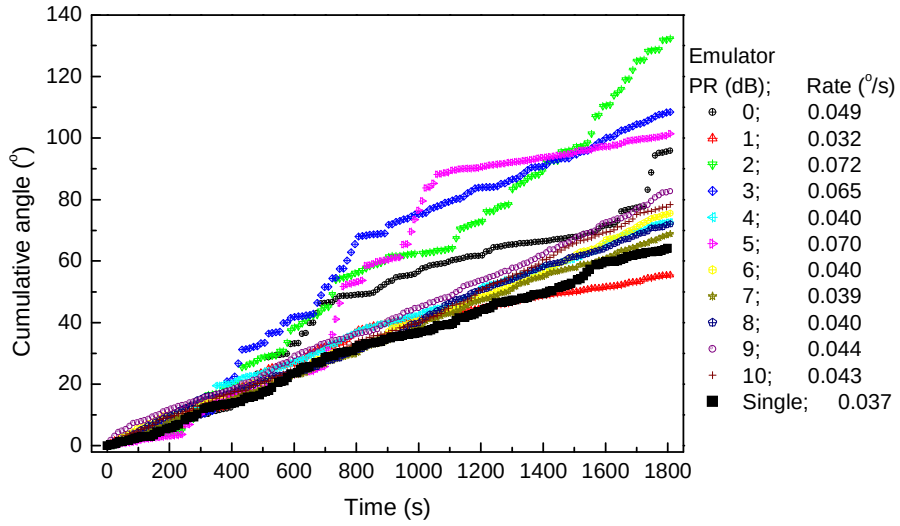

Figure 4.2 (b) Cumulative angle for the emulator over 30 minutes.

For the case of both the DSF and the emulator a reference measurement was made. The reference measurement entailed tracking the SOP for a single probe channel with no pump

signal. For a single probe channel with no pump signal present the, maximum cumulative angle for the DSF was 54.6^{o} which was the lowest cumulative angle. This drift is most probably caused by slight temperature changes within the lab, which cause the fibre jacket to contract or expand which in turn influences the fibre birefringence. However this value does not differ much with the maximum angle values for when the pump is present. From the average SOP rate it does appear that the SOP shows more activity for power ratios 0 dB, 5 dB and 10 dB (i.e. pump powers 3 dBm, 8 dBm, 13 dBm).

The cumulative angle against time for the emulator (figure 4.2 (b)) shows the same trend as for the DSF (figure 4.2 (a)), where power ratios 0 dB, 2 dB, 3 dB and 5 dB appear to have slightly more activity than the single wavelength transmission. Generally the cumulative SOP for both the DSF and emulator seem to be very stable for both scenarios of signal channel transmission as well as for double channel transmission for all pump powers indicated. The cumulative angle rate of change is calculated by dividing the cumulative angle by the total time. The rate varies between 0.029 ^{o}/s and 0.058 ^{o}/s for DSF, and 0.031 ^{o}/s and 0.072 ^{o}/s for the emulator.

An alternative manner of looking at the evolution of the SOP vectors over time as the lightwaves are transmitted through the DSF and emulator, is to compute the relative angle between the SOP vector for a particular time and the initial SOP vector for each SOP vector. Hence the initial vector acts as a reference vector. This was done in figure 4.3 (a) and (b) where the angle is called the relative angle.

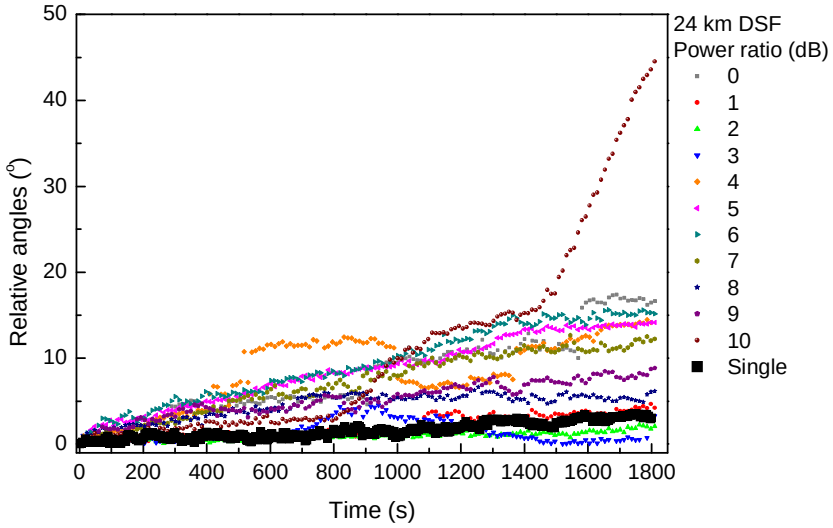

Figure 4.3 (a) Relative angle between initial and developing SOP vectors for transmission over DSF.

Figure 4.3 (a) again shows that the probe SOP vector remains stable in all scenarios. From figure 4.3 (a) it is evident that when a single optical signal is transmitted the SOP is the most stable throughout, whereas for two signal transmission the SOP move slightly away from the reference SOP. The exception is for a power ratio of 10 dB where the SOP walks away from the reference SOP to a total angle of 44.5^{o}. These results show that the probe SOP remains stable both in the absence and in the presence of a pump signal where both signals are continuous optical waves. The presence of the pump signal does appear to make the probe signal more active however this movement is not ordered.

The results for the emulator, in figure 4.3 (b), does not show any more movement than the DSF case. Hence again, the single optical wave shows the least movement with slightly more movement when the pump is transmitted with a pump signal of higher power. The probe SOP vector transmitted through the emulator appears to have an oscillating motion indicating that the probe signal no longer migrates away from the reference vector in a linear fashion but in an oscillating manner. This effect may be caused by the fibre PMD. Since the emulator has many spliced sections implying many mode coupling sections, this results in higher second order PMD. The PMD randomises the SOP vector, in the process changing its direction.

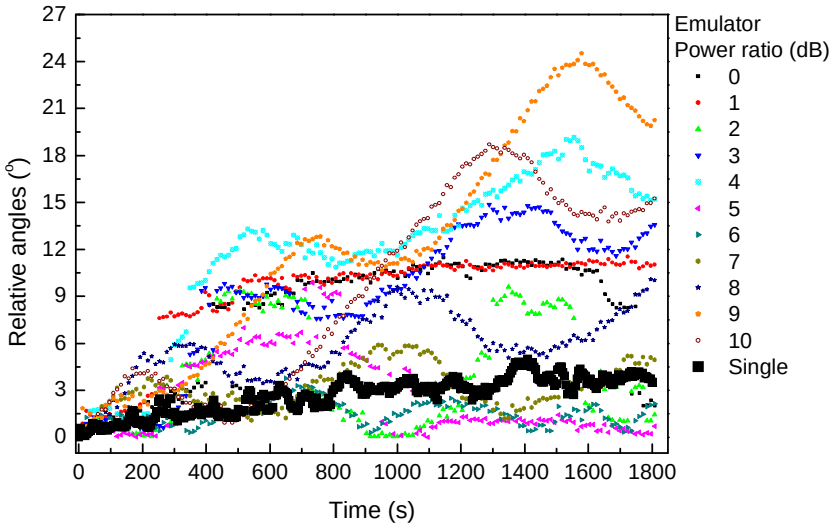

Figure 4.3 (b) Relative angle between initial and developing SOP vectors for transmission over the emulator.

4.2 Control of a low power probe SOP using a high power pump

Referring back to chapter 3 section 3.5 when two optical waves are transmitted down an optical fibre, the optical intensity of one wave will affect the refractive index experienced by the neighbouring signal. Collings and Boivin presented a mathematical expression in [15] which shows that the SOP change over distance equates to the cross product of the two neighbouring signals. This is clearly demonstrated by equations 3.26 (a) and (b).

Looking closer at equation 3.26, it states that over a small infinitesimal distance ∂z the SOP vector $\overline{S_a}$ changes by an amount $\partial\overline{S_a}$ and this change is a function of the intensity as well as orientation of the neighbouring optical wave vector $\overline{S_b}$. All the other elements in the equation are constants. A vector is described by both magnitude and direction. Firstly, the rate of change of SOP vector $\overline{S_a}$ is influenced by the intensity of the co-transmitted SOP vector $\overline{S_b}$. Secondly, as a result of the cross product the SOP rate changes as the vector $\overline{S_b}$ changes. Figure 4.4 shows an illustration of rate equations 3.26 (a) and (b); specifically it shows the cross product of two vectors $\bar{a}$ and $\bar{b}$. Here we calculate the cross product between vectors $\bar{a}$ and $\bar{b}$. Vector $\bar{a}$ is kept fixed while vector $\bar{b}$ is rotated in a circle around the Poincaré sphere. This gives an interesting result, the cross product forms an ellipse where each vector is perpendicular to both the vectors $\bar{a}$ and the corresponding vector $\bar{b}$. Figure 4.4 is an illustration of rate equations 3.26 (a) and (b).

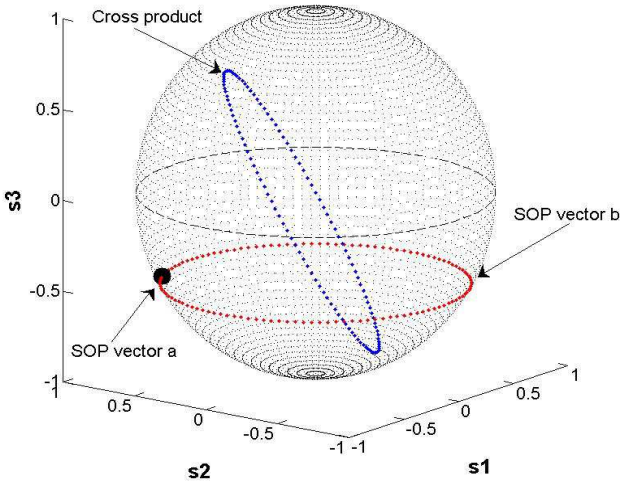

Figure 4.4 Cross product of a stationary and mobile vector.

Hence, the cross product depicted in figure 4.4 is an illustrative effect of the response of the rate of change of SOP vector $\bar{a}$ as vector $\bar{b}$ is rotated according to equation 3.26 (a) and (b). Using equation 3.30 (a) an intuitive explanation is that the SOP vector $\bar{s}$ changes slightly, by $\partial\bar{s}$, over a small distance ∂z and this change differs for different cross products with different vectors $\bar{p}$. The vector $\partial\bar{s}$ is perpendicular to the local pump and probe vector. This occurs throughout the fibre length, hence a change in the pump vector $\bar{p}$ orientation yields a change in the output probe SOP vector $\bar{s}$. Therefore the SOP vector $\bar{s}$ will develop in the same fashion as the pump vector. This gives the idea that through cross phase modulation the orientation of the probe SOP may be controlled indirectly by changing either the co-propagating pump intensity or orientation.

This phenomenon was investigated further experimentally. Figure 4.5 shows the scheme used for this experiment. The laser source used for the XPM experiments throughout this study was a WDM unit housing eight distributed feedback (DFB) laser diodes. This product is from Thorlabs. The laser diodes are all centred around 1550 nm, are tuneable over a small wavelength range and their central wavelengths differ by 50 GHz. A pump (λ_1) and probe (λ_2) signal at wavelengths 1552.12 nm and 1551.72 nm were multiplexed using a multiplexer and transmitted over 24 km of dispersion shifted fibre (DSF). A 3 dB coupler split the pivot (sum of the pump and probe signal), where the pivot goes directly to an optical switch which directs the pivot to a polarimeter. The probe signal is filtered twice by the demultiplexer as well a tuneable digital filter to ensure that the pump signal is fully suppressed. The probe signal is then passed through the same optical switch which leads the probe to a polarimeter.

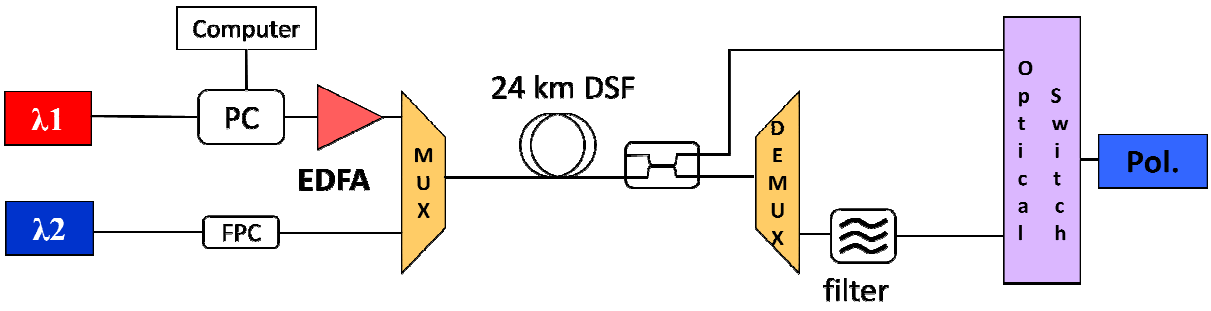

Figure 4.5 Continuous wave probe and pump signal multiplexed and transmitted over 24.7 km DSF.

A polarization controller (PC) from Adaptif was used to control the SOP of the pump signal. The Adaptif polarization controller contains five waveplates: four quarter waveplates and one

half waveplate. The waveplates are made of lithium niobate ($LiNbO_3$) crystals. The output SOP is controlled by the state of the PC. The state of the PC is set by the position of the waveplates which is expressed in terms of five angles measured in radians. An external voltage is applied to the crystals to change the refractive index of the crystals which in turn alters the SOP of the input light. A complete rotation of the quarter waveplate changes the phase difference by $\pi/2$ and a complete rotation of the half waveplate changes the phase difference by π.

In terms of the SOP on the Poincaré sphere, a complete rotation of a quarter waveplate will trace out a figure eight on the Poincaré sphere and a full rotation of the half waveplate will trace out a circle. The polarization controller was interfaced with a computer to control the PC waveplates using a Labview-based program. Instructions were sent to rotate the half waveplate to trace out a circle on the Poincaré sphere. The pump wave power was amplified with an erbium doped fibre amplifier (EDFA) to 21 dBm while the probe wavelength power was kept at a minimum of 5 dBm.

Figure 4.6 shows the resultant outcome as the pump is rotated in a circle while the input signal is kept fixed.

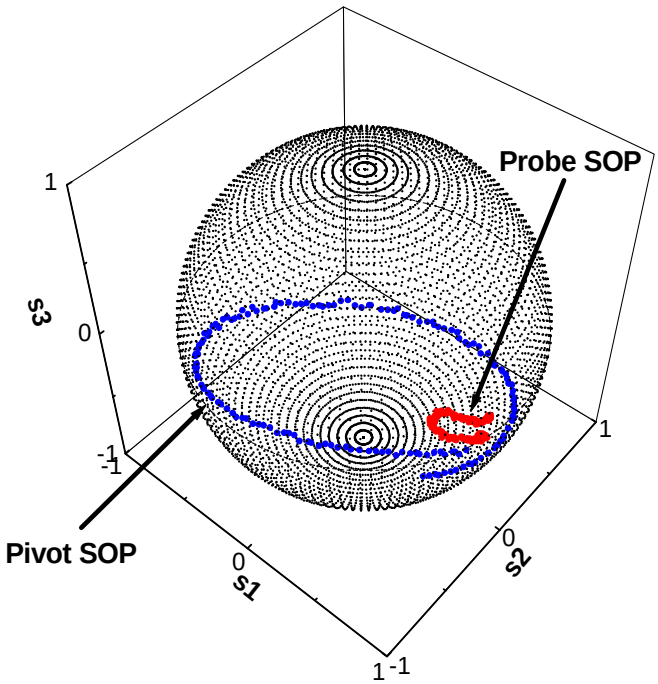

Fig. 4.6 The half waveplate of the Adaptif photonics A3200 polarization is used to rotate the SOP of the pump signal to trace a circle on the Poincaré sphere.

The blue trace represents the sum of the pump and probe SOP which is referred to as the pivot. The pivot mostly represents the pump due to the pump's significantly larger intensity by 16 dB. The probe signal generally mimics to pump signal and also traces out a circle on the Poincaré sphere. This effect is the result of XPM and agrees with the propagation equation as discussed above. This result is very similar to the illustrative result in figure 4.5. It is noted that the probe SOP traces a circle much smaller as compared to the pump SOP.

A different version of this experiment is to change the direction of rotation of the pump signal and to observe the probe signal SOP. The quarter waveplate of the PC was rotated so as to direct the pump SOP to trace a figure eight on the Poincaré sphere. Figure 4.7 shows the pivot trace out a figure eight on the Poincaré sphere, hence the pump traced out a figure eight. The probe signal traced out a similar figure eight on the sphere. Therefore it is clear that due to XPM the probe SOP vector follows and imitates the pump signal SOP vector with respect to direction.

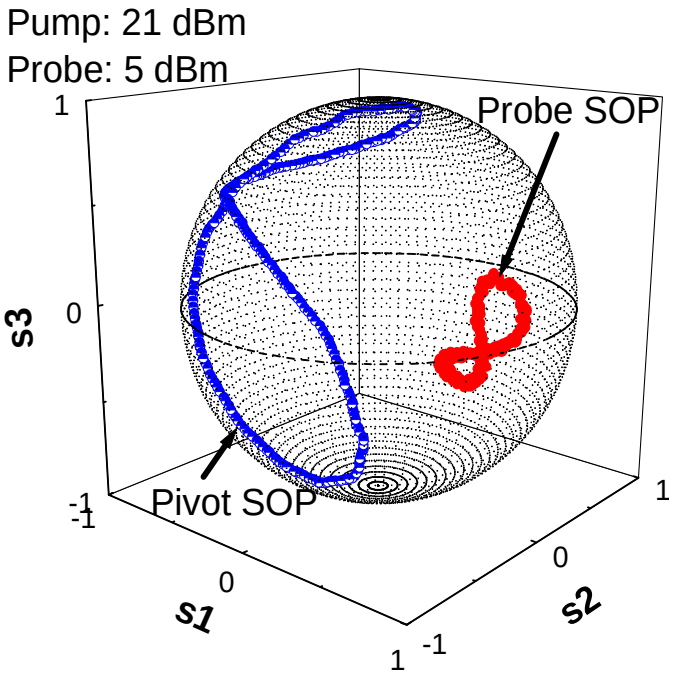

Figure 4.7 The quarter waveplate of the Adaptif photonics A3200 polarization is used to rotate the SOP of the pump signal to trace a figure 8 on the Poincaré sphere; the probe mimics the pump signal.

From figures 4.6 and 4.7 the probe SOP clearly covers a limited area on the Poincaré sphere. An experiment was performed to determine the size of the finite area covered by the probe SOP. The pump signal was randomly scrambled by using 500 random settings of all five

waveplates. Hence changing the pump SOP 500 times and spreading the pump SOP evenly over the entire Poincaré sphere. Figure 4.8 shows the resultant plot.

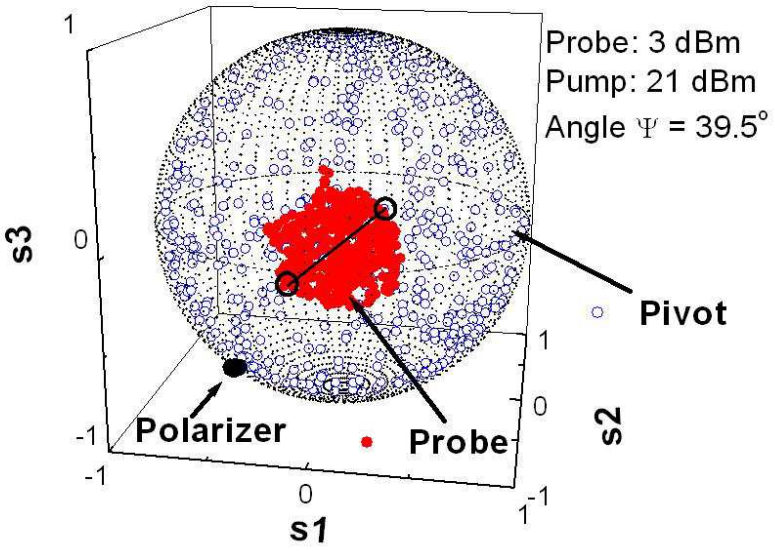

Figure 4.8 The blue circles represent 500 random SOPs of the pump signal manifested into the pivot without the polarizer in place.

As seen in figure 4.8 for a pump power of 21 dBm and a probe power of 3 dBm, the probe SOP again mimics the pump SOP vector. The probe SOP is spread out over a finite area where the maximum angle between the vectors at opposite ends of the area traced out by the probe SOP vectors is 39.5^{o}. Therefore on average, by using this technique and for these pump powers, every time the pump SOP is changed by 9^{o} the probe SOP moves by 1^{o}. The effect appears to be instantaneous.

4.3 XPM induced SOP modulation to intensity modulation

The XPM effect explained in section 4.2 could potentially be used to transfer a pattern or specific information from the pump signal to the probe signal. The principle is that the probe signal SOP vector orientation may be controlled indirectly by a co-transmitted pump signal.

Figure 4.9 shows a scheme where a pump signal was modulated with a Mach-Zehnder modulator (MZM).

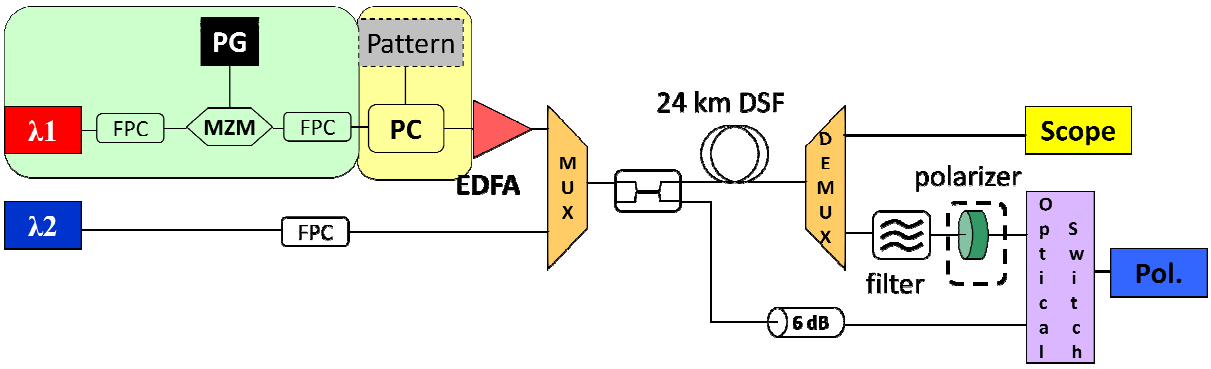

Figure 4.9 Pump signal is modulated with a MZM and multiplexed before transmission over 24.7km DSF.

The pump signal was intensity modulated at a bit rate of 10.3 Gbps with a pseudo random bit sequence (PRBS) repetition rate of 2^7-1. The fibre polarization controller (FPC) in front of the MZM ensures the correct SOP into the MZM, as the MZM is polarization sensitive. The FPC after the modulator was used to set the initial pump SOP. Right after the intensity modulation of the pump signal, the signal was passed through the Adaptif PC where it was polarization modulated. By using a computer interface to the polarization controller (PC) as before, the half waveplate inside the PC was modulated by adjusting the voltage to the waveplate such that the pump SOP covers 180^o on the Poincaré sphere. This SOP modulation is then transferred to the probe signal by cross phase modulation nonlinear polarization rotation (XPM NPR).

After transmission through the fibre the signals are demultiplexed. The probe signal passes through an additional filter and then through a polarizer. The polarizer acts as a polarization discriminator. Figure 4.8 shows the SOP position of the polarizer on the Poincaré sphere. SOPs closer to the polarizer SOP on the Poincaré sphere pass through with a higher intensity than SOPs further away from the polarizer SOP. Hence a 1 bit was made by moving the pump SOP from some arbitrary SOP to its orthogonal counterpart and back. A zero bit was made by keeping the SOP stationary over the entire bit period. Therefore the peak of the 1 bit occurs for the SOP closest to the polarizer SOP. The whole process was controlled by a LabView program written for this particular application. The polarimeter was used as an oscilloscope by recording the probe signal power against time. Figure 4.10 shows a 128 bit pattern that was transmitted over 24.7 km of DSF using this technique.

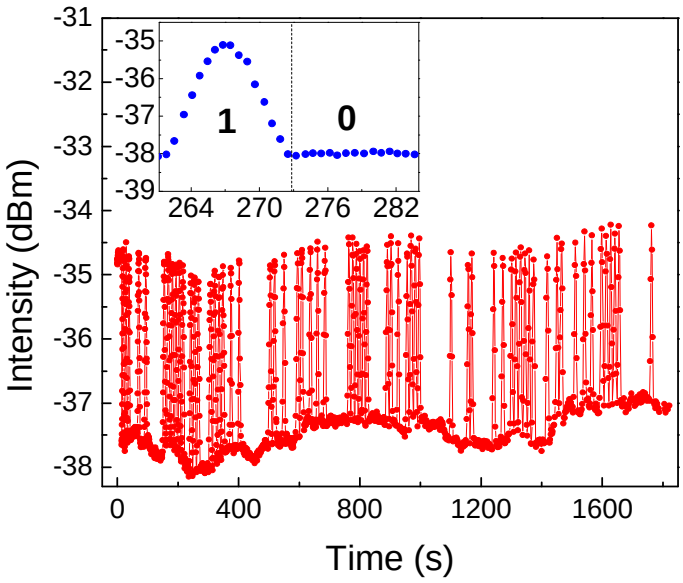

Fig. 4.10 Intensity pulses of the probe signal wavelength. XPolM induces modulation of the probe signal as a resultant from polarization modulation of the pump signal. A polarizer does the SOP modulation to intensity modulation conversion.

The dynamic range of the pulse remains relatively fixed at approximately 2.85 dB. The intensity bits (ones and zeros) in figure 4.10 are strictly that of the probe signal. Therefore as the pump signal's SOP is modulated the probe signal's SOP also changes through XPM. The polarizer then converts the probe signal's SOP modulation to intensity modulation for simpler intensity detection. The pulse period in figure 4.10 is limited by the rate of changing the SOP using the polarization controller, as well as the computer interfacing and using the polarimeter as an oscilloscope. The pulse bit period in figure 4.10 is 11 s. From the total 128 bits it is also evident that the baseline of the bit string fluctuates over time. This effect is a result of the non-stationary SOP which could be attributed to a variation in temperature or to the fact that modulating the pump leads to less stable SOPs due to cross polarization modulation (XPolM).

The fluctuating baseline in the bit string could be solved with offline signal processing by, for example, making use of the fact that the dynamic range remains relatively fixed. Figure 4.11 shows a 128 bit pattern transmitted repeatedly for 57 minutes over a buried Telkom fibre link in the field with length 28.8 km.

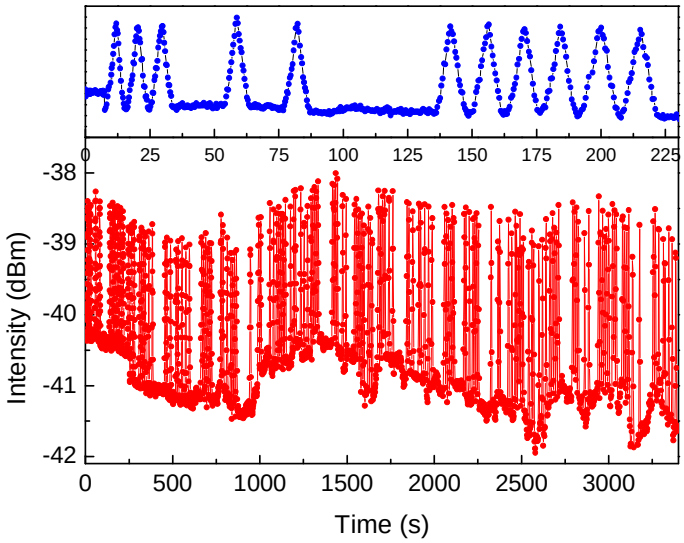

Figure 4.11 Probe intensity pulses. Here, the fibre transmission was carried out over a deployed buried fibre link 28.8 km long.

According to the FTB-5700 PMD single-ended dispersion analyser, the link had a PMD of 3.61 ps, hence its PMD coefficient is 0.67 ps/√km. The total chromatic dispersion (CD) measured in the fibre was 479.95 ps/nm, at 1550 nm, giving a CD co-efficient of 16.65 ps/nm.km. The walk-off, as defined in chapter 3, is then calculated to be 191.97 ps/km. Transmission was still possible despite the fibre length, CD and PMD values. The probe power was relatively high at 13 dB and the pump signal power was 22 dBm.

As with the DSF, the transmitted signal intensity fluctuates as the SOP does not remain completely stable. Figure 4.12 shows two traces which are measures of the probe intensity over time. These traces were created with both the pump and probe on for both cases.

The black trace shows how the probe intensity fluctuates without the pump SOP being modulated. This is referred to as the background intensity and gives an indication of how the probe signal keeps evolving. This is part of the reason why the bit train in figure 4.11 fluctuates. The fluctuation of the probe in figure 4.12 is most probably caused by slight temperature changes and external mechanical perturbations. The data points in red in figure 4.12 represent the response of the probe signal as the pump signal SOP is randomly changed. This gives a better indication of the dynamic range and shows that the range could measure to 3.5 dB. The trace also gives another means of quantifying the response of the probe signal in relation to the pump signal SOP change.

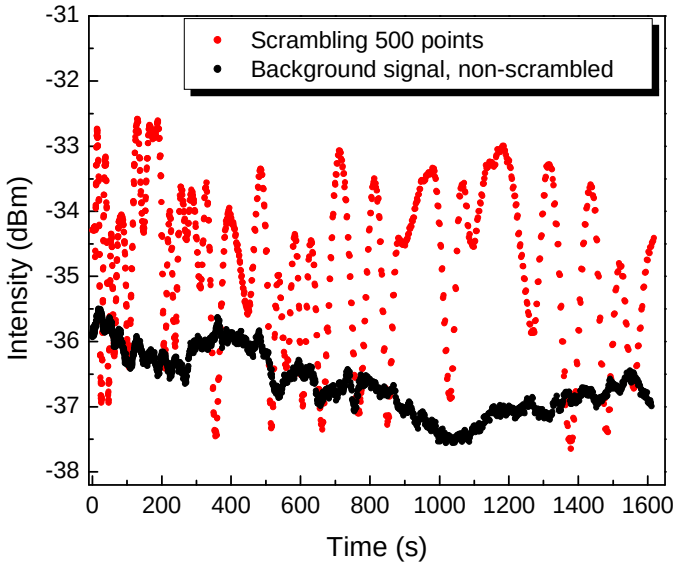

Figure 4.12 Background intensity trace (in black) and the probe intensity trace as the pump signal SOP is randomly modulated (in red).

4.4 Summary

This chapter introduced the effect of XPM in fibre experimentally. Experimental results of several experiments which were specifically designed to study the behaviour and the characteristics of XPM in fibre were presented.

Initially, the experiments set out to determine the stability of the SOP over a short period of time, for example 30 minutes. This was done by monitoring the development of the probe SOP vector over time. The cumulative angle showed that the SOP that was transmitted without the pump signal, known as the probe reference SOP, remained the most stable. However for both the DSF and the emulator, the probe SOP in the presence of a continuous wave pump did not show much more activity than the reference probe SOP. For some large pump powers, the probe SOP did appear slightly more active in comparison to the lower probe powers; however the level of activity was not correlated to an increase in pump power level. The figures of the plot of the reference angles also show a similar behaviour. However, for DSF fibre it is noted that for a power ratio of 10 dB, the probe does walk away considerable from the reference starting SOP. Oscillating behaviour is seen from the emulator.

Section 4.2 looked into the effect of controlling the SOP of a probe signal by changing the SOP of the co-propagating pump signal. It is found that XPM causes the probe signal SOP to

change as the pump signal SOP is tuned. The SOP change occurs on a much smaller scale for the probe signal. The results also show that the probe SOP imitate the direction of the pump SOP to a large extent.

The above effect is used to determine the largest SOP change of the probe as the pump SOP is changed through intensity. It is also used to transfer SOP modulation of the pump signal to SOP modulation of the probe signal using XPM. By using a polarizer the probe signal is converted to an intensity modulated signal, hence the probe was used as a carrier to transmit data over 24.7 km of DSF and over 28.8 km of buried SMF.

CHAPTER 5

DOP DEGRADATION AS A RESULT OF CROSS PHASE MODULATION

PMD in optical fibre may lead to pulse broadening. Polarization mode dispersion compensators (PMDCs) are able to compensate for PMD. A lot of these compensators are based on tracking the degree of polarization (DOP) and using it as a feedback signal. When considering new generation networks, which multiplex several optical signals into one fibre, the combination of wavelength division multiplexing and the effects of XPM on the co-propagating signals may present a problem to PMDCs. This chapter looks at the impact XPM has on a two channel WDM system and relates the effects to PMDCs.

5.1 Introduction

As mentioned previously polarization mode dispersion (PMD) broadens the input optical pulse and causes a reduction in optical power which may lead to system penalties such as inter-symbol interference. This optical effect is more prominent at bit rates higher than 10 Gbps, hence it is essential to impose control over PMD by making PMD measurements and mitigating the problem presented by PMD. One method of solving this problem is by PMD compensation. Researchers have theoretically and experimentally looked into first-order PMD compensation. Further, the derivative of first-order PMD with respect to optical angular frequency results into polarization chromatic dispersion (PCD) and principal state of polarization rate of rotation (PSPRR). These terms are collectively known as second-order PMD.

In an attempt to reduce the cost on infrastructure, system providers try to increase the transmission distance through the fibre by increasing the optical power. This increase in the fibre transmission distance is limited by non-linear optical effects such as four-wave mixing, crosstalk and cross polarization modulation (XPolM). This thesis looks at the effect of XPM. In increasing the optical power, XPM causes a signal to affect its neighbouring optical signal

which may in turn have a deleterious effect on a polarization mode dispersion compensator (PMDC).

5.2 Brief background on PMD compensation

Polarization mode dispersion broadens the input pulse which will lead to bit errors in the transmitted data. A potential solution is to insert a polarization mode dispersion compensator (PMDC) in the fibre link. Real time PMD compensation techniques require fast monitoring of a PMD related parameter from which the PMD can be determined [65]. Polarization mode dispersion compensators (PMDCs) monitor the link PMD in an indirect manner; for example, a popular monitoring technique tracks the degree of polarization (DOP) of a signal in the link [65]. PMD is a statistical phenomenon [22]. The maximum tolerable PMD is 15 % of the bit period [49]. Hence, for bit rates of 10 Gbps and 40 Gbps, the tolerable PMD values are 15 ps and 3.75 ps respectively.

Fast repeated optical monitoring enables restoration of signals degraded by impairments such as CD or PMD. This type of compensation requires monitoring of a signal which is related to the effect to be corrected. In [48, 58, 69] the instantaneous power is monitored and converted into electrical signals which are measured on an oscilloscope or a radio frequency (RF) spectrum analyser. However, as signals become faster it becomes more challenging and even impossible to compensate using electronic monitoring. This has lead to all optical PMD monitoring techniques which are able to solve this problem. Two well known optical PMD monitors are based on the frequency resolved state of polarization (FRSOP) method [5, 7] and the degree of polarization method [41].

In [7], researchers propose a novel PMD monitoring technique, the FRSOP method, which estimates the DGD by monitoring the Stokes vectors at different frequencies of the received optical pulse spectrum. The FRSOP method requires around ten SOP measurements making it too slow for real time PMD compensation which requires millisecond response times [5].

In [13, 12, 41, 49, 63] the PMDC monitors the signal DOP. The compensator consists of a polarization controller and a polarization maintaining fibre with a fixed PMD value of 15 ps. A control algorithm tries to maximize the output DOP by adjusting the polarization controller. DOP monitoring proves to be fairly accurate in tracking the PMD and has a fast response time. In [49], a 40 Gbps signal is efficiently compensated.

Typically, PMD compensators are arranged into one of two base schemes, feed-forward or feedback. In a feed-forward scheme the monitoring device is essentially placed right after the fibre link but before the PMD compensator. Figure 5.1 shows an illustration of a feed-forward PMD compensation scheme. In figure 5.1, the monitor is a DOP monitor but it could also be an RF monitor. Normally, a small percentage of the signal is passed to the monitor. The monitor information is passed on to the control algorithm which will infer the appropriate settings for the PMDC to correct the PMD in the fibre link.

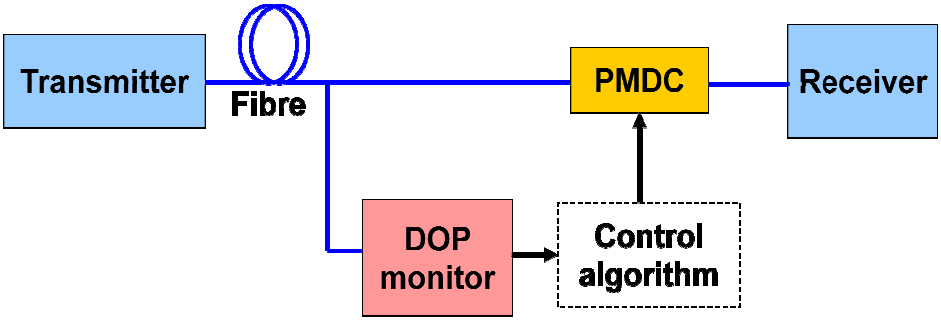

Figure 5.1 An illustrative scheme of a feed-forward PMDC that monitors the DOP signal.

In [63, 13, 12] feed-forward PMD compensation was carried out using a DOP monitor. The feed-forward scheme proves to be very fast as it requires only one control step after the required variables for compensation are obtained. The magnitude of the DOP of a transmitted signal depends on the DGD of the link as well as the power splitting ratio of the two principal states of polarization (PSPs) [63]. In Stokes space the PSPs are oriented orthogonal to each other on the Poincaré sphere. If a signal is launched into both PSPs with equal power then at the output the polarimeter measures the combination of the two [12]. Therefore the DOP is a minimum when the SOP is launched at a 45^{o} angle (in Jones space) between the two PSPs.

In [63], a scrambler covers the whole Poincaré sphere in 18 ms at the fibre input after which the DOP is measured. Hence the worst DOP belongs to the case where the PSPs splitting ratio is 0.5, therefore this allows the fibre DGD to be derived from the DOP. The PSPs are given by the SOPs with the largest DOP. Thus both the link DGD and PSPs can be inferred from measuring the DOP [63]. The link DGD is then determined from a stored response curve and the compensator DGD element is set to cancel the link PMD [63]. The PSPs

information was not used but could be used to further improve the compensator by setting the polarization controller based on the PSPs data.

Chou et al. demonstrated a feed-forward PMDC which characterises the PSPs scrambled input signal [13]. The PSPs are then aligned with the DGD compensator using a calibrated lookup table [13].

The above mentioned compensators represent simple feed-forward PMD compensators which use DOP monitoring to track the PMD parameters. More complex PMDCs with more PMD parameters and more sophisticated algorithms have been developed as well.

In a feedback PMD compensator scheme, the monitoring signal is tapped after the compensator. In [40] a 40 Gbps signal is transmitted through an emulator with 7.2 ps PMD and some second-order PMD. The PMDC consisted of a polarization controller and 15 ps PMF. The DOP was tapped after the compensator and used as a feedback signal. BER measurements showed that the compensator was able to effectively compensate for PMD in the link thereby increasing the PMD limit of the link up to 33 % of the bit period [40].

PMDCs use other feedback signals such as the electrical spectral width, the total electrical power and an estimate of the BER [50] as well. The requirements of a feedback signal are the following: it should be sensitive, it must have a high correlation with the BER and it should have a high response time to the PMD [50]. DOP as a feedback signal stands out, meeting all the above mentioned criteria. Additionally the DOP as a feedback signal is independent of the bit rate [38]. All the PMDC mentioned above are meant for link transmitting only one wavelength. They also do not factor in XPM. Therefore for WDM links these compensators would have to be adapted to factor in the effects from XPM.

5.3 Experimental background to DOP degradation

XPM affects the refractive index that a neighbouring optical beam experiences through the Kerr nonlinearity, as discussed in chapter 3. Hence in a WDM system cross talk takes place between all the optical beams. This section looks into the effect that XPM has on an optical signal in a two channel WDM system where the pump signal is modulated.

Chapter 3 showed the propagation equations of the probe and pump signals in Stokes space, equation 3.30 (a) and 3.30 (b). These equations describe the evolution of the probe and pump over distance and time. For a continuous wave pump and probe signal, the rotation angle,

given by equation 3.31, is linearly proportional to the pivot power and the effective length. In [6] another expression is derived for the rotation angle for a probe signal in the presence of an intensity modulated pump signal. This model is referred to as the Carousel model. The Carousel model yields a new expression for the rotation angle, equation 3.32, which states that the rotation angle depends on the intensity modulated pump bits that have walked past the probe signal from the input of the fibre to a particular distance [25].

The experimental setup to investigate the DOP degradation of a probe signal caused by XPM was performed using the scheme shown in figure 5.2.

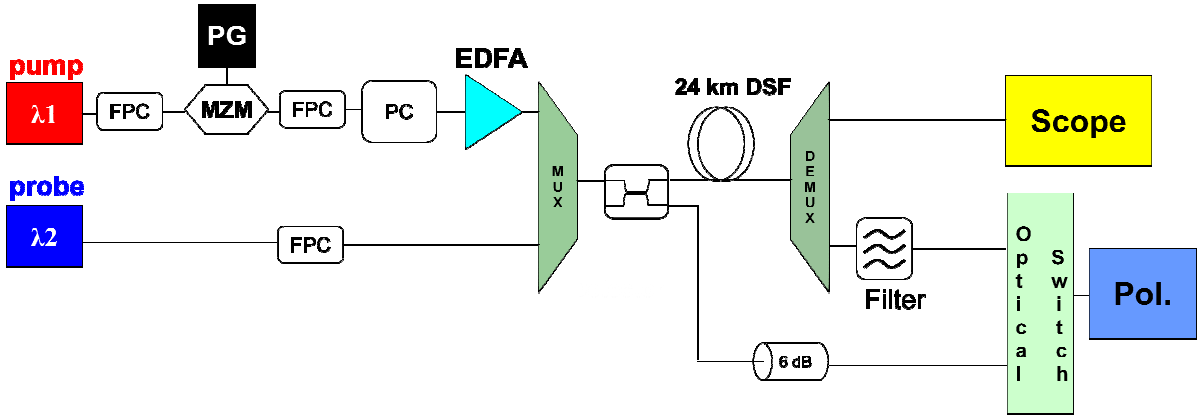

Figure 5.2 Pump signal,1552.12 nm, NRZ modulated at 10.3 Gbps is multiplexed with probe signal, at 1551.72 nm, and transmitted over 24.7 km of DSF. The filter central wavelength was 1551.7 nm.

The pump signal was non-return to zero (NRZ) intensity modulated, with an effective bit rate of 10.3 Gbps and a pseudo-random bit sequence (PRBS) of 2^7-1. A radio frequency (RF) signal with a bit rate of 10.3 Gbps was fed to a MZM. The RF single is transferred onto the pump signal by the MZM and passed through a polarization controller (PC), after which the pump signal is amplified by an EDFA. Thereafter the pump and probe signals are multiplexed and transmitted over 24.7 km of DSF. Post-transmission, a de-multiplexer decouples the signals, and directs the pump signal to the scope and the probe signal to a polarimeter. A coupler was used to tap the pivot (sum of the probe and pump signal) right before transmission over the DSF.

The input DOP into the DSF can be determined using the following expression

$$\mathrm{DOP}_{in} = \sqrt{1 - (1 - \cos\theta)\left((2\mathrm{PR})/(1 + \mathrm{PR})^2\right)} \tag{5.1}$$

where DOP_{in} is the DOP of the multiplexed signals pre-transmission, θ the relative angle between the pump and probe, and PR the power ratio [6]. This expression is plotted in figure 5.3 for power ratios within the range 10 dB to 22 dB, where PR is the power ratio of the probe and pump signal.

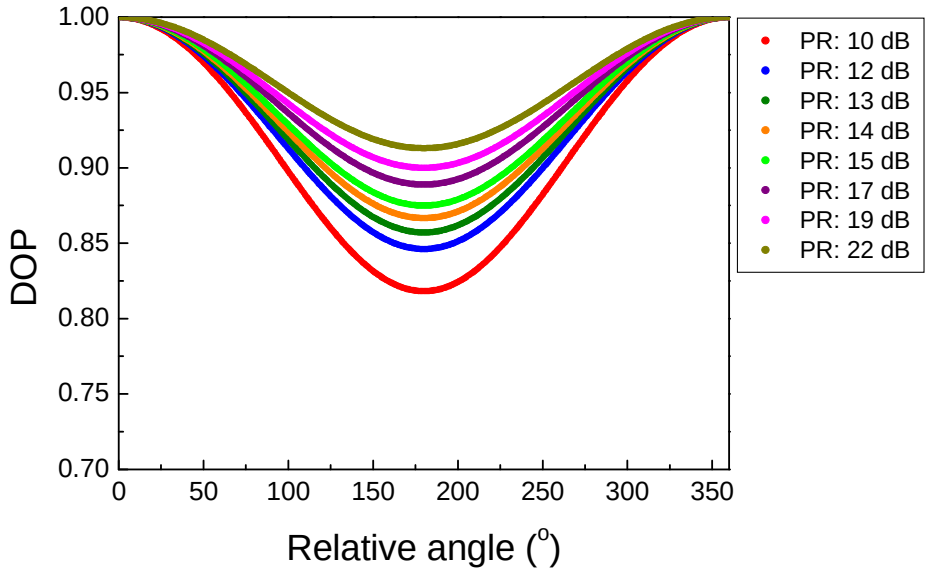

Figure 5.3 DOP of pivot pre-transmission against the relative angle between pump and probe.

Figure 5.3 shows that the DOP is a minimum at a relative angle of 180°, that is when the pump and probe signal vectors point in the opposite direction in Stokes space. Figure 5.3 serves as a good indicator to what the relative orientations between the probe and pump signal are.

An experimental plot of figure 5.3 was generated by rotating the pump SOP in a full circle using the half waveplate housed in the polarization controller; the results are plotted in figure 5.4. After optimising the orientation of the probe with respect to the pump, the next step was to measure the DOP of the pivot using a polarimeter.

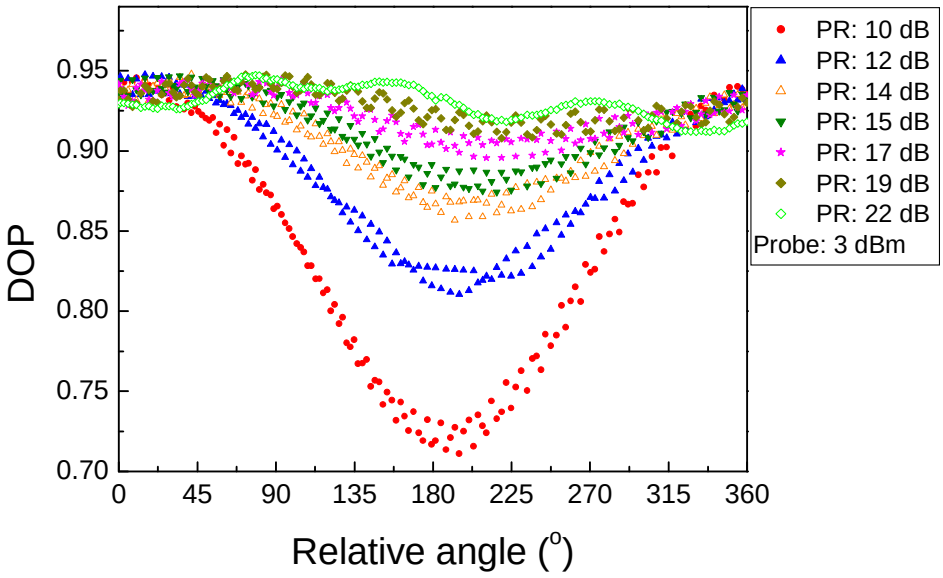

Figure 5.4 Experimental results of the DOP of the pivot vs the relative angle between pump and probe.

Figure 5.4 shows that the pump was initially co-parallel with the probe signal vector. At a relative orientation where the pump and probe were at an 180° angle, the DOP reached a minimum, while at the end of the pump rotation the two signals were again co-parallel hence the return to the maximum DOP. The DOP calculated by equation (5.1) differs from the DOP measured using the polarimeter. This is evident for the power ratio difference of 10 dB, where the DOP difference between the theoretical and experimental is 0.05 and 0.1 for relative angles 0 degrees and 180 degrees respectively. This is most likely caused by non exact SOP alignment between the pump and probe signal at the 0 degree starting point. This slight misalignment increases insignificantly with a change in the relative angle leading to the shift from a DOP of 0.05 to 0.1. In generally, this minor misalignment most likely caused the experimentally found DOP offset from the calculated DOP.

5.4 Impact of XPM on the signal DOP in a two channel WDM system

A Luceo E-BERT, bit error rate test system, was used to drive a Mach-Zehnder modulator at 10.3 Gbps. Figure 5.5 shows an eye diagram of a pre-transmitted signal. Before transmission

the signal is clearly undistorted and has a bit period of 100 ps. Only the pump signal was intensity modulated while the probe signal remained a continuous wave laser signal.

The pump and probe signals were multiplexed and transmitted over 24.7 km of DSF. Whenever the pump signal is turned on the pump and probe signal SOPs start to rotate around a pivot while when the pump is turned off the two signal SOPs stop rotating. An expression of this rotation angle was given in chapter 3, equation 3.32. This equation shows that the probe SOP rotation angle depends on the pump bits that have walked past the probe signal over a specified distance. The fact that the probe SOP undergoes a rotation depending on the pump bits that have walked past the probe signal, affects the average DOP of the probe signal.

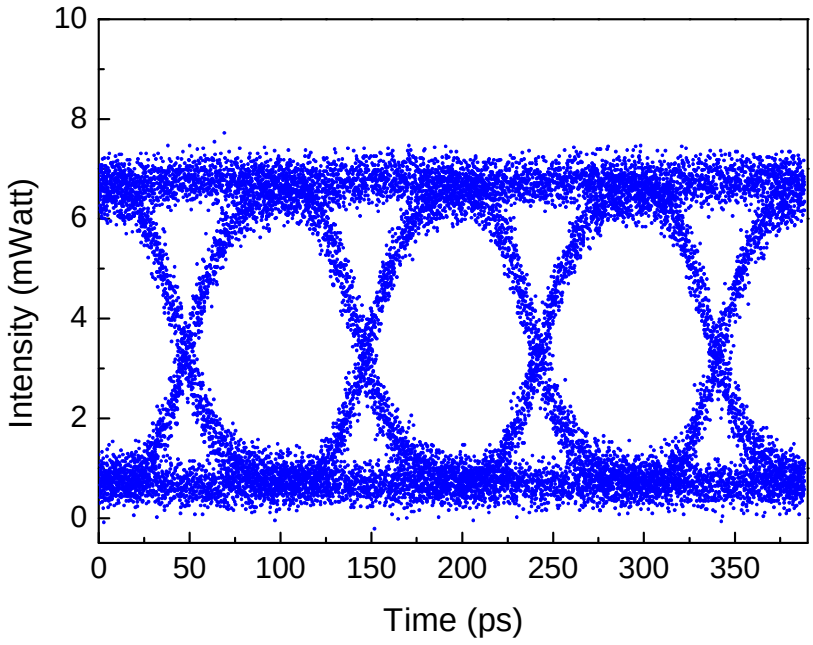

Figure 5.5 Pre-transmitted pump signal eye diagram.

Equation 3.32 shows that the rotation angle is proportional to the power of the pump signal. Hence the more intense the pump power, the greater the rotation angle traced out by the SOP of the probe signal. Equation 3.34 relates the DOP to the rotation angle and the relative angle between the pivot and probe signal. Two features stand out in equation 3.34. Firstly, the larger the rotation angle, the more the DOP is degraded. Secondly, for a relative angle of 90^{o}

and 270^{o}, in Stokes space, between the pivot and probe signal, θ_s yields a minimum DOP value. Equation 3.34 is plotted for several rotation angles in figure 5.6.

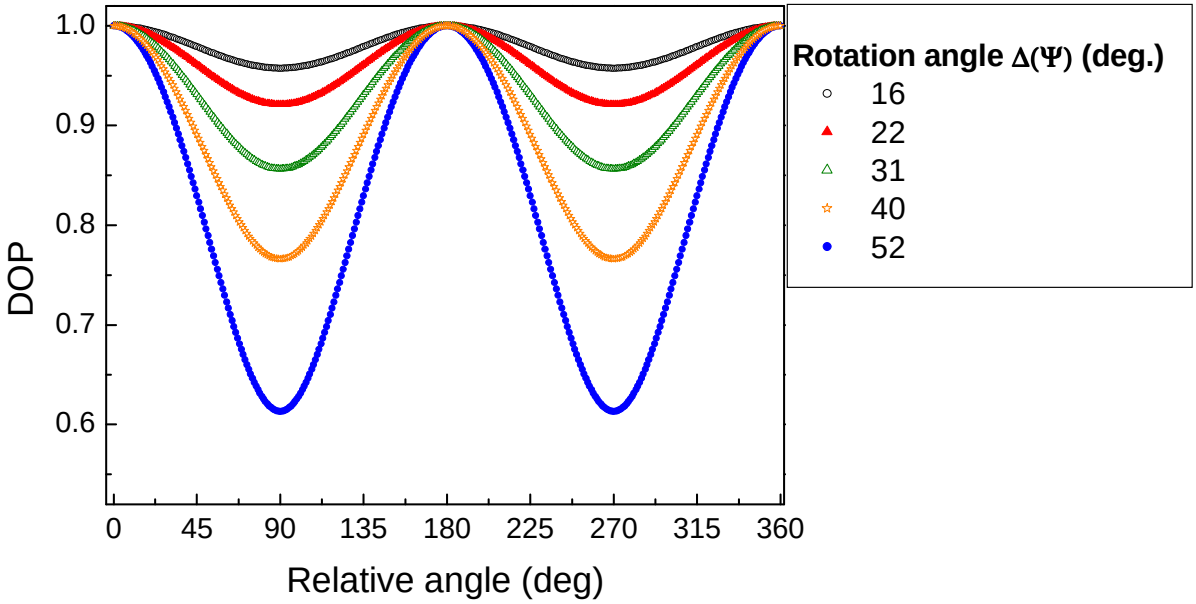

Figure 5.6 Probe DOP as a function of the relative angle between pump and probe for several rotation angles.

Figure 5.6 shows that there exists maximum interaction between the pump and probe signals at orthogonal orientation between the pump and probe signal vectors. For parallel and anti-parallel relative orientations, the DOP is a maximum.

The DOP degradation predicted by the Carousel model was experimentally verified using the scheme in figure 5.2. After intensity modulating the pump signal, it was amplified from 13 dBm to 25 dBm using an EDFA. For each pump power the pump signal, the SOP was rotated 360^{o} with a polarization controller. The pump and probe are multiplexed and transmitted over 24.7 km of DSF, after which the probe signal DOP and SOP were recovered. The experimental results are plotted in figures 5.7 and 5.8. Figure 5.4 was used as a guide to the relative alignment between the pump and probe signal. Figures 5.7 and 5.8 confirm the DOP degradation as a result of XPM. They show that the DOP is degraded to a minimum when the pump and probe are orthogonal with respect to each other, hence maximum interaction between the pump and probe takes place for these configurations. The DOP remains 1 for when the pump and probe are oriented parallel and anti-parallel with respect to each other.

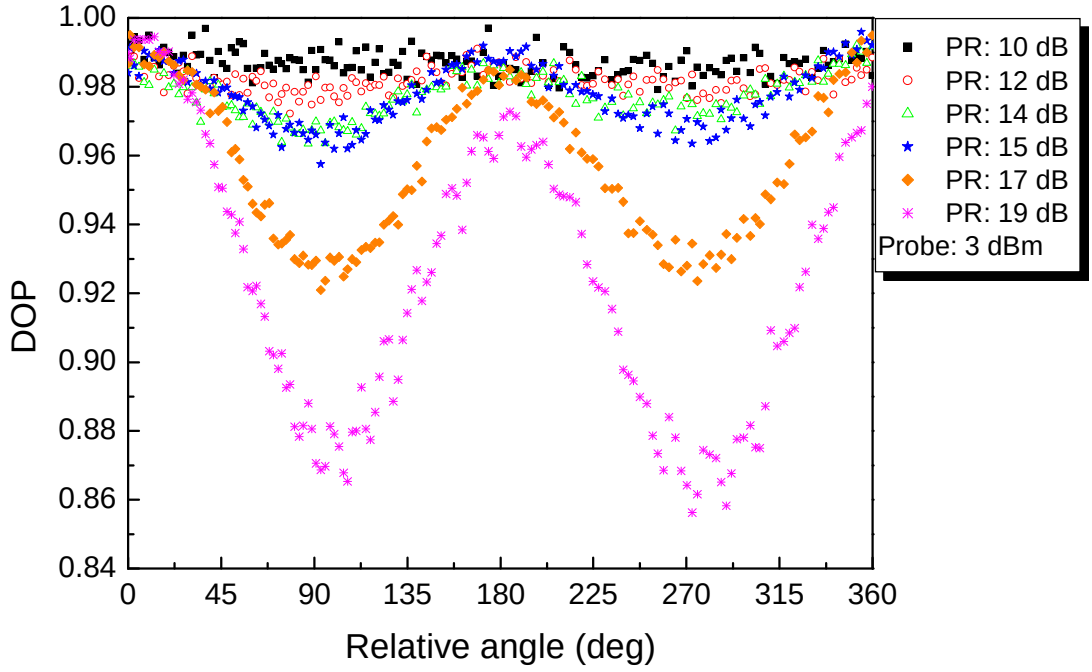

Figure 5.7 Observed DOP degradation over wavelength for power ratios within the range 10–19 dB, where the probe power was fixed at 3 dBm.

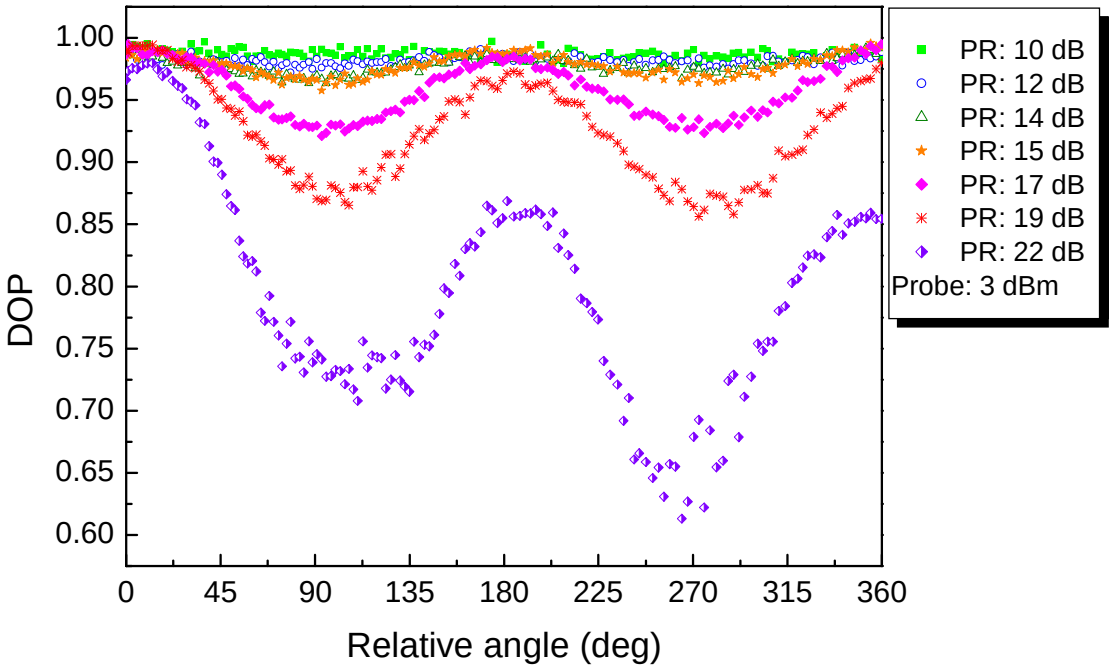

Figure 5.8 Observed probe DOP degradation plot extended to 22 dB power ratio.

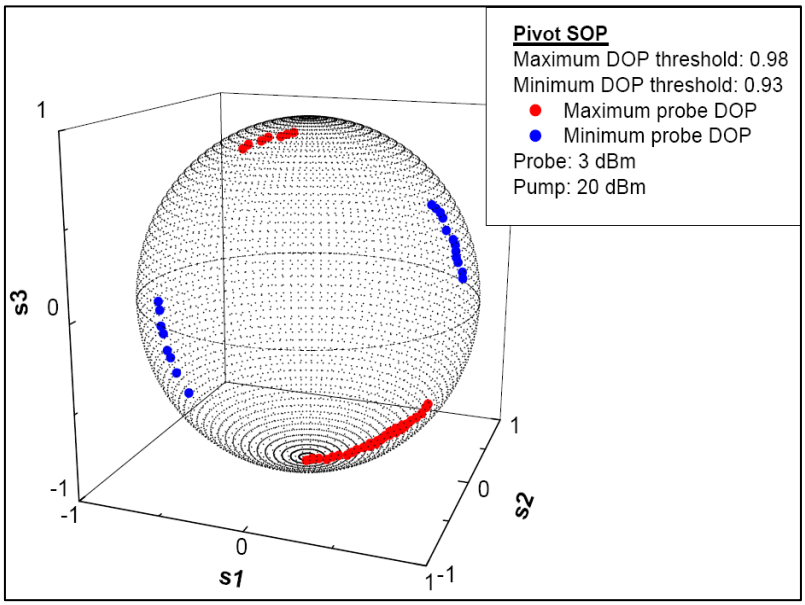

Figure 5.9 Pivot SOP corresponding to the probe SOP with maximum and minimum DOP.

The location of the pivot SOP which correlates with the probe SOP (which had a maximum and minimum DOP) is plotted in figure 5.9. These points were generated by setting a minimum threshold of 0.98 for pivot SOP where the probe DOP was maximum, and a maximum threshold of 0.93 for pivot SOP where the probe DOP was minimum. It can clearly be seen that there are two SOP regions for which the probe DOP will be minimum (blue dots) and two where the DOP will be maximum (red dots). It is also evident that the relative orientation of these SOP regions is such that they are spaced 90^{o} apart on the Poincaré sphere. From figure 5.7 and 5.8 it can be seen that for a power ratio of 10 dB, where the probe power was 3 dBm, the DOP degradation is much less than for a power ratio of 22 dB. These figures clearly show that the DOP degradation increases with power ratio.

We demonstrate this DOP degradation in [24]. DOP degradation occurs as a result of the swing of the rotation angle of the probe signal. This swing takes place at the bit rate. The average DOP is determined by the sum of the SOP vectors over time. The pump probe power ratio determines the magnitude of the rotation angle. Therefore, the larger the power ratio between the pump and probe, the larger the rotation angle of the probe SOP, which translates into a lower DOP [6, 24]. This trend is clearly visible in figures 5.7 and 5.8 where the minimum DOP between the power ratios occurs at 22 dB [24], yielding a minimum DOP of 0.61.

As mentioned above in section 5.1, PMDC systems often use DOP monitoring as a feedback signal because DOP monitoring meets the critical criteria for a feedback signal pertaining to

PMD compensation. The DOP magnitude gives an indication of the PMD in the fibre link. PMDCs do not factor in DOP degradation caused by XPM. This fact leaves PMDCs vulnerable to DOP degradation by XPM. The compensator will be unable to distinguish between DOP degradation from PMD in the fibre link and DOP degradation as a result of XPM in a WDM link. For example, if a signal's DOP is degraded as a result of XPM, the PMDC will assume the degradation is due to PMD and will try to correct the PMD based on the DOP magnitude. This will most likely worsen the overall PMD. Additional information inferred from the DOP are the PSPs as well as the second order PMD. Again both the PSPs and second order PMD determined in this scenario will be erroneous.

Figure 5.10 plots the time average probe rotation angle against the DOP of the probe signal. Here the angle between the probe and pivot is assumed to be 90^o. The time average of the rotation angle differs from the rotation angle.

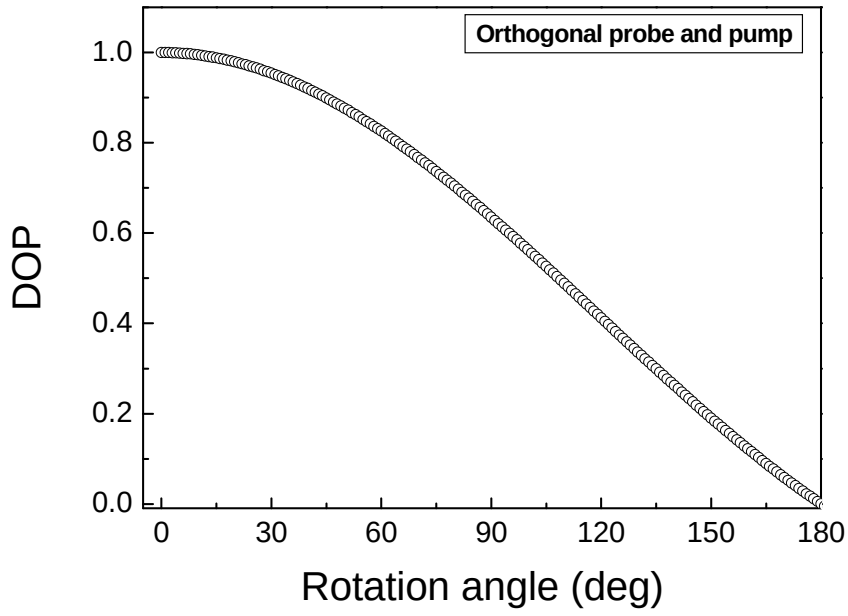

Figure 5.10 DOP plotted against the rotation angle, here the probe and modulated pump are assumed to be orthogonal.

The corresponding minimum DOP of the power ratio 15, 17, 19 and 22 dB is 0.96, 0.92, 0.86 and 0.61. Reading from figure 5.10 these power ratios yield time average rotation angles of 27^o, 29^o, 54^o and 93^o.

The minimum DOP at relative angles 90^o and 270^o will decrease as the pump power is increased. This rate of decrease is plotted in figure 5.11. Figure 5.11 shows that the DOP decreases gradually at first for low power ratios and then more rapidly for power ratios greater than 16 dB.

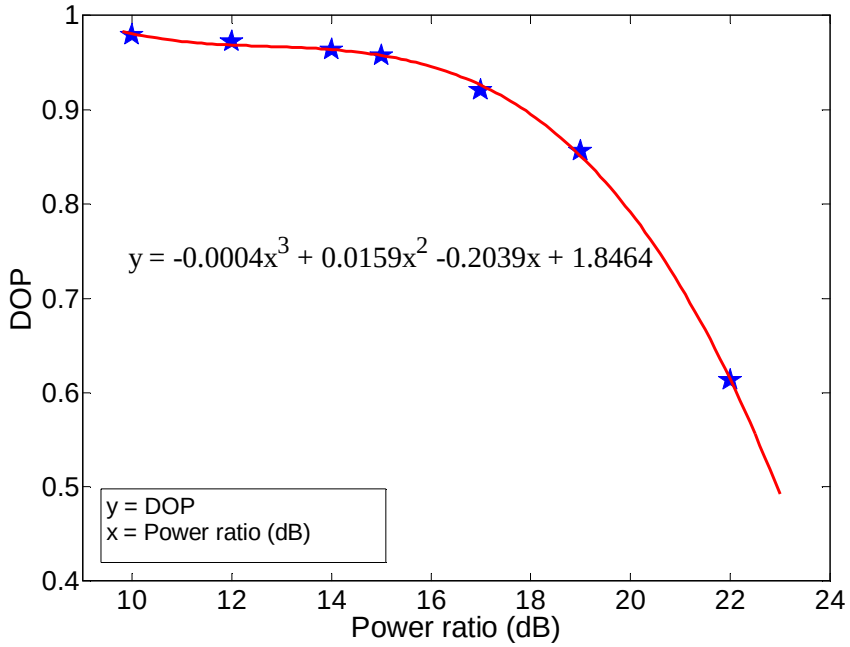

Figure 5.11 Minimum probe DOP corresponding to orthogonal pump and probe orientation.

The DOP is directly related to the probe SOP swing range. Therefore, figure 5.11 suggests that the pump and probe interaction through cross phase modulation (XPM), increases more rapidly after 16 dB power difference. The polynomial curve fit suggests that the DOP degrades according to the expression in figure 5.11 as the power ratio increases.

The above results show that the DOP was effectively degraded for the combination of a low power probe and a high power pump signal. The experiment was repeated where the probe signal was a continuous wave and the pump signal NRZ intensity modulated. The pump was then rotated and locked when the pump and probe SOP were orthogonal and a minimum DOP reached. The minimum probe DOP was monitored for 20 minutes at a time. The probe power was then increased from 3 dBm to 13 dBm while the DOP was recorded for 20 minutes each. This was repeated for two pump powers, 13 dBm and 20 dBm.

Figure 5.12 (a) shows the measured DOP of the probe and pump combination while figure 5.12 (b) summarizes these results in a single plot, where the average DOP of every power combination was plotted.

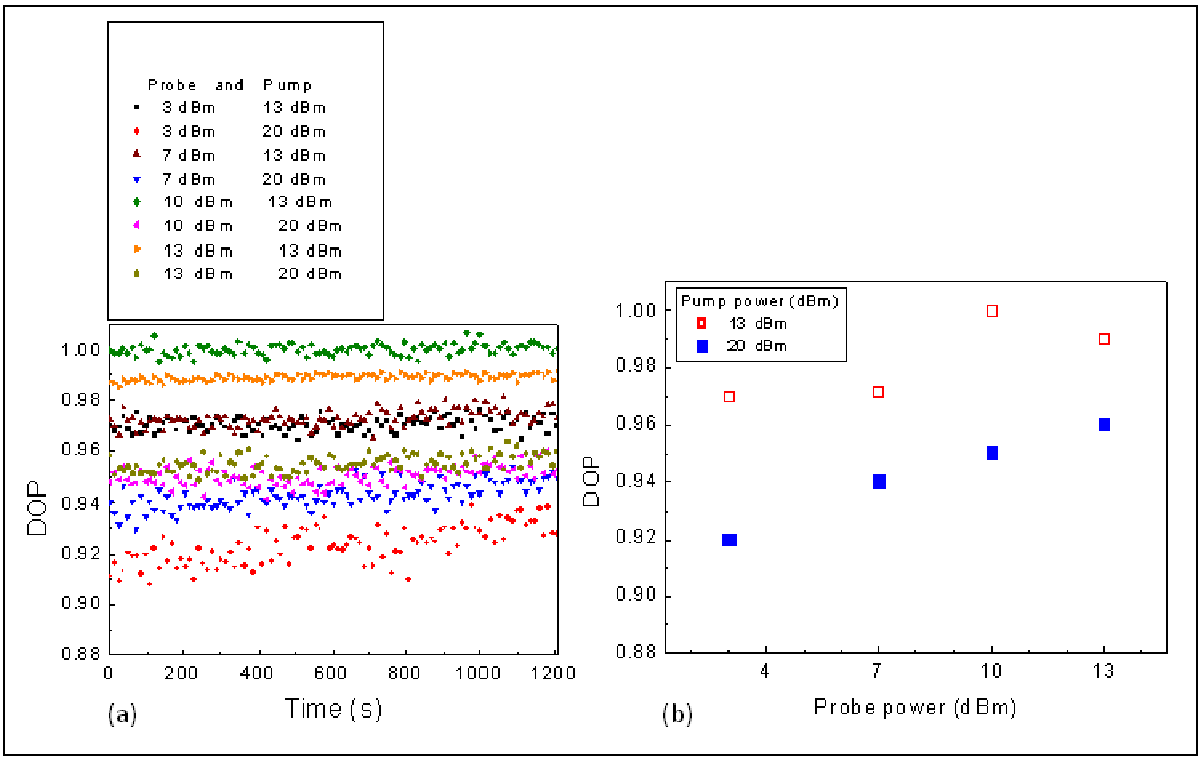

Figure 5.12 (a) Minimum DOP of probe signal over 1200 seconds, (b) DOP of probe signal as the probe power is increased relative to the pump power.

The DOP remains stable over the 20 minute period as shown in figure 5.12 (a). Reading from figure 5.12 (b) the DOP is degraded to 0.92 when the pump is 20 dBm and the probe power 3 dBm. The trend for the 20 dBm pump power shows that as the probe power is increased the probe signal is re-polarized as its DOP increases. Hence the probe SOP starts to swing less as the probe power increases. Therefore, the pump signal has less of an effect through XPM on the probe signal as the probe power is increased. For a pump power of 13 dBm, the DOP is almost unity for probe powers 10 dBm and 13 dBm which are comparable to the pump power. XPM is based on the principle that the refractive index seen by an optical wave is not only dependent on the intensity of that beam but also on the intensity of the neighbouring signal. Therefore, in the situation where the pump and probe power become comparable in intensity, the two signals impact each others phase equally.

It has been clearly demonstrated that the probe DOP is degraded for orthogonal probe and pump orientations. This degradation increases with an increase in power ratio as the probe SOP rotation angle becomes larger with an increase in power. XPM is the cause of this

degradation. This DOP degradation will definite mislead a PMDC which relies on DOP as a feedback signal. The DOP degradation due to XPM may be reduced by increasing the pump power, increasing the walk-off or by managing the probe-pump relative orientation.

CHAPTER 6

EVALUATION OF PROBE SIGNAL SOP FACTORING IN CROSS PHASE MODULATION

Intensity modulation of a pump signal leads to SOP modulation of a probe signal in a two channel WDM system, which further manifests into DOP degradation of the probe signal. The SOP modulation of the probe signal occurs as a result of XPM which results in cross polarization modulation (XPolM). The XPolM of the probe signal raises the question of the stability of the probe signal. This chapter briefly looks at the SOP drift of a low intensity probe signal for different scenarios.

6.1 Experimental setup

As in previous schemes the pump and probe signals were multiplexed and transmitted over 24.7 km of DSF. The pump signal, at 1552.12 nm, was amplified to higher powers with an EDFA. The probe signal was recovered with a polarimeter after filtering the signal using a 50 GHz multiplexer and a tuneable filter, as illustrated in figure 6.1. The probe SOP was logged for three scenarios. In the first case, the pump signal was left off and the probe signal switched on, here the probe signal is left as a continuous wave. In the second case the pump signal is switched on, modulated and amplified. The probe signal is switched on as well and left as a continuous wave. In figure 6.1 this implies replacing A with 1 and B with 2. The third scheme involved modulating both the pump and probe signal simultaneously and amplifying both signals before transmission. The SOP of the probe signal was monitored and recorded continuously for two days.

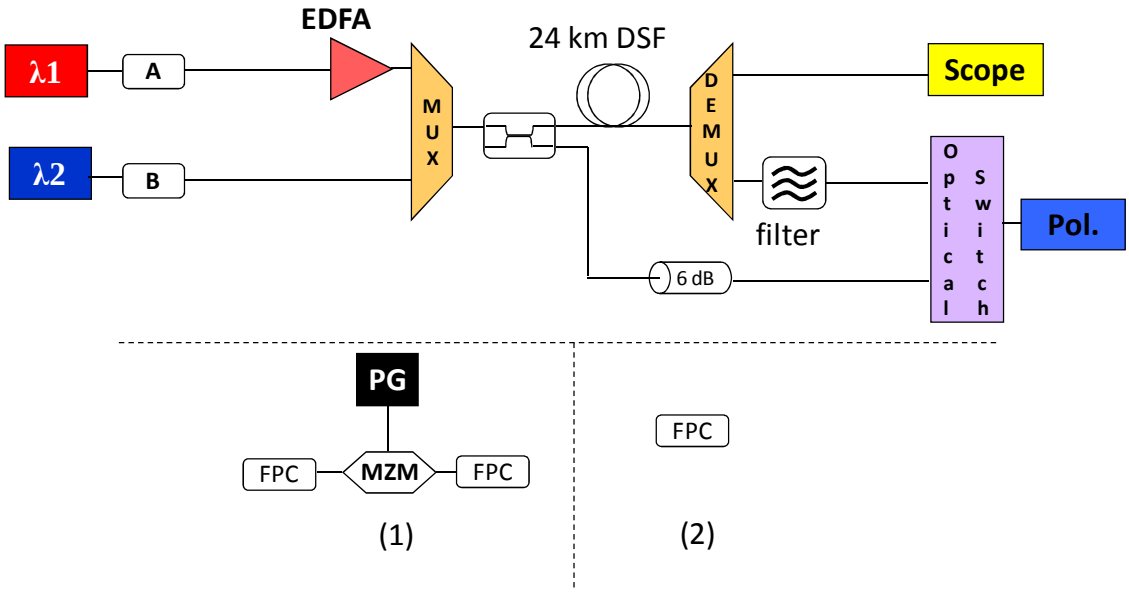

Figure 6.1 Pump and probe signal are multiplexed and transmitted over DSF. The probe signal SOP is monitored for modulating and continuous wave combinations of the pump and probe signal.

6.2 Probe SOP migration

6.2.1 Transmission of probe signal

As mentioned previously, the fibre birefringence is the difference between the refractive indices of the orthogonal polarization modes [62]. Deviation from the circular symmetry of an ideal fibre leads to an anisotropic refractive index distribution which introduces birefringence [62]. In practical optical fibres, birefringence is caused by a noncircular core, asymmetrical lateral stress, bending and twists [62], all of which bring about asymmetry within of the fibre core. Hence the two polarization modes propagate with different phase velocities. A change in the birefringence manifests as a change in the SOP and a change in the differential group delay (DGD). Fibre optic interferometric sensors and coherent communication systems rely on the polarization state of the light [62]. Temperature variation causes stress on the fibre core, this leads to stress birefringence [62]. Refer to [62] for a plot of the birefringence against temperature.

Figure 6.2 is a plot of the temperature measured over a period of two days. A thermocouple was used to measure and log the temperature. The thermocouple was placed directly next to

the DSF fibre spool in a laboratory with air conditioning that is meant to maintain a constant temperature.

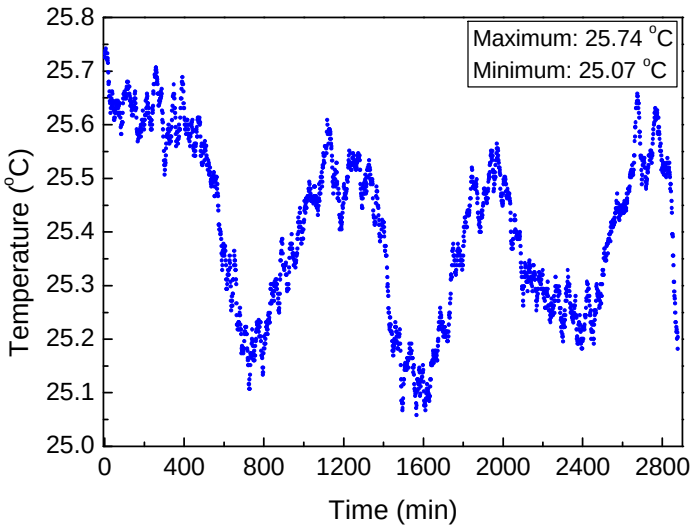

Figure 6.2 Temperature inside the laboratory next to the DSF over a two day period.

A periodic temperature fluctuation is evident in figure 6.2.The temperature measurement was found to vary between 25.07 ^{o}C and 25.74 ^{o}C, figure 6.2.

Considering scenario one as described above, the probe SOP for a continuous wave signal was recorded over a two day period. This was done in the absence of any pump signal. Figure 6.3 shows the SOP results. As seen on the Poincaré sphere in figure 6.3, the probe signal SOP drifts and traces out a path on the Poincaré sphere, figure 6.3 (a). It is evident that the SOP has migrated all the way past its orthogonal counterpart and back within the region of its original starting position. It should be kept in mind that this occurs over a two day period. This slow migration of the SOP may be attributed to the slow temperature change. As the temperature varies it causes the fibre to expand or contract, this process induces stress birefringence which leads to a change in the SOP [62].

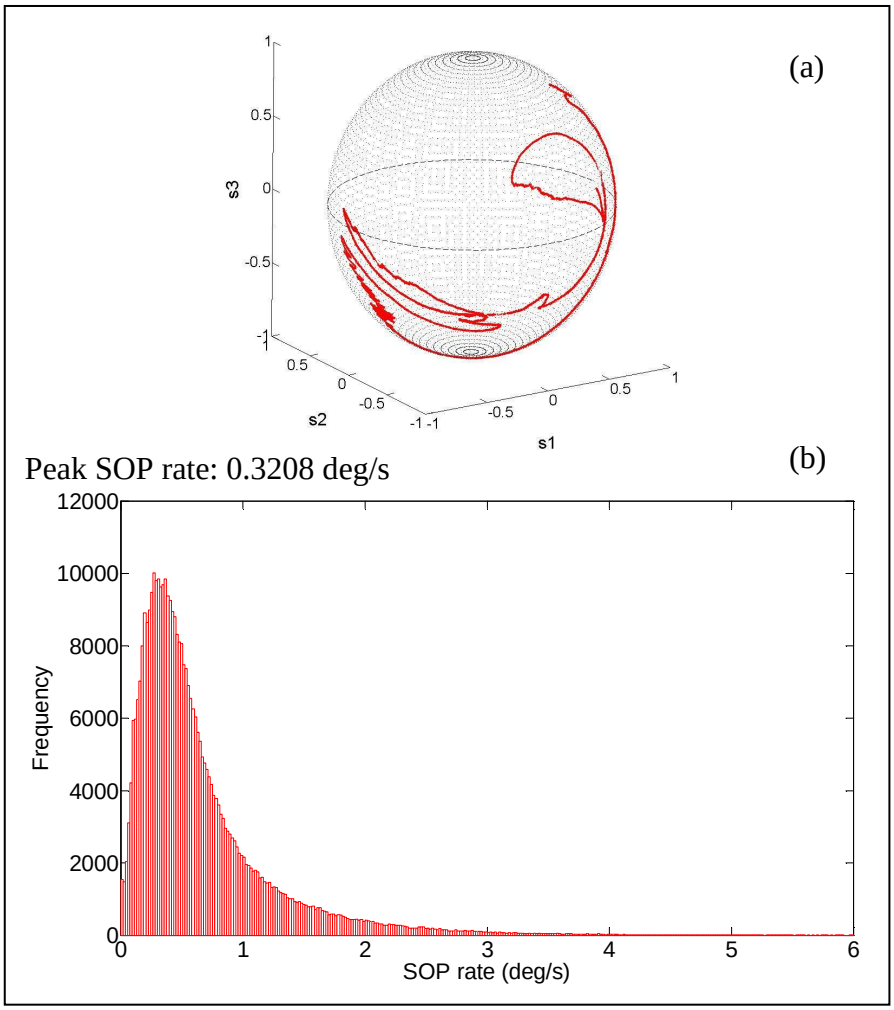

Figure 6.3 SOP response of probe signal: Continuous wave probe signal in the absence of a pump signal.

Figure 6.3 (b) is a histogram plot of the SOP rate, hence the x-axis indicates the SOP rate as the angle of rotation per second while the y-axis relates to the number of occurrences of a particular SOP rate. The angle was calculated by considering each SOP as a vector.

The rate is then the angle between the current and previous vector divided by the time it took to move from the previous to the current SOP. The peak of the histogram in figure 6.3 (b) is located at approximately 0.32 deg/s indicating that the majority of SOP movements occurred at a rate of 0.32 deg/s.

6.2.2 Co-transmission of probe and pump signals

The same experiment was repeated for scenario two where the probe signal was multiplexed with a NRZ modulated pump signal. The bit rate of the pump signal was 10.3 Gbps. The probe signal was kept as a continuous wave.

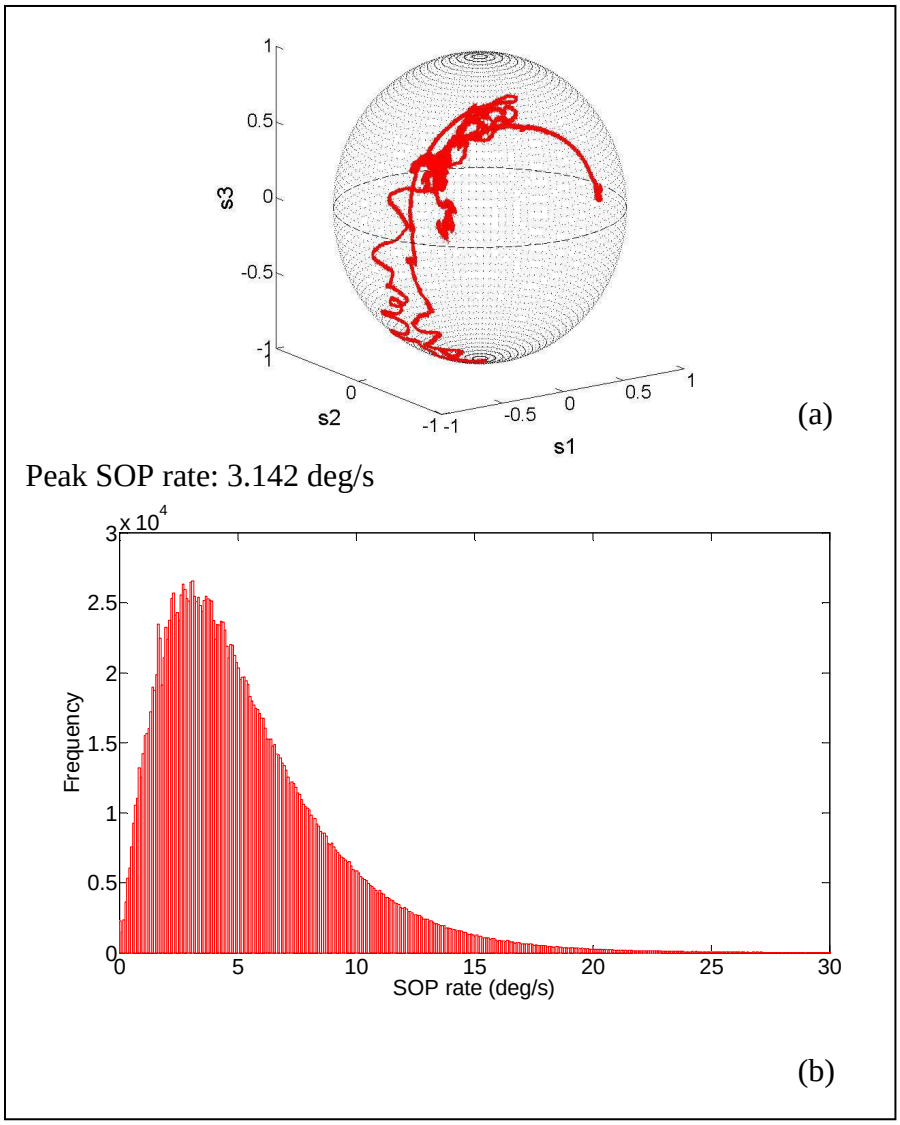

Figure 6.4 SOP response of probe signal: Continuous wave probe signal in the presence of a modulated pump signal.

Here the probe and pump signal pre-transmission power was 3 dBm for the probe and 25 dBm for the pump. From the Poincaré sphere in figure 6.4 (a), it can be seen that the probe SOP is more active as compared to singular transmission of the probe signal only. Figure 6.4 (b) is again a histogram plot of the SOP angular rate of change (measured in degrees per second). The majority SOP rate again appears at a peak value, after which the SOP rate tails off exponentially. The peak in this case appears at 3.14 deg/s. This is much faster than the 0.32 deg/s for the lone probe signal transmission. Therefore the SOP in this case is much more active. The extra activity is attributed to XPM of the probe signal by the pump signal. The pump signal is intensity modulated, hence the probe signal SOP is modulated through XPM. The polarimeter can sample at a maximum sampling rate of 1

MHz. In these experiments the SOPs were sampled at a rate of 13 Hz, which is an ample sampling rate to detect all the activity.

The same experiment was again performed for scenario three, where both the pump and signal were modulated.

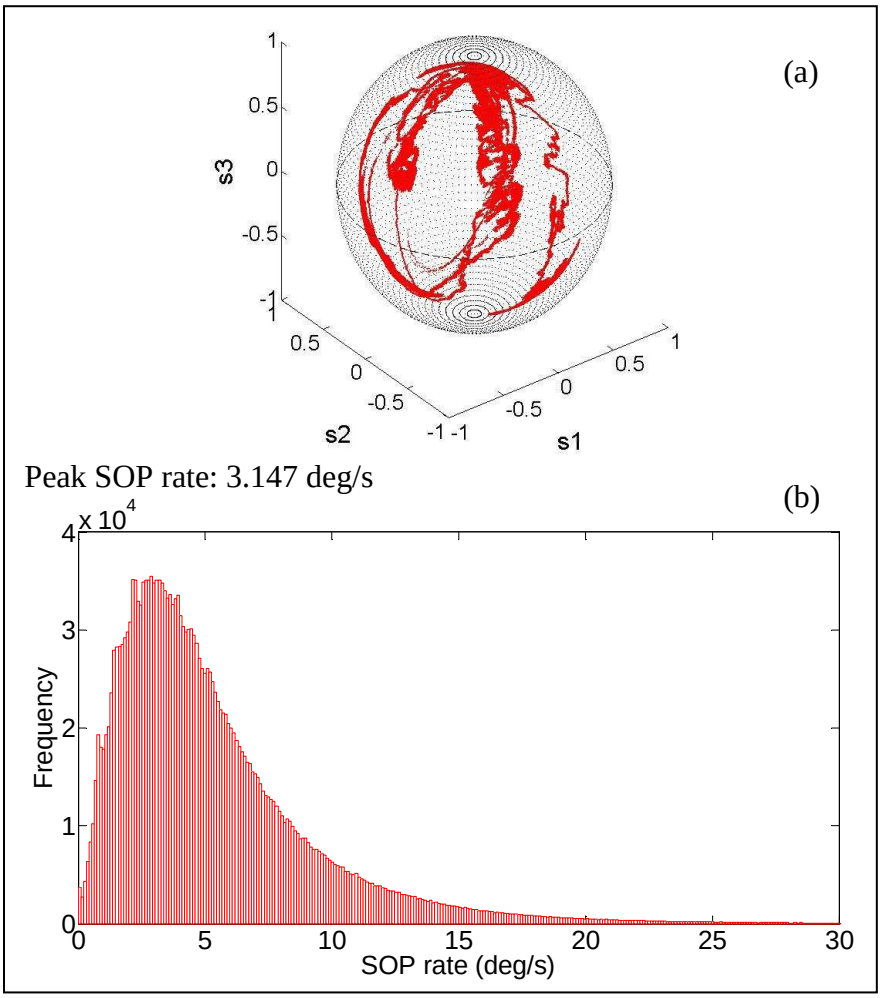

Figure 6.5 SOP response of probe signal: Multiplexed modulated pump and probe signals.

Figure 6.5 shows that the probe SOP becomes even more unstable for this last scenario. The histogram indicates that the majority probe SOP rate of change now increases to 3.15 deg/s. This does not differ much from scenario two, however the visibly increased activity on the Poincaré sphere indicates that the probe SOP covers a larger area. The maximum probe SOP rates for cases on, two and three are: 9.4 deg/s, 80.6 deg/s and 1049 deg/s. The last two scenarios suggests that the probe SOP is more active in the presence of a modulated pump wave whether the probe signal is modulated or not.

CHAPTER 7

CONCLUSIONS

WDM networks face several challenges. Cross phase modulation (XPM) is one of these critical challenges. XPM leads to modulation of the phase of co-propagating signals. This may be problematic to co-propagating wavelength channels in operational optical networks. XPM also presents difficulty to polarization mode dispersion compensators as well as to polarization sensitive receivers.

In this thesis the nature of XPM was investigated. The work was limited to observing the effects of XPM on a probe signal in the presence of a pump signal; hence the study was limited to a two channel WDM network. This allows for the observation of the direct effect a pump signal has on a co-propagating probe signal with respect to XPM. The theoretical background of nonlinear effects was covered in Chapter 3. Theoretical and experimental work from literature was reviewed for the various nonlinear effects found in optical fibre. A section in chapter 3 looks into the physics and mathematics background of XPM in optical fibre. Literature shows that in a two wave WDM system, the intensity of the two signals causes a phase shift in the neighbouring signal. It has also been proven that the Stokes vectors of a probe and pump signal rotate with the same rate around a constant vector. This vector is known as the pivot and is the resultant sum of the probe and pump signal. It has been shown that these polarization changes occur at the bit rate. Researchers have also look into the effect intensity modulation has on a neighbouring optical signal.

The refractive index experienced by an optical signal is affected by the intensity of a neighbouring optical signal. This may lead to a phase change which is dependent on the intensity of the neighbouring signal. The first experiment discussed in chapter 4 investigated the stability of a probe signal's SOP in the presence of a pump signal over a short period of time. A probe and pump signal, 50 GHz apart, were transmitted over 24.7 km DSF and over an emulator. The probe signal SOP was recorded over a 30 minute time span. The probe signal power was fixed at 3 dBm while the pump power was increased to 13 dBm in a 1 dB interval step.

The cumulative angle shows the overall migrations of the probe SOP over a period of time. The cumulative angle for different power ratios were plotted against the cumulative angle for the case of a probe signal transmitted without a pump signal. It was found the SOP is relatively stable for all cases; however for higher pump powers the probe SOP did appear to migrate more than the single signal transmission scenario for both the DSF and emulator. The relative angle for this experimental data was also computed. The relative angle refers to the displacement between any SOP vector in time to the initial SOP vector. The relative angle SOP against time plot revealed a periodic trend for transmission over the emulator. The figure plotting the relative trend showed that the SOP vector of the probe signal for cases when the pump power was high is much less stable than for single transmission, probe only. It also showed a periodic signature indicating that the probe SOP migrates away from the initial SOP in an oscillating fashion. This is most likely caused by the many mode coupling sections in the emulator.

The experiments that followed set out to examine the remote control capability of XPM. Again a pump and probe signal were co-transmitted over 24.7 km DSF. The pump and probe power difference was maintained at 16 dB. A lithium niobate based polarization controller rotated the pump signal SOP to form a large circle on the Poincaré sphere. The experimental results showed that the probe signal SOP mimicked the pump signal trajectory, but on a smaller scale. The same experiment was repeated, only this time the pump traced out a figure eight on the Poincaré sphere. The result was a smaller figure eight traced out by the probe signal. The explanation for this effect lies in the propagation equations for XPM. These equations show that the probe signal SOP is not only affected by a change in the pump signal intensity but also by the change in the pump signal SOP. The pump signal SOP was then randomly scrambled over 500 SOPs to cover the entire Poincaré sphere. The probe signal SOP responded in the same fashion; however the probe SOP covered a limited area of the sphere.

The last experiment in chapter 4 sets out to demonstrate a potential application for the effect of altering the probe SOP by changing the pump SOP. Data was imposed on the pump signal by a MZM as well as by writing data onto the pump signal using a polarization controller. The information is transmitted over 24.7 km of DSF. The pump signal's polarization modulated data is transferred to the probe signal by XPM. A de-multiplexer and digital tuneable filter separated the probe from the pump. A polarizer at the end transferred the

polarization modulated probe signal into an intensity modulated signal. Results were shown for transmission over 24.7 km DSF and 28.8 km buried single mode fibre (SMF). All the bits are recovered on the probe signal. This is an example of a wavelength converter. The dynamic range of the recovered intensity pulses was found to be constant at 2.85 dB. The baseline of the bit period was found to fluctuate over time which is a result of the non stationary SOP. Hence the probe SOP is changing not only because the pump SOP is hanging but from other effects. This additional activity may be attributed to temperature fluctuations, external mechanical activity and possibly from the effects of XPM by the intensity modulation of the pump signal.

Polarization mode dispersion has a pulse broadening effect on optical pulses and may lead to inter-symbol interference. Modern fibres have much lower PMD coefficients than legacy fibre, hence bit rate transmission up to 40 Gbps does not present a problem. However beyond 40 Gbps PMD is most likely to be problematic. To avoid replacing legacy fibre and to counter the problem presented by PMD for high bit rates, network operators make use of polarization mode dispersion compensators (PMDCs). PMDCs are based on the operating principle of monitoring a feedback signal and correcting the PMD. The link PMD is monitored indirectly. The signal's degree of polarization (DOP) has been proven to be the preferred monitoring signal. It tracks the link PMD fairly well, it has a fast response time and is independent of the bit rate. XPM may present misleading information to a polarization mode dispersion compensator (PMDC). In a two signal WDM network a change in the intensity of a pump signal will lead to a change in the phase of a probe signal caused by XPM. This in turn implies a change in the SOP of the probe signal. Therefore rapid intensity modulation of a pump signal leads to rapid polarization modulation of a neighbouring probe signal as a result of XPM. This polarization modulation of the probe signal, manifests as DOP degradation of the probe signal.

Experimental results show the DOP degradation of a probe signal in the presence of a high intensity pump signal. A pump signal was intensity modulated, multiplexed with a probe signal 50 GHz away and transmitted over 24.7 km DSF. The pump signal was amplified with an EDFA. A half waveplate rotated the pump SOP to trace out a circle on the Poincaré sphere. This process was repeated for several pump powers. The results show that the DOP degrades to a maximum for two distinct probe and pump orientations. Maximum DOP degradation is achieved when the probe and pump signal SOP vectors are 90^{o} and 270^{o} apart.

Therefore maximum XPM interaction occurs between the probe and pump signal, when the signals are positioned orthogonal with respect to each other. Further, the probe signal DOP at these pivotal angles decreases with an increase in pump power. The probe signal power was maintained at 3 dBm whereas the pump signal power was varied from 13 dBm to 25 dBm. Maximum DOP degradation of the probe signal, a DOP of 0.61, was shown for a pump power of 25 dBm. We show these result in [24]. This DOP degradation caused by XPM may be misleading to a PMDC because the DOP degradation can be mistaken for PMD in the link. Thus the compensator will react by trying to compensate for the PMD which will most likely worsen the PMD in the link. Theoretical computation agrees with the experimental results in that the greater the rotation angle the lower the DOP for orthogonal pump and probe orientation. It is shown that the decrease in DOP for orthogonal probe and signal orientations for higher pump power levels follows the trend of a third degree polynomial. The probe signal DOP degradation can be minimized by reducing the pump power and operating with low probe and signal powers. Another method is to increase the walk-off. The walk-off, as defined in chapter 3, is the product of the chromatic dispersion and the channel spacing between signals. The walk-off can be increased by using fibres with some dispersion or by increasing the channel spacing between signals. The results also suggest that the DOP degradation can be managed by controlling the SOP orientation of the pump and probe.

Polarization sensitive receivers require a stable SOP. Coherent receivers have many advantages but are sensitive to the phase and SOP of the incoming signal. Chapter 6 investigated the stability of a probe signal in the absence and presence of a continuous and modulated wave pump signal. The probe SOP was monitored over a two-day period. The experiment was performed for three scenarios. First, the continuous wave probe signal SOP was monitored in the absence of a pump signal. Second, a 3 dBm continuous wave probe signal was multiplexed with a 25 dBm pump signal which was NRZ modulated at a bit rate of 10.3 Gbps. For the third scenario, both the pump and probe signal were modulated and multiplexed. The transmission was over 24.7 km DSF. The histogram plot of all three scenarios showed the SOP rate of change of the probe signal peaks at a specific rate and then tails off, similar to a Maxwellian distribution. For scenario one the SOP rate peaks at 0.321 deg/s, scenario two at 3.142 deg/s and scenario three at 3.147 deg/s. This clearly indicates that the probe SOP shows more activity in the presence of a modulated pump signal.

Future generation optical networks will implement DWDM. Network operators are looking into solutions such as wavelength switched optical networks (WSON). It is envisioned that these networks will be much more dynamic, capable of adapting to network demands. A good understanding of XPM will be crucial to make such networks feasible. This thesis investigated the characteristics of XPM using different scenarios. It is evident that at high power levels XPM will clearly pose a threat to optical networks. As mentioned previously the effects of XPM can be lowered by; operating below the threshold power for XPM, increasing the walk-off using larger channel spacing as well as ensuring that the fibre has some dispersion and by managing the pump-probe SOP vector orientation to minimise their interaction. Future work should look into other potential solutions to minimise the effects of XPM. These solutions may be applied in the decision making process in WSON networks, when needed. Not much is understood regarding the statistical nature of XPM. Researchers are now looking into defining degrees of freedom of a system in order to analyse the impairments XPolM place on polarization division multiplexed (PolDM) systems [73, 74]. Phase modulated signals have a low tolerance to XPM, in [39] stochastic parameters such as the variance of the XPM induced phase noise is determined. This leads to quantification of the impact of XPM. In addition to extending the understanding statistical nature of XPM and XPolM, researchers have also been looking into compensation of XPM. Simple intensity dependent phase modulation has been shown to improve the transmission penalty by 4 dB in a coherent optical orthogonal frequency division multiplexing (CO-OFDM) system [18]. The effect XPM has on other modulation formats and multiple modulation formats, still needs further investigation as well. Phase modulation, together with coherent detection has also been proposed as a viable solution to XPM. Other solutions such as bit-synchronous polarization scrambling to suppress nonlinear effects as well as PMD, are also currently under investigation.

APPENDIX 1

Research Outputs during Doctoral Study

Conference

T. V. Chabata, E. Rotich, **R. R. G. Gamatham**, A. W. R. Leitch and T. B. Gibbon, "Performance comparison of OOK, NRZ and DPSK modulation formats in an optical transmission system", 5th African Laser Centre workshop, University of Namibia, Windhoek, Namibia, 14-18 November (2012).

Publications in conference proceedings

R. Gamatham, T. B. Gibbon and A. W. R. Leitch, "Experimental Demonstration of an Adaptive Poincaré sphere analysis and the Fixed Analyzer Polarization Mode Dispersion Measurement Techniques", Proc. of the Southern Africa Telecommunication Networks and Applications Conference (SATNAC), Royal Swazi Spa, Swaziland, ISBN: 9780620441063, pp. 233 – 236, 30 August – 2 September (2009).

T. B. Gibbon, X. Yu, **R. Gamatham**, N. G. Gonzalez and I. T. Monroy, "3.125 Gb/s Impulse Radio UWB over Fiber Transmission", ECOC, Vienna, Austria, ISBN 978-1-4244-5096-1, 20-24 September (2009).

R. R. G. Gamatham, T. B. Gibbon and A. W. R. Leitch, "Cross phase modulation induced depolarization of a probe signal and its impact on polarization mode dispersion compensators", 56th SAIP conference, University of South Africa, Pretoria, Proc. SAIP, Section-C, Lasers, Optics and Spectroscopy, pp. 398-402, ISBN: 978-1-86888-688-3, 12-15 July (2011).

H. Y. S. Kourouma, E. K. Rotich, D. Waswa, **R. Gamatham**, T. B. Gibbon and A. W. R. Leitch, "The Effects of Polarization States on a Reference Signal for Timing and Signal

Distribution", SATNAC, Fancourt in George, Western Cape, South Africa, 2-5 September (2012).

Journal publications

T. B. Gibbon, X. Yu, **R. Gamatham**, N. G. Gonzalez, R. Rodes, J. B. Jensen, A. Caballero and I. T. Monroy, "3.125 Gbps Impulse Radio Ultra-Wideband Photonic Generation and Distribution over a 50 km Fiber with Wireless Transmission" IEEE Microw. Wireless Compon. Lett., Vol. 20, No. 2, pp. 127 – 129, February (2010).

R. R. G. Gamatham and A. W. R. Leitch, "Characterization of cross-polarization modulation on a two channel WDM system", Opt. Commun., Vol. 285, pp. 4125-4129, July (2012).

F. Chiarello, L. Palmieri, M. Santagiustina, **R. Gamatham** and A. Galtarossa, "Experimental characterization of the counter-propagating Raman polarization attraction", Opt. Express, Vol. 20, No. 23, pp. 26050 – 26055, November (2012).

REFERENCES

1. G. P. Agrawal, “Nonlinear Fibre Optics”, Third edition, Academic press, United Kingdom, (2001).

2. B. J. Ainslie and C. R. Day, “A Review of Single Mode Fibers with Modified Dispersion Characteristics”, J. of Lightwave Technol., Vol. 4, No. 8, pp. 967-979, (1986).

3. E. Bartholinus, “Experimenta crystalli islandici disdiaclastici quibus mira & insolita refractio detegitur”, Copenhagen: Hafniæ, Denmark: Daniel Paulli (1669).

4. E. Bartholinus, “Experiments with the double refracting Iceland crystal which led to the discovery of a marvelous and strange refraction”, tr. by Werner Brandt, Westtown, Pa., (1959).

5. J. L. Blows, P. Hu and B. J. Eggleton, “Differential group delay monitoring using an all-optical signal spectrum-analyser”, Opt. Commun., Vol. 260, pp. 288-291, (2006).

6. A. Bononi, A. Vannucci, A. Orlandini, E. Corbel, S. Lanne and S. Bigo, “Degree of Polarization Degradation Due to Cross-Phase Modulation and Its Impact on Polarization –Mode Dispersion Compensators”, J. Lightwave Technol., Vol. 21, No. 9, pp. 1903 – 1913, (2003).

7. G. Bosco, B. E. Olsson and D. J. Blumenthal, “Pulsewidth Distortion Monitoring in a 40 Gb/s Optical System Affected by PMD”, Photon. Technol. Lett., Vol.14. No. 3, pp. 307-309, (2002).

8. C. Brisseau, “Fundamentals of Polarized Light: A Statistical Optics Approach”, John Wiley & Sons, (1998).

9. F. Bruyère, “Impact of First and Second order PMD in Optical Digital Transmission Systems”, Opt. Fibre Tech., Vol. 2, pp. 269-280, (1996).

10. R. Y. Chiao, C. H. Townes, and B. P. Stoicheff, “Stimulated Brillouin Scattering and Coherent Generation of Intense Hypersonic Waves”, Phys. Rev. Lett. 12, pp. 592-595, (1964).

11. F. Chiarello, L. Ursini, L. Palmieri and M. Snatagiustina, “Polarization Attraction in Counterpropagating Fiber Raman Amplifiers”, IEEE Photon. Technol. Lett., Vol. 23, no. 20, pp. 1457-1459, (2011).

12. P. C. Chou, J. M. Fini and H. A. Haus, “Real-Time Principal State Characterization for use in PMD Compensators”, IEEE Photon. Technol. Lett., Vol. 13, no. 6, pp. 568-570 (2001).

13. P. C. Chou, J. M. Fini and H.A. Haus, “Demonstration of a Feed-Forward PMD Compensation Technique”, IEEE Photon. Technol. Lett., Vol. 14, no. 2, pp. 161-163 (2002).

14. A. R. Chraplyvy and J. Stone, “Measurement of Crossphase Modulation in Coherent Wavelength-Division Multiplexing Using Injection Lasers”, IEEE Electron. Lett., Vol. 20, No. 24, pp. 996-997, (1984).

15. B. C. Collings and L. Boivin, “Nonlinear Polarization Evolution Induced by Cross-Phase Modulation and its Impact on Optical Transmission Systems”, IEEE Photon. Technol. Lett., Vol. 12, no. 11, pp. 1582-1584, (2000).

16. F. Curti, B. Daino, G. De Marchis, and F. Matera, “Statistical treatment of the evolution of the principal states of polarization in single-mode fibers” IEEE J. Lightwave Technol., Vol. 8, no. 8, pp. 1162-1166, (1990).

17. D. Derickson, “Fiber Optic Test and Measurement”, Prentice Hall Inc., (1998).

18. L. B. Du, and J. Lowery, “Practical XPM compensation method for coherent optical OFDM systems”, Photon. Technol. Lett., Vol. 22, No. 5, (2010).

19. H. J. R. Dutton, “Understanding Optical Communications”, First edition, International Business Machine Corporation, (1998).

20. T. H. Elmer, “Dehydroxylation of Porous Glass by means of Chlorine”, Journal of the American Ceramic Society, Vol. 64, Issue 3, pp. 150-154, (1981).

21. M. Ferrario, V. Gilardone, P. Martelli, L. Marazzi, and M. Martinelli, “Effective all-optical polarization control induced by Raman nonlinear amplification,” in Proc. ECOC, Torino, Italy, Sep. 19–23, p. P1.19, print ISBN: 978-4244-8536-9, pp. 1-3, (2010).

22. G. J. Foschini and C. D. Poole, “Statistical Theory of Polarization Dispersion in Single Mode Fibers”, J. Lightwave Technol., Vol. 9. No. 11, pp. 1439-1456, (1991).

23. A. Galtarossa, L. Palmieri, M. Santagiustina and L. Ursini, “Polarized backward Raman amplification in randomly birefringent fibers,” J. Lightwave Technol., Vol. 24, no. 11, pp. 4055–4063, (2006).

24. R. R. G. Gamatham and A. W. R. Leitch, “Characterization of cross-polarization modulation on a two channel WDM system”, Opt. Commun., Vol. 285, Issue 20, pp. 4125-4129, (2012).

25. N. Gisin, J. P. Von der Weid and J. P. Pellaux, “Polarization Mode Dispersion of Short and Long Single-Mode Fibers”, J. Lightwave Technol., Vol. 9, No. 7, pp. 821-827, (1991).

26. N. Gisin and J. P. Pellaux, “Polarization mode dispersion time versus frequency domains”, Opt. Commun., Vol. 89, pp. 316-323, (1992).

27. N. Gisin, R. Passy, P. Blasco, M. O. Van Deventer, R. Distl, H. Gilgen, B. Perny, R. Keys, E. Krause, C. C. Larsen, K. Mörl, J. Pelayo and J. Vobian, “Definition of polarization mode dispersion and first results of the COST 241 round-robin measurements”, Pure Appl. Opt., Vol. 4, pp. 511-522, (1995).

28. D. Gloge, “Dispersion in Weakly Guiding Fibers”, Appl. Opt., Vol. 10, No. 11, pp. 2442-2445, (1971).

29. J. P. Gordon and H. Kogelnik, “PMD Fundamentals: Polarization Mode Dispersion in Optical Fibers”, Proceedings of the National Academy of Sciences (PNAS), Vol. 97, No. 9, pp. 4541-4550, (2000).

30. C. Headley and G. Agrawal, “Raman Amplification in Fiber Optical Communication Systems”, Elsevier, (2005).

31. F. Heismann, “Tutorial: Polarization mode dispersion: Fundamentals and impact on optical communication systems,” in European Conference on Optical Communication (ECOC’98), Vol. 2, pp. 51–79, (1998).

32. C. Huyghens, “Treatise on Light”, tr. by S. P. Thompson, University of Chicago press, (2005).

33. IEC TR 61282-9 Technical Report (2006-2007), “Fibre optic communication system design guides – Part 9: Guidance on Polarization Mode Dispersion measurement and theory”, 1st edition (2006-2007).

34. ITU-T Recommendation G.655, “Characteristics of a non-zero dispersion shifted single-mode optical fibre and cable”, November, (2009).

35. ITU-T Recommendation G.653, “Characteristics of a dispersion-shifted, single-mode optical fibre and cable”, July, (2010).

36. R. C. Jones, “A New Calculus for the Treatment of Optical Systems”, J. Opt. Soc. Am., Issue 7, pp. 488-493, Vol. 31, (1941).

37. G. Keiser, “Optical Fiber Communication”, Third edition, McGraw-Hill Companies, (2000).

38. N. Kikuchi, “Analysis of Signal Degree of Polarization Degradation Used as Control Signal for Optical Polarization Mode Dispersion Compensation”, J. Lightwave Technol., Vol. 19, No. 4, pp. 480-486, (2001).

39. D. I. Kroushkov, S. Warm, M. Winter, and K. Petermann, “Simple estimation of the XPM-induced phase error variance in hybrid OOK-PSK systems”, Photon. Technol. Lett., Vol. 24, no. 9, (2012).

40. S. Lane, W. Idler, J. P. Thiéry and J. P. Hamaide, “Demonstration of adaptive PMD compensation at 40 Gb/s”, Optical Fiber Communications Conference, print ISBN: 1-55752-655-9, TuP3-1-4, (2001).

41. S. Lanne, W. Idler, J. P. Thiery and J. P. Hamaide, “Fully automatic PMD compensation at 40 Gbit/s”, Electron. Lett. Vol. 38, No. 1, pp. 40-41, (2002).

42. Q. Lin and G. P. Agrawal, “Vector theory of stimulated Raman scattering and its application to fiber-based Raman amplifiers,” J. Soc. Amer. B, Vol. 20, no. 8, pp. 1616–1631, (2003).

43. S. V. Manakov, “On the theory of two-dimensional stationary self-focusing of electromagnetic waves”, Zh. Eksp. Teor. Fiz. 65, 505 (1973) [Sov. Phys. JETP 38, 248 (1974)].

44. M. Martinelli, M. Cirigliano, M. Ferrario, L. Marazzi and P. Martelli, “Evidence of Raman-induced polarization pulling,” Opt. Express, Vol. 17, no. 2, pp. 947–955, (2009).

45. J. C. Maxwell, “A Dynamical Theory of the Electromagnetic Field”, Trans. Camb. Phil. Soc. Lond. Vol. 155, pp. 495-512, (1865).

46. A. Méndez and T. F. Morse, “Speciality Optical Fiber Handbook”, Elsevier Inc., (2007).

47. L. F. Mollenauer, J. P. Gordon and F. Heismann, “Polarization scattering by soliton-soliton collisions”, Opt. Lett. Vol. 20, Issue 20, pp. 2060-2062, (1995).

48. R. No´e, D. Sandel, M. Yoshida-Dierolf, S. Hinz, V. Mirvoda, A. Sch¨opflin, C. Glingener, E. Gottwald, C. Scheerer, G. Fischer, T. Weyrauch, and W. Haase, “Polarization Mode Dispersion Compensation at 10, 20, and 40 Gb/s with Various Optical Equalizers”, J. Lightwave Technol., Vol. 17, No. 9, pp. 1602-1616, (1999).

49. D. Penninckx, F. Roy, S. Lanne and J. P. Thiery, “Statistical study of dynamic polarization mode dispersion compensation based on degree of polarization monitoring”, Microw. Opt. Technol. Lett., Vol. 26, Issue 1, pp. 37 – 39, (2000).
50. D. Penninckx and S. Lanne, “Reducing PMD impairments”, Optical Fiber Communications Conference, TuP1, print ISBN: 1-55752-655-9, (2001).

51. F. L. Pedrotti and L. S. Pedrotti, “Introduction to Optics”, Second edition, Prentice Hall Inc., (1993).

52. S. Pitois, A. Sauter and G. Millot, “Simultaneous achievement of polarization attraction and Raman amplification in isotropic optical fibers,” Opt. Lett. Vol. 29, pp. 599-601 (2004).

53. S. Pitois, J. Fatome and G. Millot, “Polarization attraction using counter-propagating waves in optical fiber at telecommunication wavelengths,” Opt. Express, Vol, 16, pp. 6646-6651 (2008).

54. C. D. Poole and R. E. Wagner, “Phenomenological Approach to Polarisation Dispersion in Long Single-Mode Fibres”, Electron. Lett., Vol. 22, No. 19, pp. 1029-1030, (1986).

55. C. D. Poole, “Statistical treatment of polarization dispersion in single mode fiber”, Opt. Lett., Vol. 13, pp. 687-689, (1988).

56. C. D. Poole, N. S. Bergano, R. E. Wagner and H. J. Schulte, “Polarization Dispersion and Principal States in a 147-km Undersea Lightwave Cable”, J. Lightwave Technol., Vol. 6, No. 7, pp. 1185-1190, (1988).

57. C. D. Poole and J. A. Nagel, “Polarization effects in lightwave systems,” in Optical Fiber Telecommunications IIIA, I. P. Kaminow and T. L. Koch, eds. (Academic Press, San Diego), pp. 114-161, (1997).

58. H. Y. Pua, K. Peddanarappagari, B. Zhu, C. Allen, K. Demarest, and R. Hui, “An adaptive first-order polarization-mode dispersion compensation system aided by polarization scrambling: theory and demonstration”, J. Lightwave Technol., Vol. 18, Issue 6, pp. 832 – 841, (2000).

59. C. V. Raman, “The Raman Effect”, Indian J. Phys., Vol. 2**,** 387 (1928).

60. C. V. Raman, “The Raman Effect”, *Nature, Vol.* **125**, pp. 205-207, (1930).

61. R. Ramaswami, K. N. Sivarajan, “Optical Networks A Practical Perspective”, Second edition, Academic press, United Kingdom, (2002).

62. S. C. Rashleigh, “Origins and control of polarization effects in single-mode fibers”, J. Lightwave Technol., Vol. LT-1, pp. 312-331, June (1983).

63. H. Rosenfeldt, R. Ulrich, E. Brinkmeyer, U. Feiste, C. Schubert, J. Berger, R. Ludwig, H.G. Weber and A. Ehrhardt, “Feed-Forward Approach for Automatic PMD Compensation at 80 Gbit/s over 45 km Installed Single Mode Fiber”, Proc. European Conference on Optical Communication (ECOC), Amsterdam, The Netherlands (PD.4.8), print ISBN: 0-7803-6705-7, (2001).

64. R. G. Smith, "Optical Power Handling Capacity of Low Loss Optical Fibers as Determined by Stimulated Raman and Brillouin Scattering" Appl. Opt. **11**, pp. 2489-2494 (1972).

65. Y. W. Song, S. M. R. Motaghian, Z. Pan and A. E. Willner, “Efficient DOP monitoring of WDM channels for simultaneous PMD compensation”, Opt. Commun., Vol. 225, pp. 225-229, (2005).

66. G. G. Stokes, “On the composition and resolution of streams of polarized light from different sources”, Trans. Camb. Phil. Soc. Vol. 9, pp. 399, (1852).

67. R. H. Stolen, E. P. Ippen, and A. R. Tynes, “Raman Oscillation in Glass Optical Waveguide”, Appl. Phys. Lett., Vol. 20, pp. 62–64 (1972).

68. R. H. Stolen, J. P. Gordon, W. J. Tomlinson and H. A. Haus, “Raman response function of silica-core fibers”, J. Opt. Soc. Am. B, Vol. 6, Issue 6, pp. 1159-1166, (1989).

69. T. Takahashi, T. Imai and M. Aiki “Automatic compensation technique for timewise fluctuating polarisation mode dispersion in in-line amplifier systems”, Electron. Lett., Vol. 30, Issue 4, pp. 348-349 (1994).

70. L. Thévenaz, A. Zadok, A. Eyal and M. Tur, “All-optical polarization control through Brillouin amplification,” in Optical Fiber Communication Conference, 2008 OSA Technical Digest CD (2008), paper OML7.

71. L. Ursini, M. Santagiustina, and L. Palmieri, “Raman nonlinear polarization pulling in the pump depleted regime in randomly birefringent fibers,” IEEE Photon. Technol. Lett., Vol. 23, no. 4, pp. 254–256, (2011).

72. D. Wang and C. R. Menyuk, “Polarization evolution due to the Kerr nonlinearity and chromatic dispersion”, J. Lighwave Technol., Vol. 17, pp. 2520-2529, (1999).

73. M. Winter, D. Kroushkov, and K. Petermann, “Polarization-Multiplexed transmission system outage due to nonlinearity-induced depolarization”, ECOC 2010, Torino, Italy, Th. 10. E.3, (2010).

74. M. Winter, D. Kroushkov and K. Petermann, “Cross-Polarization Modulation in Polarization-Division Multiplexed transmission systems”, IEEE Photonic Society Summer Topical Meeting Series, MA2.1, (2010).

75. A. Yariv, “Optical Electronics in Modern Communications”, Fifth edition, Oxford University press, (1997).

76. T. Young, “The Bakerian lecture: On the Theory of Light”, Phil. Trans. R. Soc. Lond. 92, pp. 12-48, (1802).

77. A. Zadok, E. Zilka, A. Eyal, L. Th´evenaz and M. Tur, “Vector analysis of stimulated Brillouin scattering amplification in standard single-mode fibers,” Opt. Express, Vol. 16, pp. 21692-21707, (2008).